Entanglement detection and quantum metrology in quantum optical systems

(Összefonódottság észlelése és kvantummetrológia kvantumoptikai rendszerekben)

Doctoral Dissertation
submitted to the Hungarian Academy of Sciences

Géza Tóth
Wigner Research Centre for Physics

Budapest
2019

Contents

Chapter 1

Introduction

Although the most important principles of quantum mechanics were laid down by Schrödinger, Neumann and their contemporaries by the 1930's, a novel development started in the 1980's with applying information theoretical concepts to quantum mechanics. The new interdisciplinary field, Quantum Information Theory (QIT), is concerned with fundamental issues such as entanglement, non-locality, as well as applications. The notion of entanglement was introduced by Schrödinger in 1935. In spite of its long past, several questions remain unanswered. Only quite recently, significant progress has been achieved in understanding entanglement [1, 2].

Entanglement appears in most of the sub-fields of QIT, for example in quantum computation. Quantum computers can outperform classical ones in certain tasks, such as prime factoring and searching, since they exploit superposition and entanglement [3, 4]. Quantum teleportation can be used to move the state of a particle to a distant particle [5]. For quantum cryptography, one can use entangled particles to provide secure communication between two parties. In all these cases, successful experiments have already been carried out while quantum cryptography is perhaps not far from becoming a real life application. Moreover, entangled quantum states are shown to outperform non-entangled ones in certain metrological application and might lead to more exact atomic clocks [6, 7]. Entanglement also appears as a natural goal in today's quantum experiments (e.g., [8–12]). In this way, quantum information science, and in particular entanglement theory, can play a crucial role in the technological development of quantum control and quantum engineering. Finally, the realization of larger and larger entangled quantum systems might also help to answer fundamental questions concerning quantum theory, such as the appearance of a classical macroscopic world based on a quantum microworld (e.g., [13]).

Next, we will first review quantum systems that make it possible to create many-particle entanglement. Then, we present short reviews of entanglement theory and quan-

tum metrology. Finally, we outline the theory of Bell inequalities.

1.1 Interesting quantum states

In this section, we present some quantum states relevant for quantum information. This will help us to have an idea about the recent quantum experiments preparing highly entangled quantum states.

A pure **product state** of an N-particle system can be given as

$$|\Psi_1\rangle \otimes |\Psi_2\rangle \otimes ... \otimes |\Psi_N\rangle, \tag{1.1.1}$$

where $|\Psi_n\rangle$ is the state of the nth particle. If the system is in such a state, then there are no correlations between the particles, that is, $\langle A_n B_m\rangle = \langle A_n\rangle\langle B_m\rangle$ for any A_n and B_m operators measured on particle n and m, respectively.

For quantum information applications, we need highly correlated quantum states. One of such states is the **singlet state** given as

$$\frac{1}{\sqrt{2}}\left(|01\rangle - |10\rangle\right). \tag{1.1.2}$$

The singlet state is often called maximally entangled among two-qubit states, where "qubit" means a two-state system.

Highly entangled states are studied also in multiparticle systems. One of the most interesting states is the **Greenberger-Horne-Zeilinger (GHZ) state** [14], which is just a superposition of a state in which all particles are in state "0" and another one in which all particles are in state "1"

$$|\mathrm{GHZ}_N\rangle = \frac{1}{\sqrt{2}}\left(\underbrace{|00..0\rangle}_{N \text{ qubits}} + |11..1\rangle\right), \tag{1.1.3}$$

where N is the number of two-state particles. In a sense, one can call this state a Schrödinger cat state.

GHZ states are in the symmetric subspace. They are very fragile to noise, since even after a single particle is lost, we obtain a trivial mixture of two product states. There are symmetric entangled states that are more robust to noise. One of them is called **W-state**,

and is defined as

$$\frac{1}{\sqrt{N}}\left(|100..00\rangle + |010..00\rangle + ... + |000..01\rangle\right). \tag{1.1.4}$$

It is just a superposition of all permutations of the states in which a single particle is in state "1" and all the others are in state "0" .

States with more than 1 excitations are also studied intensively. An N-qubit symmetric **Dicke state** with m excitations is defined as [15, 16]

$$|m, N\rangle := \left(\begin{array}{c} N \\ m \end{array}\right)^{-\frac{1}{2}} \sum_k P_k(|1_1, 1_2, ..., 1_m, 0_{m+1}, ..., 0_N\rangle), \tag{1.1.5}$$

where $\{P_k\}$ is the set of all distinct permutations of the spins. $|1, N\rangle$ is the N-qubit W state given in Eq. (1.1.4). In the literature and also in this thesis, for an even N, Dicke state often means just the state $|N/2, N\rangle$, since it is the most studied state and the most entangled one among the states (1.1.5).

Finally, quite recently another family of quantum states, called **cluster states**, have raised considerable interest. While the multiparticle states mentioned so far were symmetric, the cluster state is a state in a one-dimensional spin chain. It can be given explicitly with an Ising dynamics starting from a product state as

$$|\mathrm{C}_N\rangle = U_\mathrm{C} \underbrace{|00..0\rangle_x}_{N \text{ qubits}}, \tag{1.1.6}$$

where x indicates that the state is given in the x-basis, the unitary evolution is defined as

$$U_\mathrm{C} = \exp(-iH_\mathrm{C}\frac{\pi}{4}), \tag{1.1.7}$$

and the Hamiltonian is

$$H_\mathrm{C} = \sum_{n=1}^{N-1}(\mathbb{1} - \sigma_z^{(n)})(\mathbb{1} - \sigma_z^{(n+1)}), \tag{1.1.8}$$

where $\sigma_l^{(n)}$ for $l = x, y, z$ denotes Pauli spin matrices in the thesis[1]. Note that $U_\mathrm{C}^2 = \mathbb{1}$. Hence, applying U_C again we arrive at the initial product state. Cluster states are interesting, since they can be used for a quantum computation scheme which is not based on a unitary evolution, but on single-particle measurements. With two-dimensional cluster states, even universal quantum computation can be realized. In the literature, it is called measurement-based quantum computing [17].

[1]We also use the $X^{(n)}, Y^{(n)}, Z^{(n)}$ notation in some part of the thesis, following the literature.

1.2 Physical systems

In this section, we will discuss some quantum optical systems, in which entanglement has been created.

(i) Systems in which the particles are addressable, with typically 5-10 particles

Photons are one of the most versatile systems for quantum experiments. They encode the "0" and "1" in the horizontal and vertical polarization of the photons, respectively. While photons do not interact with each other, parametric down-conversion and selective detection makes it possible to obtain a large variety of quantum states. Photonic setups can typically create a single quantum state, or a family of states. If we would like to obtain another state, we need to build another experimental setup. However, the quantum state that we are aiming to create can be obtained with a large fidelity. Using more than one degrees of freedom for a single photon, even a ten-qubit GHZ state has been created [18]. Since a photon can take more than two degrees of freedom, a rapid increase is expected above 10 qubits [19].

Trapped ions are another possibility to create multi-particle quantum states. Ions do not interact directly, only through phonons. Thus two-qubit gates must be realized through involving the vibrational states of the chain of ions. Applying different pulse sequences can be used, in principle, to realize various entangled states with the same ion trap. In practice, there are states that are more suitable for the realization in an ion trap than other states. Ion traps have a limit of around $10 - 20$ atoms, hence they are now aiming to combine several such traps to increase to number of ions further. An eight-qubit W-state has been realized with ion traps [20], as well as GHZ states up to 14 qubits [21].

(ii) Systems in which only collective quantities can be measured, with typically $10^6 - 10^{12}$ particles

In experiments with **cold atomic ensembles**, the quantum information is stored in the internal states of the atoms. The atoms are in a vacuum chamber and do not interact with each other [22]. However, by shining light through the chamber and subsequently detecting it, it is possible to entangle the atoms. This way, it is also possible to decrease the variances of collective spin observables to a considerable extent, which is called spin squeezing [23]. Quantum states obtained this way become useful for quantum metrology, as shown in Fig. 1.1. That is, they can provide a better accuracy in measurements than a state in which the spins are not correlated. In such systems, continuous variable quantum teleportation was realized [24], two large ensembles were entangled with each other [10], and a quantum memory for light was realized [25]. The optical depth can be enhanced much further if the ensemble is placed inside an optical cavity. With that technique, very

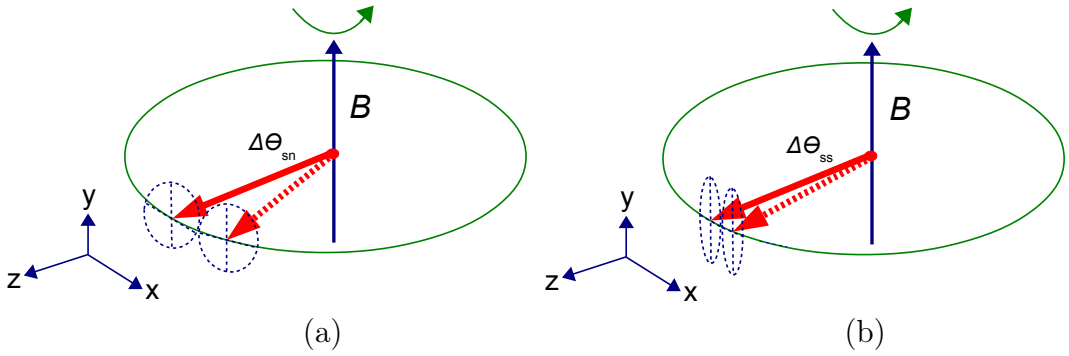

Figure 1.1: (a) Magnetometry with an ensemble of spins. All spins point into the z direction. (Solid arrow) The large collective spin precesses around the magnetic field pointing into the y direction. (Dashed arrow) After a precession of an angle $\Delta\theta_{\rm sn}$, the uncertainty ellipse of the spin is not overlapping with the uncertainty ellipse of the spin at the starting position. Hence, $\Delta\theta_{\rm sn}$ is close to the uncertainty of the phase estimation, which coincides with the shot-noise limit, indicated by the subscript "sn." (b) Magnetometry with an ensemble of spins. All spins point to the z direction and are spin squeezed along the x direction. The uncertainty of the phase estimation is close to the angle $\Delta\theta_{\rm ss}$, which is smaller than $\Delta\theta_{\rm sn}$ due to spin squeezing, indicated by the subscript "ss."

recently, they achieved a 100 times squeezing in such systems [26].

Bose-Einstein condensates can also be used to create correlated states of an ensemble of two-state atoms. The quantum information is stored again in the internal states of the atoms. However, now the atoms interact with each other which can be used to create spin squeezed states [7, 27–29] and Dicke states [30, 31]. Clearly, a bosonic particle has an integer spin. Often, they use particles with a spin $j = 1$, hence such a particle has three states corresponding to the three eigenvectors of the spin component j_z. Often, the experimenters would like to work with two-state atoms. Then, the two-state subsystems are created artificially, such that they keep one of the three levels, typically the $j_z = 0$ level, unpopulated. There are also experiments aiming to realize quantum states with particles with more than two internal states (e.g., Ref. [11]). The advantage of such experiments is that the two-state subsystems need not be created artificially.

Bosonic atoms can also be placed in a lattice. In a paradigmatic experiment they filled around 100 000 cold atoms in a 3D optical lattice [32]. The quantum information was again stored in the internal states of the atoms. Atoms with different states were trapped with different trapping potentials. Moving one of these potentials relative to the other one, they could achieve that atoms get delocalized and interact with atoms at different lattice sites. They used these techniques to realize a 2D array of Ising spin chains and create large scale entanglement [33]. We note that nowadays in some optical lattice experiments they even have access to individual lattice sites [34].

1.3 Entanglement detection

In this section we will discuss, how to interpret the results of various experiments aiming at creating highly entangled quantum states. A review can be found in Ref. [2].

When a quantum state is created, we can obtain lots of data about the state. However, we must be able to characterize the success of the experiment with few data. For example, one can measure the fidelity of the state with respect to the state we intended to create. This is a number between 0 and 1. If the fidelity is large, then the experiment was successful. Another possibility is to prove that the quantum state is entangled. This, as we later discuss, tells us that the state is qualitatively different from non-entangled or separable states.

The theory of entanglement started with the seminal paper of R. F. Werner in 1989 [35], that defined entangled states as they are defined now. Next, we summarize some important aspects of entanglement theory. Let us imagine for a moment, that we have only pure quantum states in nature. In this case, it would be sufficient to talk about *pure product states* and *pure entangled states*. The pure product states are also called pure separable states. This classification is considered in condensed matter, when they talk about the properties of ground states of certain spin chain Hamiltonians. In this case, product states have the property that they do not exhibit any correlation between the particles.

In the real word, we cannot prepare pure states in an experiment. We can only aim at preparing a pure state, but the result will be a mixed state. (We have to remember that when a quantum state is prepared, we always have to talk about a series of experiments, not only a single one.) Thus, we have to generalize the notion of pure separable states to mixed separable states. A mixed *separable state* is just a mixture of pure product states. Any state that is not separable is called an *entangled state*.

Since separable states are just mixtures of trivial product states, quantum interaction is not needed to produce them. This does not exclude the possibility that such an interaction was present. However, we cannot prove it based on the density matrix. In the case of entangled density matrices, we can know that quantum interaction provably contributed to the creation of the state.

Note that separability does not exclude the possibility that the measurements find correlations in separable states, which is not possible for pure product states. However, these correlations can be achieved by operations acting locally on the subsystems, and classical communication among the subsystems, which is the quantum information theoretical analogue of classical interaction. Such operations are called local operations and classical communication (LOCC), see Sec. 2.1.2.

Since entanglement is an important property of the quantum state, there has been a large effort to decide whether a quantum state is entangled. In short, we have to decide whether the density matrix of a two-particle or multi-particle quantum state can be written as a mixture of product states. It turns out that this problem is not solvable in general [36]. There are only necessary conditions for separability. If they are violated, then we know that the state is entangled. However, we do not detect all entangled states this way.

After a general review on entanglement theory, let us discuss how entanglement can be detected in various systems. First, we consider few particle states, corresponding to systems of type (i) of Sec. 1.2. After a multi-particle quantum state is created, one can try to obtain the density matrix of the quantum state by quantum state tomography. This is possible only for small systems (i.e., 10-20 two-state particles), since the number of degrees of freedom (i.e., the number of independent real parameters) increases exponentially with the number of particles. There are also other methods that do not recover the full density matrix, only a part of it, such as permutationally invariant tomography (Sec. 6). They can be used for larger systems.

One of the necessary conditions for separability is the criterion based on the positivity of the partial transpose (PPT). It is based on transposing a density matrix of a two-particle system according to one of the subsystems. Simple algebra shows that the matrix obtained is positive-semidefinite for all separable states. Hence, if the result of the transformation above is not positive-semidefinite, then the state was entangled. This way, we can detect all entangled states in 2×2 and 2×3 systems (i.e., composite systems consisting of two two-state systems, and a two-state system and a three-state system, respectively). There are other criteria, such as the Computable Cross Norm-Realignment Criterion (CCNR), that detects some entangled states that are not detected by the PPT criterion. However, the CCNR criterion is in general not stronger than the PPT criterion.

So far we discussed entanglement detection in the case that the density matrix is fully known. As we mentioned, this can happen only for small systems. Moreover, even for small systems typically it is not possible to measure all the correlations needed to obtain the density matrix. Fortunately, it is possible to detect entanglement by measuring only a single operator. Such an operator is called an *entanglement witnes*. Clearly, entanglement witneses detect only some entangled states. However, the infinitely many entanglement witnesses altogether detect all entangled states.

There is a large literature on how to design entanglement witnesses. There are witnesses which detect entanglement close to Greenberger-Horne-Zeilinger states [37–39], cluster states [39–41], and Dicke states [42–46]. A multi-particle quantum operator cannot typically be measured directly. It must be decomposed into the sum of product

operators. When looking for entanglement witnesses, it is important to look for ones that can be decomposed into the sum of few terms, hence they are easy to measure.

So far, we considered quantum systems of few particles. Next, we discuss entanglement detection in the many-particle ensembles corresponding to systems of type (ii) of Sec. 1.2. On the one hand, in large systems it is impossible to obtain the density matrix due to the very large number of degrees of freedom. On the other hand, typically the particles are not individually addressable and there are few means that can be used to manipulate them, both for creating highly entangled quantum states or to verify their entanglement content.

In a system of many particles, typically one can measure the expectation values of collective quantities, such as the collective angular momentum components. We can also measure the variance of these quantities. These are already sufficient to detect entanglement in an ensemble of many, say 10^3 or 10^{12}, particles. The most known entanglement criterion of this type is the spin-squeezing inequality. Later, the full set of such conditions have been determined for spin-1/2 particles [47]. That is, we cannot find further conditions that detect more states based on the expectation values and variances of collective angular momentum components. Spin squeezing conditions can detect not only entanglement, but can obtain a lower bound on the *entanglement depth*. In other words, apart from telling "entangled", they can also say, how many particles are entangled with each other.

1.4 Quantum metrology

Apart from detecting entanglement, it is also desirable to prove that the quantum state is useful for some application. One of the most important applications is quantum metrology [48–54]. Indeed, spin-squeezed states mentioned above can be used for quantum metrology and they provide a better precision in magnetometry than non-entangled states [23].

The central notion of the field is the quantum Fisher information. It determines the best achievable precision in linear interferometers for a given quantum state. The larger the quantum Fisher information, the better the precision.

Recently, it has even been proven that entanglement is needed to reach the maximal quantum Fisher information and hence, the best precision in metrology [52, 55, 56]. Hence, proving metrological usefulness can also be used for entanglement detection. In more details, higher and higher values of the quantum Fisher information in linear interferometers can be achieved only by quantum states with a larger and larger entanglement depth. This makes it possible to detect the entanglement depth by measuring precision

in some interferometric task carried out with the quantum state.

1.5 Bell inequalities

In this section, we briefly describe the theoretical development leading later to modern entanglement theory. First of all, we have to mention the seminal paper about the Einstein-Podolsky-Rosen (EPR) paradox published in 1935 [57]. It studied quantum measurements on a two-particle singlet, when the particles are far away from each other. It pointed out several effects unusual from the point of view of classical physics, which they called "spooky action at a distance".

Based on these ideas, Bell developed his famous inequalities in 1964 [58], which were followed by other similar relations [59]. In general, Bell inequalities are inequalities that are constructed for bipartite or multipartite systems. They are inequalities with correlations terms that are fulfilled by all so-called local hidden variable (LHV) models (Sec. 9.1.2), which assume that the results of a quantum measurement exist before the measurement. There are quantum states, such as the trivial product states, that do not violate any Bell inequality. They noticed that pure states violating Bell inequalities are often highly correlated.

In Ref. [35], entangled states have been shown that do not violate any Bell inequality.[2] It has been conjectured by A. Peres in 1999, that bound entangled states, i.e., entangled states with a positive partial transpose mentioned before, does not violate a Bell inequality [60]. The conjecture is reasonable since bound entangled states possess a weak form of entanglement. After a long search for counterexamples, the conjecture has been proven to be false in 2014 since some bound entangled states have been found that violate a Bell inequality [61].

On the other hand, all states violating a Bell inequality are entangled. Hence, Bell inequalities can be used for entanglement detection, even if entanglement theory did not exist when they were created. There are also other connections to entanglement theory. Bell inequalities, like entanglement witnesses, are typically also designed for specific quantum states. There are Bell inequalities that detect states close to two-spin singlets [62], GHZ states [63], or cluster states [64–66].

[2] In some cases, when several copies of these states are provided, they do violate a Bell inequality. See S. Popescu, Phys. Rev. Lett. 74, 2619 (1995).

1.6 Structure of the thesis

Next, we will present the topics considered in this thesis, mentioning also the relevant publications. First of all, we would draw the attention to the review articles on quantum entanglement theory [2] and quantum metrology [52].

The thesis is organized as follows. At the beginning of each Chapter, we give a short reference to relevant publications belonging to thesis. In each Chapter, we present some sections explaining the background. Then, sections with our own results follow.

In Chapter 2, we discuss entanglement detection with few correlation terms. In particular, we will consider entanglement detection with spin chain Hamiltonians [67, 68]. In Chapter 3, we consider detection of multipartite entanglement close to graph states, which also include cluster states and GHZ states [39, 41, 69]. We also discuss how to estimate the fidelity with respect to such states [39, 41]. An experimental application of this scheme is described in Ref. [40]. In Chapter 4, entanglement detection close to Dicke states is discussed [42]. We will also show how to measure the entanglement conditions efficiently [46]. We also show examples of entanglement conditions that need only collective measurements [42]. The experimental applications of this scheme are in Ref. [43, 44]. In Chapter 5, the relation between entanglement and permutational symmetry is discussed. We will present symmetric states that are not detected by the PPT criterion [70]. In Chapter 6, we discuss an efficient tomographic method for permutationally invariant systems [71]. Its advantage is that the number of measurements needed scales quadratically with the number of qubits. This makes it possible to carry out tomography of large systems. In Chapter 7, entanglement detection with collective observables are discussed. A generalized spin sqeeezing entanglement condition is presented that detects entanglement close to singlet states [69]. Later, a complete set of entanglement criteria based on collective observables is presented [47, 72]. In Chapter 8, the relation of multipartite entanglement and quantum metrology is discussed. We show that full multipartite entanglement is needed to reach the maximum sensitivity [56]. In Chapter 9, Bell inequalities for graph states are presented [66].

Chapter 2

Entanglement detection with correlations

In this Chapter, we will consider entanglement detection with spin chain Hamiltonians, described in Refs. [67, 68].

2.1 Background

2.1.1 Entanglement

What kind of quantum states should experiments aim at creating? Let us consider first pure states. Clearly, product states of the type

$$|\Psi^{(1)}\rangle \otimes |\Psi^{(2)}\rangle \otimes ...|\Psi^{(N)}\rangle \tag{2.1.1}$$

are not that interesting. Such states can be created without any interaction between the parties. On the other hand, pure multipartite quantum states that are not product states have to be created via an interaction between the parties.

Let us turn now to mixed states. A mixed quantum state is (fully) separable if it can be written as [35]

$$\varrho_{\text{sep}} = \sum_m p_m \rho_m^{(1)} \otimes \rho_m^{(2)} \otimes ... \otimes \rho_m^{(N)}, \tag{2.1.2}$$

where $\rho_m^{(n)}$ are single-particle pure states and N is the number of the particles. Separable states are essentially states that can be created without an inter-particle interaction, just by mixing product states. More precisely, separable states can be created with LOCC operations from product states. Such operations have been mentioned in the introduction,

and will be described in the next section.

States that are not separable are called entangled. Entangled states are more useful than separable ones for several quantum information processing tasks, such as quantum teleportation, quantum cryptography, and, as we will show later, for quantum metrology [1, 2]. Entanglement is connected to older notions of quantum physics, such as Bell inequalities, as we have mentioned in Sec. 1.5. Entanglement is also related to non-classicality, a central concept in quantum optics [73].

2.1.2 Local Operations and Classical Communication

Local Operations and Classical Communication (LOCC) are some series of the following operations.

- Local unitaries, i.e., unitaries of the type

$$U^{(1)} \otimes U^{(2)} \otimes ... \otimes U^{(N)}, \tag{2.1.3}$$

  where $U^{(n)}$ acts on n^{th} party of the N-partite state.

- Local von Neumann measurements and local generalized measurements, i.e., local positive-operator valued measures (POVM).

- Local unitaries or measurements conditioned on measurement outcomes on the other party.

Such operations cannot produce an entangled state from a separable one given in Eq. (2.1.2) [1, 2]. Note, however, that such operations can create correlations starting from a product state.

2.1.3 Multipartite entanglement and entanglement depth

In the many-particle case, it is not sufficient to distinguish only two qualitatively different cases of separable and entangled states. For example, an N-particle state is entangled, even if only two of the particles are entangled, as in the state

$$|\Psi\rangle = \frac{1}{\sqrt{2}} \left(|00\rangle + |11\rangle\right) \otimes |0\rangle^{\otimes(N-2)}. \tag{2.1.4}$$

Usually, we would not call the state given in Eq.(2.1.4) multipartite entangled. On the other hand, there are quantum states in which all the N particles are entangled with each

other. One of the most important such highly entangled states is the GHZ state defined in Eq. (1.1.3). Hence, the notion of genuine multipartite entanglement [37, 38] has been introduced to distinguish partial entanglement from the case when all the particles are entangled with each other. It is defined as follows. A pure state is biseparable, if it can be written as a tensor product of two multi-partite states

$$|\Psi\rangle = |\Psi_1\rangle \otimes |\Psi_2\rangle. \tag{2.1.5}$$

A mixed state is biseparable if it can be written as a mixture of biseparable pure states. A state that is not biseparable is genuine multipartite entangled. Genuine multipartite entanglement is one of the notions most used in nowadays experiments with ions and photons [18, 19, 21, 38, 43–45, 74–77]. A quantum system possessing entanglement of this type cannot be obtained from entangled systems of smaller size by trivial operations, without real quantum interaction. For example, by merely adding a particle to a system with N-qubit genuine multipartite entanglement, without interaction, it is not possible to get a state with $(N + 1)$-qubit genuine multipartite entanglement. This way, if in an experiment genuine multipartite entanglement of $(N + 1)$ qubits is detected, then this experiment provides something qualitatively new compared to N-particle experiments.

In the many-particle scenario, further levels of multi-partite entanglement must be introduced since verifying full N-particle entanglement for $N = 1000$ or 10^6 particles is not realistic. In order to characterise the different levels of multipartite entanglement, we start first with pure states. We call a state k-producible, if it can be written as a tensor product of the form

$$|\Psi\rangle = \otimes_m |\psi_m\rangle, \tag{2.1.6}$$

where $|\psi_m\rangle$ are multiparticle states with $k_m \leq k$ particles. A k-producible state can be created in such a way that only particles within groups containing not more than k particles were interacting with each other. This notion can be extended to mixed states by calling a mixed state k-producible if it can be written as a mixture of pure k-producible states. A state that is not k-producible contains at least $(k + 1)$-particle entanglement [78, 79]. Using another terminology, we can also say that the entanglement depth of the quantum state is larger than k [23]. An N-qubit state with an entanglement depth N is genuine multipartite entangled.

It is instructive to depict states with various forms of multipartite entanglement in set diagrams as shown in Fig. 2.1. Separable states are a convex set since if we mix two separable states, we can obtain only a separable state. Similarly, k-producible states also form a convex set. In general, the set of k-producible states contains the set of l-producible states if $k > l$.

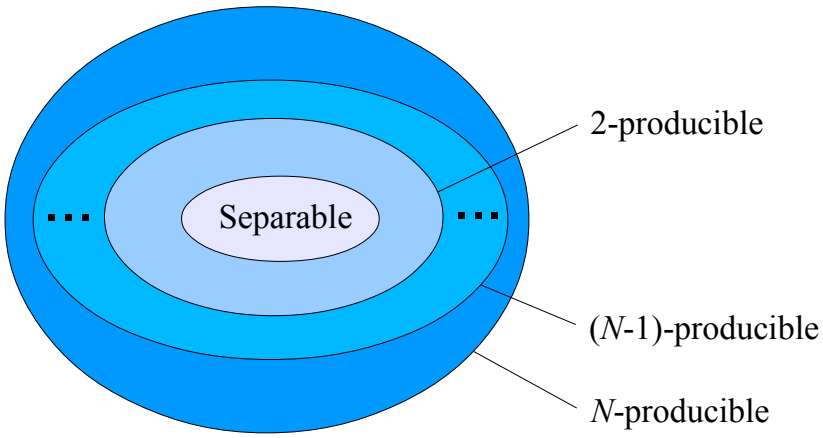

Figure 2.1: Sets of states with various forms of multipartite entanglement. k-producible states form larger and larger convex sets. 1-producible states are equal to the set of separable states. The set of physical quantum states is equal to the set of N-producible states.

An even more detailed classification of multipartite entangled states is possible, into which the k-producibility based classification fits naturally. It is called partial separability classification [80, 81], and it takes into account all the possible ways how the states can be mixed by the use of pure states separable with respect to different splits.

2.1.4 Entanglement witnesses

An observable $\mathcal{W}$ is entanglement witness if it fulfils the following two requirements [82, 83]:

(i) $\langle \mathcal{W} \rangle \geq 0$ for all separable states,

(ii) $\langle \mathcal{W} \rangle < 0$ for some entangled state.

In another context, entanglement witnesses are entanglement criteria that are linear in operator expectation values.

Entanglement witnesses can also be designed such that they detect no entanglement in general, but a certain type of entanglement, i.e., only genuine multipartite entanglement.

2.1.5 Robustness to noise for entanglement witnesses

There are infinite number of entanglement witnesses that can be used to detect a given quantum state as entangled. We have to choose one of them, by evaluating the witnesses

based on their usefulness. One of the most important requirements is that the witness should have a large robustness to noise. In an experiment that aims to prepare a pure state $|\Psi\rangle$, the result is, of course, a mixed state, which can typically be very well approximated by the original pure state mixed with white noise (i.e., the completely mixed state) as

$$\varrho(p_{\text{noise}}) = (1 - p_{\text{noise}})|\Psi\rangle\langle\Psi| + p_{\text{noise}}\varrho_{\text{cm}}, \tag{2.1.7}$$

where the completely mixed state is defined as

$$\varrho_{\text{cm}} = \frac{1}{d^N}\mathbb{1}, \tag{2.1.8}$$

where $\mathbb{1}$ is the identity matrix, p_{noise} is the fraction of the noise, and we considered a system of N qudits with a dimension d. It is important that the witness used is able to detect not only the ideal state as entangled, but also the noisy state. The largest noise fraction p_{noise} for which the state is still detected as entangled is the robustness of the witness to noise. Alternatively, it is also called noise tolerance. Simple calculation shows that if the witness $\mathcal{W}$ detects $|\Psi\rangle$ as entangled (i.e., $\langle\mathcal{W}\rangle_{|\Psi\rangle} < 0$) then a state of the type (2.1.7) is detected as entangled if

$$p_{\text{noise}} < \frac{\langle\mathcal{W}\rangle_{|\Psi\rangle}}{\langle\mathcal{W}\rangle_{|\Psi\rangle} - \langle\mathcal{W}\rangle_{\varrho_{\text{cm}}}}. \tag{2.1.9}$$

2.2 Using correlations to witness entanglement

Beside constructing entanglement witnesses, it is also important to find a way to measure them. For example, they can easily be measured by decomposing them into a sum of locally measurable terms [8]. Here we follow a different route. We will construct witness operators of the form

$$\mathcal{W}_O := O - \inf_{\Psi\in S}\left[\langle\Psi|O|\Psi\rangle\right], \tag{2.2.10}$$

where S is the set of separable states, "inf" denotes infimum, and O is a fundamental quantum operator of a spin system which is easy to measure. In the general case $\inf_{\Psi\in S}\langle\Psi|O|\Psi\rangle$ is difficult, if not impossible, to compute [84, 85]. Thus we will concentrate on operators that contain only two-particle interactions and have certain symmetries. We derive a general method to find bounds for the expectation value of such operators for separable states. This method will be applied to spin lattices. We will also consider models with a different topology.

If observable O is taken to be the Hamiltonian then our method can be used for detect-

ing entanglement by energy measurement.[3] While our approach does not require that the system is in thermal equilibrium, it can readily be used to detect entanglement for a range of well-known systems in this case. The energy bound for separable states correspond to a temperature bound. Below this temperature the thermal state is necessarily entangled.

Let us consider first a simple example.

Example 2.2.1 *For two-qubit separable states we have*

$$\langle \sigma_x^{(1)} \sigma_x^{(2)} \rangle + \langle \sigma_y^{(1)} \sigma_y^{(2)} \rangle + \left\langle \sigma_z^{(1)} \sigma_z^{(2)} \right\rangle \leq 1. \tag{2.2.11}$$

Proof. Let us consider first pure two-qubit product states of the form $|\psi_1\rangle \otimes |\psi_2\rangle$. Then, for such states we have

$$\langle \sigma_l^{(1)} \sigma_l^{(2)} \rangle = \langle \sigma_l^{(1)} \rangle \langle \sigma_l^{(2)} \rangle \tag{2.2.12}$$

for $l = x, y, z$. Hence, the left-hand side of Eq. (2.2.11) can be written as a scalar product of two vectors

$$\langle \sigma_x^{(1)} \sigma_x^{(2)} \rangle + \langle \sigma_y^{(1)} \sigma_y^{(2)} \rangle + \left\langle \sigma_z^{(1)} \sigma_z^{(2)} \right\rangle = \vec{s}_1 \cdot \vec{s}_2, \tag{2.2.13}$$

where

$$\vec{s}_n = \begin{pmatrix} \langle \sigma_x^{(n)} \rangle \\ \langle \sigma_y^{(n)} \rangle \\ \langle \sigma_z^{(n)} \rangle \end{pmatrix} \tag{2.2.14}$$

for $n = 1, 2$. Finally, applying the Cauchy-Schwarz inequality we get

$$\vec{s}_1 \vec{s}_2 \leq |\vec{s}_1||\vec{s}_2| = 1. \tag{2.2.15}$$

With that, we proved Eq. (2.2.11) for pure product states. Keeping in mind that separable states are the mixtures of product states, Eq. (2.2.11) is also valid for separable states given in Eq. (2.1.2). ■

After the simple example, we consider spin lattice Hamiltonians. Calculations similar to this one are widely used in statistical physics, however, we still think that it will help to understand the basic goals of entanglement theory by connecting it to other areas of physics. We would like to find the minimal expectation value of such Hamiltonians for product states. The calculations can be simplified if the lattice can be divided into two sublattices, A and B, such that every correlation term involves one spin component from sublattice A and another one from sublattice B. Such sublattices are shown in Fig. 2.2. If

[3] Independently, a pre-print with a similar approach has appeared: Č. Brukner and V. Vedral, quant-ph/0406040.

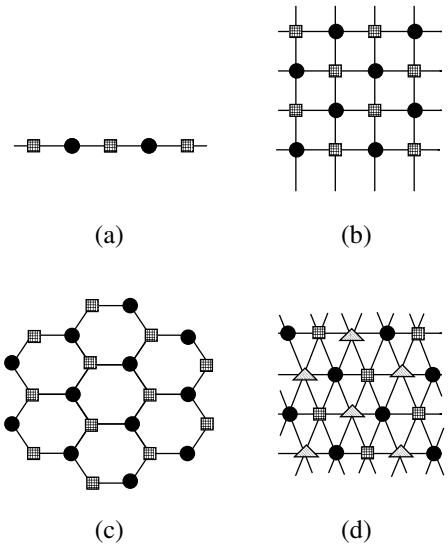

Figure 2.2: Some of the most often considered lattice models: (a) Chain, (b) two-dimensional cubic lattice, (c) hexagonal lattice and (b) triangular lattice. Different symbols at the vertices indicate a possible partitioning into sublattices. Figure is taken from Ref. [67].

we also assume that all interaction terms are the same then we can write the expectation value of the Hamiltonian for such systems as

$$\langle H\rangle = \sum_k f(\vec{s}_{a_k}, \vec{s}_{b_k}), \tag{2.2.16}$$

where f is some two-spin function, and a_k and b_k denotes the indices of spins of sublattice A and B, respectively. The minimum over product states can be obtained as

$$\min_{\Psi_1\otimes\Psi_2\otimes\ldots\otimes\Psi_N} \langle H\rangle = \min_{\{\vec{s}_k\}_{k=1}^N, |\vec{s}_k|=1} \sum_k f(\vec{s}_{a_k}, \vec{s}_{b_k}). \tag{2.2.17}$$

It is possible to minimize the terms in Eq. (2.2.17) idependently, hence we arrive at

$$\min_{\Psi_1\otimes\Psi_2\otimes\ldots\otimes\Psi_N} \langle H\rangle = N_{\text{corr}} \min_{\vec{s}^m, |\vec{s}^m|=1} f(\vec{s}^A, \vec{s}^B), \tag{2.2.18}$$

where N_{corr} is the number of correlation terms.

Finally, we need the minimum of $\langle H\rangle$ for separable states. Since separable states are just mixtures of product states, and the expectation value is $\langle H\rangle = \text{Tr}(\varrho H)$ is linear in ϱ, the bound we obtain in Eq. (2.2.18) is also valid for separable states. Hence, if $\langle H\rangle$ is lower than this minimum, then the quantum state must be entangled. This way we can detect entanglement based on energy measurement. With the formalism of Sec. 2.1.4, we

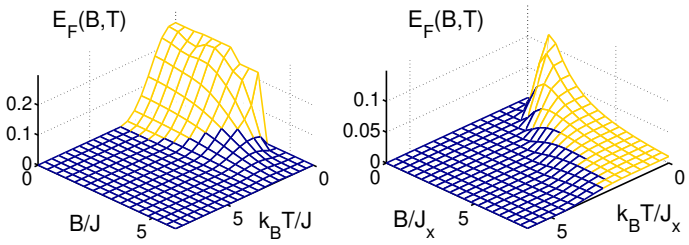

(a) (b)

Figure 2.3: (a) Heisenberg chain of 8 spins. Nearest-neighbor entanglement as a function of magnetic field B and temperature T. (b) The same for an Ising spin chain. Here k_B is the Boltzmann constant, J and J_x are coupling constants. Light color indicates the region where entanglement is detected by our method. Figure is taken from Ref. [67].

can say that

$$W = H - N_{\text{corr}} \min_{\vec{s}^m, |\vec{s}^m|=1} f(\vec{s}^A, \vec{s}^B), \tag{2.2.19}$$

is an entanglement witness.

If the nondegenerate ground state or the $T = 0$ thermal state of a system is entangled, then it is expected that the thermal state remains entangled even at finite temperatures up to a temperature bound. Let us define the temperature T_{E} such that the energy of the thermal state equals to the bound obtained in Eq. (2.2.18), that is,

$$\frac{\text{Tr}\left(He^{\frac{H}{T_{\text{E}}}}\right)}{\text{Tr}\left(e^{\frac{H}{T_{\text{E}}}}\right)} = N_{\text{corr}} \min_{\vec{s}^m, |\vec{s}^m|=1} f(\vec{s}^A, \vec{s}^B). \tag{2.2.20}$$

For $T < T_{\text{E}}$ the thermal state will have lower energies than the bound (2.2.18), hence it must be entangled. It is straightforward to calculate T_{E} based on our approach. We add that we do not claim that the system is separable for all $T > T_{\text{E}}$.

2.3 Entanglement detection with well-known spin Hamiltonians

Let us consider an anti-ferromagnetic Heisenberg Hamiltonian with periodic boundary conditions on a d-dimensional cubic lattice

$$H_{\text{H}} := \sum_{\langle k,l \rangle} \sigma_x^{(k)} \sigma_x^{(l)} + \sigma_y^{(k)} \sigma_y^{(l)} + \sigma_z^{(k)} \sigma_z^{(l)} + B\sigma_z^{(k)}. \tag{2.3.21}$$

The strength of the exchange interaction is set to be $J = 1$, B is the magnetic field, and $\langle k, l\rangle$ denotes spin pairs connected by an interaction. The expectation value of Eq. (2.3.21) for separable states is bounded from below

$$\langle H_{\rm H}\rangle \geq E_{H,\rm sep} := \begin{cases} -dN[(B/d)^2/8+1] & \text{if } |B/d| \leq 4, \\ -dN(|B/d|-1) & \text{if } |B/d| > 4, \end{cases} \tag{2.3.22}$$

where N is the total number of spins. This bound was obtained using two sublattices, minimizing the expression $f_{\rm H}(\vec{s}^A, \vec{s}^B) := \vec{s}^A\vec{s}^B + B(s_z^A + s_z^B)/(2d)$. Based on this $E_{\rm H,sep} = dN\inf[f_{\rm H}]$.[4]

Another important question is how the temperature bound T_E depends on the number of particles. For the Heisenberg model of even number of spins with $B = 0$ this temperature decreases slowly with N and saturates at $T \approx 3.18$. Refs. [86, 87] find the same temperature bound for nonzero concurrence for an infinite system.

For the XY Hamiltonian on a d-dimensional cubic lattice with periodic boundary conditions

$$H_{\rm XY} := \sum_{\langle k,l\rangle} J_x\sigma_x^{(k)}\sigma_x^{(l)} + J_y\sigma_y^{(k)}\sigma_y^{(l)} + B\sum_k^N \sigma_z^{(k)} \tag{2.3.23}$$

the energy of separable states is bounded from below as

$$\langle H_{\rm XY}\rangle \geq E_{\rm XY,sep} := \begin{cases} -dNM\big(1+b^2/4\big) & \text{if } b \leq 2, \\ -dNMb & \text{if } b > 2. \end{cases} \tag{2.3.24}$$

Here J_x and J_y are the nearest-neighbor coupling along the x and y direction, respectively. B is the magnetic field, $M := \max(|J_x|, |J_y|)$ and $b := |B|/M/d$. This bound is simply the mean-field ground state energy. It was obtained using two sublattices and minimizing $f_{\rm XY}(\vec{s}^A, \vec{s}^B) := J_x s_x^A s_x^B + J_y s_y^A s_y^B + B(s_z^A + s_z^B)/(2d)$.

A one-dimensional spin-1/2 Ising chain is a special case of an XY lattice with $J_x = 1$ and $J_y = 0$. Fig. 2.3(b) shows the nearest-neighbor entanglement as a function of B and T for this system. According to numerics, T_E (computed for $B = 1$) decreases with increasing N. For $N = \infty$ we obtain $T_E \approx 0.41$ [88].

[4] If the number of sites along one dimension is odd, then a lattice with periodic boundary conditions cannot be partitioned into two sublattices such that neighboring sites correspond to different sublattices. In this case $E_{\rm sep}$ given here is still a lower bound for the energy of separable states, but not necessarily the highest possible lower bound.

2.4 Connected work

We review some works connected to this topic. A similar approach has been reported in independent works in Ref. [89, 90]. Optimal temperature bounds have been calculated in Ref. [91]. References [78, 79] consider the detection of various forms of multipartite entanglement, described in Sec. 2.1.3, with a similar approach.

Chapter 3

Entanglement detection close to graph states

In this Chapter, we consider detection of multipartite entanglement close to graph states, which also include cluster states and GHZ states described in Refs. [39, 41, 69]. We present criteria that detect any type of entanglement, as well as criteria that detect only genuine multipartite entanglement. We also discuss how to estimate the fidelity with respect to such states based on Refs. [39, 41].

3.1 Background

3.1.1 GHZ states, as stabilizer states

There are various quantum states that appear often in experiments. One of them is the Greenberger-Horne-Zeilinger (GHZ) state [14] given in Eq. (1.1.3), which is the superposition of two states: all atoms in state '0' and all atoms in state '1'. For large number of particles, this is the superposition of two macroscopically different states, i.e., a Schrödinger-cat state.

We introduce very briefly the *stabilizer theory* [92], which will be used for entanglement detection. This theory already plays a determining role in quantum information science. Its key idea is describing the quantum state by its so-called *stabilizing operators* rather than the state vector. This works as follows: An observable S_k is a stabilizing operator of an N-qubit state $|\psi\rangle$ if the state $|\psi\rangle$ is an eigenstate of S_k with eigenvalue 1

$$S_k|\psi\rangle = |\psi\rangle. \tag{3.1.1}$$

Many highly entangled N-qubit states can be uniquely defined by N stabilizing operators which are locally measurable, i.e., they are products of Pauli matrices.

We now show how the stabilizer theory can be used to give a set of correlations that determine the GHZ state uniquely. An N-qubit GHZ state is given by Eq. (1.1.3). Besides this explicit definition one may define the GHZ state also in the following way: Let us look at the observables

$$\begin{aligned} S_1^{(\mathrm{GHZ}_N)} &:= \prod_{k=1}^{N} X^{(k)}, \\ S_k^{(\mathrm{GHZ}_N)} &:= Z^{(k-1)}Z^{(k)} \text{ for } k = 2, 3, ..., N, \end{aligned} \tag{3.1.2}$$

where $X^{(k)}, Y^{(k)}$, and $Z^{(k)}$ denote the Pauli matrices acting on the k-th qubit. Now we can *define* the GHZ state as the state $|\mathrm{GHZ}_N\rangle$ which fulfills

$$S_k^{(\mathrm{GHZ}_N)}|\mathrm{GHZ}_N\rangle = |\mathrm{GHZ}_N\rangle \tag{3.1.3}$$

for $k = 1, 2, ..., N$. One can straightforwardly calculate that the GHZ state is uniquely defined by Eq. (3.1.3). From a physical point of view the definition via Eq. (3.1.3) stresses that the GHZ state is uniquely determined by the fact that it exhibits perfect correlations for the observables $S_k^{(\mathrm{GHZ}_N)}$.

Note that $|\mathrm{GHZ}_N\rangle$ is stabilized not only by $S_k^{(\mathrm{GHZ}_N)}$, but also by their products. These operators, all having perfect correlations for a GHZ state, form a group called *stabilizer* [92]. This 2^N-element group of operators will be denoted by $\mathcal{S}^{(\mathrm{GHZ}_N)}$. The operators $S_k^{(\mathrm{GHZ}_N)}$ are the generators of this group.

3.1.2 Cluster states and graph states

Cluster states are multipartite states arising naturally in Ising spin systems. In the two-dimensional case, they can be used for measurement based quantum computing as a resource [17].

For simplicity let us consider a one-dimensional cluster state defined in Eq. (1.1.6). One can use the stabilizer theory described in Sec. 3.1.1 to define cluster states. In this case, a cluster state $|\mathrm{C}_N\rangle$ is defined to be the state fulfilling the equations $|\mathrm{C}_N\rangle = S_k^{(\mathrm{C}_N)}|\mathrm{C}_N\rangle$ with the following stabilizing operators

$$\begin{aligned} S_1^{(\mathrm{C}_N)} &:= X^{(1)}Z^{(2)}, \\ S_k^{(\mathrm{C}_N)} &:= Z^{(k-1)}X^{(k)}Z^{(k+1)}; k = 2, 3, ..., N-1, \\ S_N^{(\mathrm{C}_N)} &:= Z^{(N-1)}X^{(N)}. \end{aligned} \tag{3.1.4}$$

Analogously to the case of GHZ states described in Sec. 3.1.1, the cluster state is uniquely given by the N stabilizing operators (3.1.4).

Let us now describe graph states. They are the generalizations of cluster states [93]. A graph state corresponds to a graph G consisting of N vertices and some edges. The connectivity of this graph is defined by $\mathcal{N}(i)$, which gives the set of neighbors for vertex i. Let us define for each vertex a locally measurable observable

$$S_k^{(\mathrm{G}_N)} := X^{(k)} \prod_{l \in \mathcal{N}(k)} Z^{(l)}. \tag{3.1.5}$$

A graph state $|\mathrm{G}_N\rangle$ of N qubits is now defined to be the state which has the operators $S_k^{(\mathrm{G}_N)}$ given in Eq. (3.1.5) as stabilizing operators. This means that the $S_k^{(\mathrm{G}_N)}$ have the state $|\mathrm{G}_N\rangle$ as an eigenstate with eigenvalue $+1$,

$$S_k^{(\mathrm{G}_N)} |\mathrm{G}_N\rangle = |\mathrm{G}_N\rangle. \tag{3.1.6}$$

We can see that cluster states correspond to graph states with

$$\begin{aligned} \mathcal{N}(1) &= \{2\}, \\ \mathcal{N}(n) &= \{n-1, n+1\}, \text{ for } n = 2, 3, ..., N-1, \\ \mathcal{N}(N) &= \{N-1\}. \end{aligned} \tag{3.1.7}$$

3.1.3 Local decomoposition of entanglement witnesses

An entanglement witness $\mathcal{W}$ is typically a multipartite operator. In principle, it is an observable, and can be measured. In practice, it is very difficult to measure a multipartite operator. Fortunately, we do not need a von Neumann measurement of $\mathcal{W}$, we need only its expectation value. $\langle \mathcal{W} \rangle$ can be obtained from a series of correlation measurements using the local decomposition

$$\mathcal{W} = \sum_k c_k A_k^{(1)} \otimes A_k^{(2)} \otimes ... A_k^{(N)}, \tag{3.1.8}$$

where N is the number of parties and $A_k^{(n)}$ are operators acting on party (n). Then, $\langle \mathcal{W} \rangle$ is obtained as a weighted average of the expectation values of correlation measuements

$$\langle \mathcal{W} \rangle = \sum_k c_k \left\langle A_k^{(1)} \otimes A_k^{(2)} \otimes ... A_k^{(N)} \right\rangle. \tag{3.1.9}$$

3.1.4 Local measurement settings

Based on the previous section, one might think that the experimental effort needed for measuring such an operator is characterized by the number of correlation terms we need for a decompositon. In fact, this is not the case. The experimental effort needed for measuring a witness can be characterized by the number of local measurement settings needed for its implementation [83, 94].

A local measurement setting

$$\mathcal{L} = \{O^{(k)}\}_{k=1}^{N} \tag{3.1.10}$$

consists of performing simultaneously the von Neumann measurements $O^{(k)}$ on the corresponding parties. By repeating the measurements many times one can determine the probabilities of the possible outcomes. Given these probabilities it is possible to compute all two-point correlations $\langle O^{(k)}O^{(l)}\rangle$, three-point correlations $\langle O^{(k)}O^{(l)}O^{(m)}\rangle$, etc. Hence, there are several correlation terms that can be measured with a single setting.

Optimal decompositions for various system sizes and operators has been intensively studied [95–97]. The number of measurement settings needed to decompose any projector to an N-qubit symmetric state is at most $(N^2 + 3N + 2)/2$ [71].

3.2 Detection of entanglement

Based on Sec. 3.1.1, we construct our witness from two locally non-commuting stabilizing operators:

Observation 3.2.1 *A witness detecting entanglement around an N-qubit GHZ state is*

$$\mathcal{W}_m^{(\mathrm{GHZ}_N)} := \mathbb{1} - S_1^{(\mathrm{GHZ}_N)} - S_m^{(\mathrm{GHZ}_N)}, \tag{3.2.11}$$

where $m = 2, 3, ..., N$.

Proof. The proof is based on the Cauchy-Schwarz inequality. Using this and $\langle X^{(i)}\rangle^2 + \langle Z^{(i)}\rangle^2 \leq 1$, for pure product states we obtain

$$\begin{aligned}
&\langle S_1^{(\mathrm{GHZ}_N)}\rangle + \langle S_m^{(\mathrm{GHZ}_N)}\rangle = \\
&\quad = \langle X^{(1)}\rangle\langle X^{(2)}\rangle ... \langle X^{(N)}\rangle + \langle Z^{(m-1)}\rangle\langle Z^{(m)}\rangle \\
&\quad \leq |\langle X^{(m-1)}\rangle| \cdot |\langle X^{(m)}\rangle| + |\langle Z^{(m-1)}\rangle| \cdot |\langle Z^{(m)}\rangle| \\
&\quad \leq \sqrt{\langle X^{(m-1)}\rangle^2 + \langle Z^{(m-1)}\rangle^2}\sqrt{\langle X^{(m)}\rangle^2 + \langle Z^{(m)}\rangle^2} \\
&\quad \leq 1.
\end{aligned} \tag{3.2.12}$$

It is easy to see that the bound is also valid for mixed separable states. ■

This proof can straightforwardly be generalized to arbitrary two locally non-commuting elements of the stabilizer. Using the definitions of Sec. 3.1.2, a derivation similar to the one above yield the following.

Observation 3.2.2 *A witness detecting entanglement around an N-qubit cluster state is*

$$\mathcal{W}_m^{(\mathrm{C}_N)} := \mathbb{1} - S_m^{(\mathrm{C}_N)} - S_{m+1}^{(\mathrm{C}_N)}, \tag{3.2.13}$$

where $m = 1, 3, ..., N-1$.

Proof. The proof is analogous to the poof of the previous Observation 3.2.1. ■

3.3 Detection of multipartite entanglement

The measurement of the fidelity with respect to some pure quantum state, and the detection of genuine multipartite entanglement are needed in numerous quantum experiments (e.g., Refs. [40, 44, 98]). In most of these experiments, only local measurements can be carried out. For such systems, many methods need a measurement effort increasing exponentially with the number of qubits [39]. This also means that measuring the quantum fidelity and measuring witness operators is impractical in many cases apart from very small particle numbers. Hence, it has been noted that it is not clear that entanglement witnesses have really an advantage over full state tomography (e.g., Ref. [83]). It seems that we cannot obtain any useful information in an experiment about the quantum state prepared. Indeed, there is no a priori reason that the detection of multipartite entanglement is possible in a scalable way with local measurements.

In this section, we will present efficient methods, which need few local measurements, to detect genuine multipartite entanglement in the vicinity of stabilizer states, and also for obtaining a very good lower bound on the fidelity. Next, we present efficient witnesses for GHZ states.

Observation 3.3.1 *The following entanglement witness detects genuine N-qubit entanglement for states close to an N-qubit GHZ state:*

$$\mathcal{W}_{\mathrm{GHZ}_N} := 3\mathbb{1} - 2\left[\frac{S_1^{(\mathrm{GHZ}_N)} + \mathbb{1}}{2} + \prod_{k=2}^{N} \frac{S_k^{(\mathrm{GHZ}_N)} + \mathbb{1}}{2}\right]. \tag{3.3.14}$$

Another witness for this task is given by

$$\mathcal{W}'_{\mathrm{GHZ}_N} := (N-1)\mathbb{1} - \sum_{k=1}^{N} S_k^{(\mathrm{GHZ}_N)}. \tag{3.3.15}$$

Proof. First, we need to know that

$$\widetilde{\mathcal{W}}_{\mathrm{GHZ}_N} = \frac{1}{2}\mathbb{1} - |\mathrm{GHZ}_N\rangle\langle\mathrm{GHZ}_N| \tag{3.3.16}$$

detects genuine N-qubit entanglement. This follows from the methods presented in Ref. [8]. We will now show that the witness $\widetilde{\mathcal{W}}_{\mathrm{GHZ}_N}$ is finer than the witness $\mathcal{W}_{\mathrm{GHZ}_N}$, *i.e.*, that for all states with $\mathrm{Tr}(\varrho\mathcal{W}_{\mathrm{GHZ}_N}) < 0$ also $\mathrm{Tr}(\varrho\widetilde{\mathcal{W}}_{\mathrm{GHZ}_N}) < 0$ holds [82]. For that we have to show that

$$\mathcal{W}_{\mathrm{GHZ}_N} - \alpha\widetilde{\mathcal{W}}_{\mathrm{GHZ}_N} \geq 0, \tag{3.3.17}$$

where α is some positive constant. Then for any state ϱ detected by $\mathcal{W}_{\mathrm{GHZ}_N}$ we have $\alpha\mathrm{Tr}(\varrho\widetilde{\mathcal{W}}_{\mathrm{GHZ}_N}) \leq \mathrm{Tr}(\varrho\mathcal{W}_{\mathrm{GHZ}_N}) < 0$ thus the state is also detected by $\widetilde{\mathcal{W}}_{\mathrm{GHZ}_N}$. This implies that $\mathcal{W}_{\mathrm{GHZ}_N}$ is also a multi-qubit witness. Let us now look at the observable

$$X := \mathcal{W}_{\mathrm{GHZ}_N} - 2\widetilde{\mathcal{W}}_{\mathrm{GHZ}_N}, \tag{3.3.18}$$

and show that $X \geq 0$. We can express X in the GHZ state basis. Since $\mathcal{W}_{\mathrm{GHZ}_N}$ as well as $\widetilde{\mathcal{W}}_{\mathrm{GHZ}_N}$ are diagonal in this basis, X is also diagonal. By direct calculation it is straightforward to check that the entries on the diagonal are all non-negative, which proves our claim. For the other witness one can show similarly that $\mathcal{W}'_{\mathrm{GHZ}_N} - 2\widetilde{\mathcal{W}}_{\mathrm{GHZ}_N} \geq 0$ ■

In Fig. 3.1(b) the measurement settings are shown that are needed to measure $\mathcal{W}_{\mathrm{GHZ}_N}$ and $\mathcal{W}'_{\mathrm{GHZ}_N}$. We need only two measurement settings for these witnesses that detect genuine multipartite entanglement, for any particle number. This is the main point of these witnesses. Since the number of settings does not increase with the particle number, these witnesses are feasible for large systems. In contrast, the number of settings needed to detect genuine multipartite entanglement with Bell inequalities [63] is increasing exponentially with the number of qubits.

Next, we present efficient witnesses for cluster states.

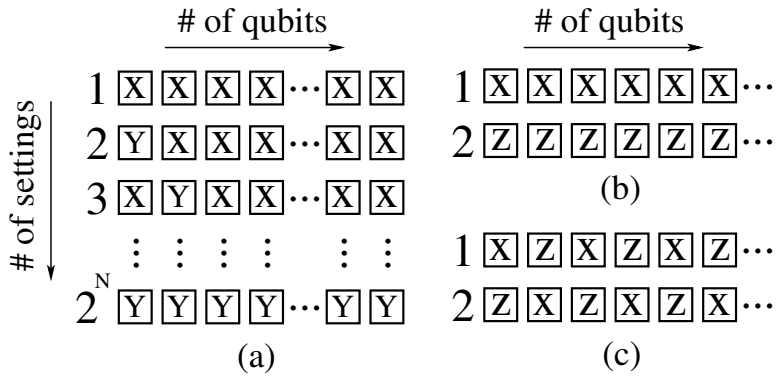

Figure 3.1: (a) Measurement settings needed for detecting genuine multi-qubit entanglement close to GHZ states with Bell inequalities. For each qubit the measured spin component is indicated. (b) Settings needed for the approach presented here for detecting entangled states close to GHZ states and (c) cluster states. Figure is taken from Ref. [39].

Observation 3.3.2 *The following witnesses detect genuine N-party entanglement close to a cluster state*

$$\begin{aligned} \mathcal{W}_{\mathrm{C}_N} &:= 3\mathbb{1} - 2\Big[\prod_{even\ k}\frac{S_k^{(\mathrm{C}_N)}+\mathbb{1}}{2} + \prod_{odd\ k}\frac{S_k^{(\mathrm{C}_N)}+\mathbb{1}}{2}\Big], \\ \mathcal{W}'_{\mathrm{C}_N} &:= (N-1)\mathbb{1} - \sum_{k=1}^{N} S_k^{(\mathrm{C}_N)}. \end{aligned} \tag{3.3.19}$$

Proof. In order to show that these observables are witnesses, we first show that

$$\widetilde{\mathcal{W}}_{\mathrm{C}_N} := \frac{1}{2}\mathbb{1} - |\mathrm{C}_N\rangle\langle\mathrm{C}_N|. \tag{3.3.20}$$

is a witness. To do this we have to show that for all pure biseparable states $|\phi\rangle$ the bound

$$|\langle\phi|\mathrm{C}_N\rangle| \leq \frac{1}{\sqrt{2}} \tag{3.3.21}$$

holds. This is equivalent to showing that the Schmidt coefficients do not exceed $1/\sqrt{2}$ when making a Schmidt decomposition of $|\mathrm{C}_N\rangle$ with respect to an arbitrary bipartite splitting, since they bound the overlap with the biseparable states [8]. It is known that one can produce a singlet between an arbitrary pair of qubits from a cluster state by local operations and classical communication [99]. For a singlet both Schmidt coefficients are $1/\sqrt{2}$. Furthermore, it is known that the largest Schmidt coefficient cannot decrease [100] under these operations. This proves our claim. Knowing that $\widetilde{\mathcal{W}}_{\mathrm{C}_N}$ is a witness, one can show as in the GHZ case that $\mathcal{W}_{\mathrm{C}_N}$ and $\mathcal{W}'_{\mathrm{C}_N}$ are also witnesses. ■

In Fig. 3.1(c) the measurement settings are shown that are needed to measure $\mathcal{W}_{\mathrm{C}_N}$ and $\mathcal{W}'_{\mathrm{C}_N}$. We need only two measurement settings for these witnesses that detect genuine multipartite entanglement, for any particle number. This again makes the witness feasible for large systems.

We examine the robustness of the witnesses defined above to noise. First, we consider noisy GHZ sates of the type

$$\varrho_{\text{noisy GHZ state}} = (1 - p_{\text{noise}})|\mathrm{GHZ}_N\rangle\langle\mathrm{GHZ}_N| + p_{\text{noise}}\varrho_{\text{cm}}, \tag{3.3.22}$$

where the completely mixed state is defined in Eq. (2.1.8).

Let us see now how much white noise can be mixed to the GHZ state such that it is still detected as entangled by the witness $\mathcal{W}_{\mathrm{GHZ}_N}$, that is, $\langle\mathcal{W}_{\mathrm{GHZ}_N}\rangle < 0$. For that, we calculate the expectation value of $\mathcal{W}_{\mathrm{GHZ}_N}$ for the GHZ state and the completely mixed state, which we obtain as

$$\begin{aligned} \langle\mathcal{W}_{\mathrm{GHZ}_N}\rangle_{|\mathrm{GHZ}_N\rangle} &= -1, \\ \langle\mathcal{W}_{\mathrm{GHZ}_N}\rangle_{\varrho_{\text{cm}}} &= 3 - 2\left(\tfrac{1}{2} + \tfrac{1}{2^{N-1}}\right) = 2 - 2^{-(N-2)}. \end{aligned} \tag{3.3.23}$$

Similar expectation values for the witness $\mathcal{W}'_{\mathrm{GHZ}_N}$ are

$$\begin{aligned} \left\langle\mathcal{W}'_{\mathrm{GHZ}_N}\right\rangle_{|\mathrm{GHZ}_N\rangle} &= -1, \\ \left\langle\mathcal{W}'_{\mathrm{GHZ}_N}\right\rangle_{\varrho_{\text{cm}}} &= N - 1. \end{aligned} \tag{3.3.24}$$

Based on these and on Eq. (2.1.7), simple calculation shows that $\mathcal{W}_{\mathrm{GHZ}_N}$ detects the GHZ states as entangled if

$$p_{\text{noise}} < \frac{1}{3 - 2^{-(N-2)}}. \tag{3.3.25}$$

while $\mathcal{W}'_{\mathrm{GHZ}_N}$ detects such states if

$$p_{\text{noise}} < \frac{1}{N}. \tag{3.3.26}$$

The bounds in Eqs. (3.3.25) and (3.3.26) characterize the robustness of our entanglement witnesses to white noise. Note that the bound in Eq. (3.3.25) converges to $\frac{1}{3}$ for large N, while the bound in Eq. (3.3.26) converges to zero. Hence, $\mathcal{W}_{\mathrm{GHZ}_N}$ is much more robust to white noise than $\mathcal{W}'_{\mathrm{GHZ}_N}$.

Let us see now how much white noise can be mixed to the cluster state such that it is still detected as entangled by $\mathcal{W}_{\mathrm{C}_N}$ for an even N. For that, we define the noisy cluster

state as

$$\varrho_{\text{noisy cluster state}} = (1 - p_{\text{noise}})|\mathrm{C}_N\rangle\langle\mathrm{C}_N| + p_{\text{noise}}\varrho_{\text{cm}}. \tag{3.3.27}$$

We now calculate the expectation value of $\mathcal{W}_{\mathrm{C}_N}$ for the cluster state and the completely mixed state, which we obtain as

$$\begin{aligned} \langle\mathcal{W}_{\mathrm{C}_N}\rangle_{|\mathrm{C}_N\rangle} &= -1, \\ \langle\mathcal{W}_{\mathrm{C}_N}\rangle_{\varrho_{\text{cm}}} &= \begin{cases} 3 - 4\cdot 2^{-N/2}, & \text{for even } N, \\ 3 - 6\cdot 2^{-(N+1)/2}, & \text{for odd } N. \end{cases} \end{aligned} \tag{3.3.28}$$

Similar expectation values for the witness $\mathcal{W}'_{\mathrm{C}_N}$ are

$$\begin{aligned} \left\langle\mathcal{W}'_{\mathrm{C}_N}\right\rangle_{|\mathrm{C}_N\rangle} &= -1, \\ \left\langle\mathcal{W}'_{\mathrm{C}_N}\right\rangle_{\varrho_{\text{cm}}} &= N - 1. \end{aligned} \tag{3.3.29}$$

Based on these, simple calculation shows that $\mathcal{W}_{\mathrm{C}_N}$ detects the noisy cluster state as entangled if

$$p_{\text{noise}} < \begin{cases} \frac{1}{4-4\cdot 2^{-N/2}}, & \text{for even } N, \\ \frac{1}{4-6\cdot 2^{-(N+1)/2}}, & \text{for odd } N, \end{cases} \tag{3.3.30}$$

while $\mathcal{W}'_{\mathrm{C}_N}$ detects such states if

$$p_{\text{noise}} < \frac{1}{N}. \tag{3.3.31}$$

Note that the bound in Eq. (3.3.30) converges to $\frac{1}{4}$ for large N, while the bound in Eq. (3.3.31) converges to zero. Hence, $\mathcal{W}_{\mathrm{C}_N}$ is much more robust to white noise than $\mathcal{W}'_{\mathrm{C}_N}$.

We can compare the noise tolerance of the above witnesses to that of the projector-based witnesses $\widetilde{\mathcal{W}}_{\mathrm{C}_N}$ and $\widetilde{\mathcal{W}}_{\mathrm{GHZ}_N}$. Both of them detect a state as entangled if

$$p_{\text{noise}} < \frac{1}{2 - 2^{-(N-1)}}. \tag{3.3.32}$$

For large N, the bound in Eq. (3.3.32) converges to $\frac{1}{2}$ for large N.

In summary, our witnesses are easy to measure, while they are somewhat less robust to noise than the projector-based witnesses. We can see that $\mathcal{W}'_{\mathrm{GHZ}_N}$ and $\mathcal{W}'_{\mathrm{C}_N}$ have a simple structure, but their robustness to noise is decreasing rapidly with the particle number. On the other hand, for $\mathcal{W}_{\mathrm{GHZ}_N}$ and $\mathcal{W}_{\mathrm{C}_N}$ the robustness to noise converges to a constant for large N. These statements are summarized in Fig. 3.2. It has also been proved that $\mathcal{W}_{\mathrm{GHZ}_N}$ and $\mathcal{W}_{\mathrm{C}_N}$ are optimal from the point of view of noise tolerance among witnesses that need two measurement settings [41].

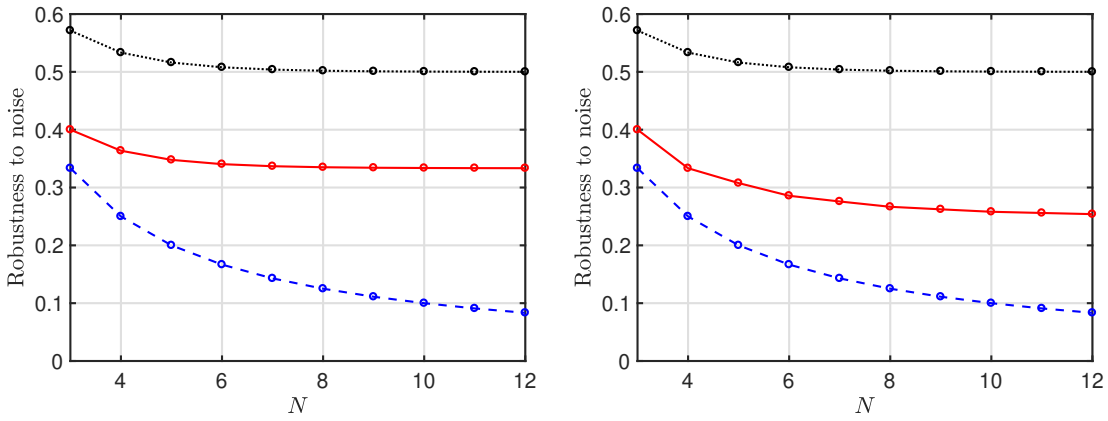

Figure 3.2: Robustness to noise for our entanglement witnesses as a function of the number of qubits. (a) Witnesses for GHZ states. (dotted) $\widetilde{\mathcal{W}}_{\mathrm{GHZ}_N}$, (solid) $\mathcal{W}_{\mathrm{GHZ}_N}$, and (dashed) $\mathcal{W}'_{\mathrm{GHZ}_N}$. (b) Witnesses for cluster states. (dotted) $\widetilde{\mathcal{W}}_{\mathrm{C}_N}$, (solid) $\mathcal{W}_{\mathrm{C}_N}$, and (dashed) $\mathcal{W}'_{\mathrm{C}_N}$.

3.4 Estimation of the fidelity

Let us say that in an experiment we intend to create a GHZ state. Beside knowing that the prepared state ϱ is entangled, we would also like to know how good its fidelity is. The fidelity could be measured by measuring the projector on the GHZ state

$$F_{\mathrm{GHZ}_N} := \mathrm{Tr}(|\mathrm{GHZ}_N\rangle\langle\mathrm{GHZ}_N|\rho). \tag{3.4.33}$$

However, we would encounter the same problem as with witnesses: The number of local settings needed for measuring the projector increases rapidly with the size.

Fortunately it is possible to obtain a lower bound on the fidelity from the expectation value of our witnesses. For example, for our GHZ witness defined in Observation 3.3.1 we have $\mathcal{W}_{\mathrm{GHZ}_N} - 2\widetilde{\mathcal{W}}_{\mathrm{GHZ}_N} \geq 0$, that is, $\mathcal{W}_{\mathrm{GHZ}_N} - 2\widetilde{\mathcal{W}}_{\mathrm{GHZ}_N}$ is a positive semidefinite matrix. Let us define now the operator [39]

$$\begin{aligned} P^{(\mathrm{est})}_{\mathrm{GHZ}_N} &= \frac{\mathbb{1}}{2} - \frac{1}{2}\mathcal{W}_{\mathrm{GHZ}_N} \\ &= \frac{S_1^{(\mathrm{GHZ}_N)} + \mathbb{1}}{2} + \prod_{k=2}^{N} \frac{S_k^{(\mathrm{GHZ}_N)} + \mathbb{1}}{2} - \mathbb{1}, \end{aligned} \tag{3.4.34}$$

where $\mathcal{W}^{(\mathrm{GHZ}_N)}$ is given in Eq. (3.3.14). We can see that

$$P^{(\mathrm{est})}_{\mathrm{GHZ}_N} \leq |\mathrm{GHZ}_N\rangle\langle\mathrm{GHZ}_N|. \tag{3.4.35}$$

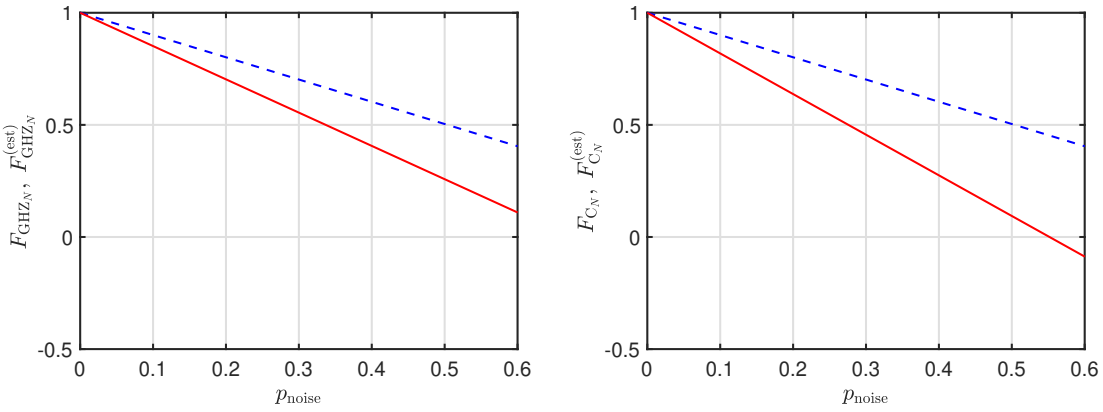

(a) (b)

Figure 3.3: Estimation of the fidelity with our witnesses for $N = 8$ qubits for a quantum state mixed with white noise as a function of the noise fraction. (a) (solid) estimation of the fidelity with $\mathcal{W}_{\text{GHZ}_N}$ and (dashed) the actual fidelity value. (b) (solid) estimation of the fidelity with $\mathcal{W}_{\text{C}_N}$ and (dashed) the actual fidelity value.

Hence, a lower bound on the fidelity, (3.4.33), can be obtained as

$$F^{(\text{est})}_{\text{GHZ}_N} = \text{Tr}(P^{(\text{est})}_{\text{GHZ}_N}\rho). \tag{3.4.36}$$

Note that for measuring $P^{(\text{est})}_{\text{GHZ}_N}$ only two local measurement settings are needed. Let us see how good this lower bound is for the noisy GHZ state (3.3.22). For this state, the fidelity and our lower bound on the fidelity, respectively, are

$$\begin{aligned} F_{\text{GHZ}_N} &= 1 - p_{\text{noise}}(1 - 2^{-N}), \\ F^{(\text{est})}_{\text{GHZ}_N} &= 1 - p_{\text{noise}}\left(\frac{3}{2} - 2^{-(N-1)}\right). \end{aligned} \tag{3.4.37}$$

The difference is $\Delta F \approx p_{\text{noise}}/2$ for large N.

Bounds can be obtained similarly for the fidelity with respect to the cluster state based on the operator [39]

$$\begin{aligned} P^{(\text{est})}_{\text{C}_N} &= \frac{\mathbb{1}}{2} - \frac{1}{2}\mathcal{W}_{\text{C}_N} \\ &= \prod_{\text{even k}} \frac{S^{(\text{C}_N)}_k + \mathbb{1}}{2} + \prod_{\text{odd k}} \frac{S^{(\text{C}_N)}_k + \mathbb{1}}{2} - \frac{5}{2}\mathbb{1}. \end{aligned} \tag{3.4.38}$$

Note that for measuring $P^{(\text{est})}_{\text{C}_N}$ only two local measurement settings are needed. We can

see that

$$P_{\mathrm{C}_N}^{(\mathrm{est})} \leq |\mathrm{C}_N\rangle\langle\mathrm{C}_N|. \tag{3.4.39}$$

Hence, a lower bound on the fidelity with respect to the cluster state

$$F_{\mathrm{C}_N} = \mathrm{Tr}(|\mathrm{C}_N\rangle\langle\mathrm{C}_N|\rho) \tag{3.4.40}$$

can be obtained as

$$F_{\mathrm{C}_N}^{(\mathrm{est})} = \mathrm{Tr}(P_{\mathrm{C}_N}^{(\mathrm{est})}\rho). \tag{3.4.41}$$

Let us consider now the noisy cluster state given in Eq. (3.3.27). For this state, the fidelity and our lower bound on the fidelity, respectively, are

$$\begin{aligned} F_{\mathrm{C}_N} &= 1 - p_{\mathrm{noise}}(1 - 2^{-N}), \\ F_{\mathrm{C}_N}^{(\mathrm{est})} &= \begin{cases} 1 - p_{\mathrm{noise}}(2 - 2 \cdot 2^{-N/2}), & \text{for even } N, \\ 1 - p_{\mathrm{noise}}(2 - 3 \cdot 2^{-(N+1)/2}), & \text{for odd } N. \end{cases} \end{aligned} \tag{3.4.42}$$

The difference is $\Delta F \approx p_{\mathrm{noise}}$ for large N. Our calculations for estimating the fidelity with the presented entanglement witnesses is summarized in Fig. 3.3.

3.5 Experimental applications of our results

Our findings have already been used in several experiments for detecting entanglement in cluster states created with photons through parametric down-conversion and selective detection. Such are the experiments, for example, by the Weinfurter group (Max Planck Institute for Quantum Optics, Munich, 2005) [40], by the De Martini group (University "La Sapienza", Rome, 2007) [101], and by the group of J.-W. Pan (Hefei, China, 2007) [102]. The results of the paper have also been used in Refs. [103] and [104]. The ideas of the witnesses have been generalized and used in further experiments for graph states of qubits (e.g., Ref. [105]). The ideas of cluster state witnesses have been used even for cluster states of qudits with a dimension higher than two in Ref. [106, 107]. It has been shown that schemes needing few measurements can even be used to quantify entanglement with two mutually unbiased bases [108, 109].

Chapter 4

Entanglement detection close to Dicke states

In this Chapter, entanglement detection close to Dicke states is discussed based on Ref. [42]. We will also show how to measure the entanglement conditions efficiently [46]. We also show examples of entanglement conditions that need only collective measurements [42].

4.1 Background

4.1.1 Definition of the Dicke state

In his seminal paper Ref. [16], Dicke considered the spontaneous emission of light by a cloud of two-state atoms, which are coupled to the electromagnetic field as electric dipoles. He found that when the cloud acts as a coherent quantum system, the maximal light intensity is roughly proportional to the square of the number of atoms. This Dicke called superradiance. The highly correlated Dicke states, defined to describe the system above, are the simultaneous eigenstates of the squared collective angular momentum, J^2 and its z-component, J_z.

In a typical many-qubit experiment, in which the qubits cannot be individually accessed, both the initial state and the dynamics are symmetric under the permutation of qubits. Thus, here we will consider only symmetric Dicke states. These are also the states with maximal J^2. An N-qubit symmetric Dicke state with m excitations $|m, N\rangle$ is defined as in Eq. (1.1.5). $|1, N\rangle$ is the well known N-qubit W state.

4.1.2 Collective measurements

In large ensembles, only collective quantities can be measured, which are the sum of single-particle quantities. For qubits, the collective quantities most often referred to are

$$J_l = \frac{1}{2}\sum_{n=1}^{N}\sigma_l^{(n)}, \tag{4.1.1}$$

where $l = x, y, z$ and $\sigma_l^{(n)}$ is a Pauli spin matrix corresponding to the n^{th} particle. Any other collective quantity can be given as a linear combintation of the form

$$J_{\vec{n}} = \sum_l n_l J_l, \tag{4.1.2}$$

where for the vector $\vec{n}$ the condition $|\vec{n}| = 1$ holds.

In a usual experiment, one can measure the expectation values of J_l. Based on Eq. (4.1.2) we can see that if we know $\langle J_x\rangle, \langle J_y\rangle$, and $\langle J_z\rangle$, then we can calculate $\langle J_{\vec{n}}\rangle$ for any $\vec{n}$. One can typically also measure the variances of the angular momentum components

$$(\Delta J_l)^2 = \langle J_l^2\rangle - \langle J_l\rangle^2. \tag{4.1.3}$$

In principle, one can try to measure higher moments of the angular momentum components. However, measuring higher order moments needs longer experiments in order to obtain a better statistics of the measured data.

4.2 Detecting entanglement close to Dicke states

We will first discuss some of the advantages of using Dicke states [16] to study the non-classical phenomena of quantum mechanics. We will present a criterion for detecting entanglement around symmetric Dicke states, which is described in Ref. [42].

Observation 4.2.1 *For biseparable quantum states ρ*

$$\mathrm{Tr}(\rho|N/2,N\rangle\langle N/2,N|) \leq \frac{1}{2}\frac{N}{N-1} =: C_{N/2,N}. \tag{4.2.4}$$

Any state that violates Eq. (4.2.4) *is genuine multipartite entangled. This condition detects entanglement close to an N-qubit symmetric Dicke state with $N/2$ excitations. Here N is assumed to be even.*

Proof. The Schmidt decomposition of $|m, N\rangle$ according to the bipartition $(1, 2, ..., N_1|N_1+1, N_1+2, ..., N)$ is [15]

$$|m, N\rangle = \sum_k \lambda_k |k, N_1\rangle \otimes |m-k, N-N_1\rangle, \tag{4.2.5}$$

where the Schmidt coefficients are

$$\lambda_k = \left(\begin{array}{c} N \\ m \end{array} \right)^{-\frac{1}{2}} \left(\begin{array}{c} N_1 \\ k \end{array} \right)^{\frac{1}{2}} \left(\begin{array}{c} N-N_1 \\ m-k \end{array} \right)^{\frac{1}{2}}. \tag{4.2.6}$$

We do not have to consider other bipartitions due to the permutational symmetry of our Dicke states. For $|N/2, N\rangle$ we have $m = N/2$. Now we use that

$$\left(\begin{array}{c} N_1 \\ k \end{array} \right) \left(\begin{array}{c} N-N_1 \\ \frac{N}{2}-k \end{array} \right) \leq \left(\begin{array}{c} 2 \\ 1 \end{array} \right) \left(\begin{array}{c} N-2 \\ \frac{N}{2}-1 \end{array} \right). \tag{4.2.7}$$

The proof of Eq. (4.2.7) can be found in the Ref. [42]. Thus we find that the maximal Schmidt coefficient can be obtained for $N_1 = 2$ and $k = 1$. For $N_1 = 2$ we obtain $\lambda_1^2 = N/(N-1)/2$. ■

Equation (4.2.4) indicates that for large N, it is sufficient to have a fidelity larger than $1/2$ to detect genuine multipartite entanglement. This is the minimal value one can obtain when detecting genuine multipartite entanglement with fidelity based entanglement witnesses, which makes the Dicke state especially suitable for experimental detection of multipartite entanglement. So far, other states known to have a fidelity bound $1/2$ are the GHZ states, cluster states and the generalizations of cluster states called graph states (see Sec. 3.1.1 and 3.1.2).

4.3 Efficient measurement of the witness

After determining the entanglement condition Eq. (4.2.4), we need to find a way to measure the fidelity with respect to the Dicke state efficiently in order to evaluate the condition. This is possible by decomposing the projector to Dicke states into the linear combination of multi-qubit correlations, as explained in Sec. 3.1.3.

Next we present explicitly two decompositions that have been used in experiments, described in Ref. [46]. It seems that there are no other decompositions that need fewer local measurement settings.

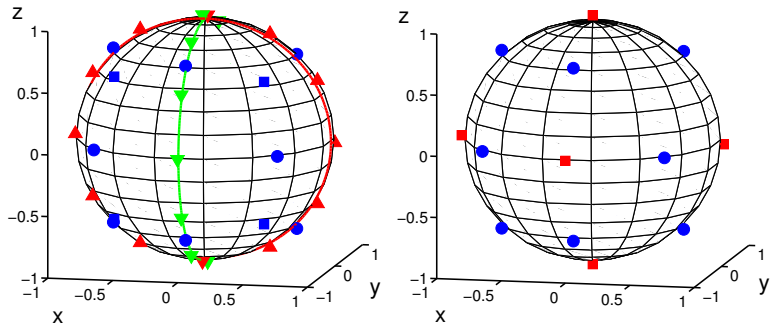

Figure 4.1: (a) The measurement settings needed to measure the projector to the six-qubit symmetric Dicke state with three excitations based on the decomposition Eq. (4.3.8). A point at (x, y, z) indicates measuring $x\sigma_x + y\sigma_y + z\sigma_z$ on all qubits. ($\triangle$) Settings for $\text{Mermin}_{x,z}$, ($\bigtriangledown$) settings for $\text{Mermin}_{y,z}$, ($\square$) $\sigma_x \pm \sigma_y \pm \sigma_z$, and ($\bigcirc$) rest of the settings. (b) Settings for the four-qubit Dicke state with two excitations based on Eq. (4.3.11). ($\square$) $\pm\sigma_x, \pm\sigma_y, \pm\sigma_z$, and ($\bigcirc$) $\sigma_x \pm \sigma_y, \sigma_x \pm \sigma_z$, and $\sigma_y \pm \sigma_z$. Figure taken from Ref. [46].

Observation 4.3.1 *The projector to the six-qubit Dicke state can be decomposed as*

$$\begin{aligned} 64|3,6\rangle\langle 3,6| \;=\; & -0.6[\mathbb{1}] + 0.3[x \pm \mathbb{1}] - 0.6[x] + 0.3[y \pm \mathbb{1}] - 0.6[y] \\ & +0.2[z \pm \mathbb{1}] - 0.2[z] + 0.2\,\text{Mermin}_{0,z} \\ & +0.05[x \pm y \pm \mathbb{1}] - 0.05[x \pm z \pm \mathbb{1}] - 0.05[y \pm z \pm \mathbb{1}] \\ & -0.05[x \pm y \pm z] + 0.2[x \pm z] + 0.2[y \pm z] + 0.1[x \pm y] \\ & +0.6\,\text{Mermin}_{x,z} + 0.6\,\text{Mermin}_{y,z}. \end{aligned} \tag{4.3.8}$$

Here we use the notation $[x + y] = (\sigma_x + \sigma_y)^{\otimes 6}$, $[x + y + \mathbb{1}] = (\sigma_x + \sigma_y + \mathbb{1})^{\otimes 6}$, *etc. The* $\pm$ *sign denotes a summation over the two signs, i.e.,* $[x \pm y] = [x + y] + [x - y]$.

The Mermin operators are defined as

$$\text{Mermin}_{a,b} := \sum_{k \text{ even}} (-1)^{k/2} \sum_m \mathcal{P}_m(\otimes_{i=1}^{k} \sigma_a \otimes_{i=k+1}^{N} \sigma_b), \tag{4.3.9}$$

where $\sigma_0 = \mathbb{1}$, and the summation over m is just the summation over all distinct permutations of the qubits. That is, it is the sum of terms with even number of σ_a's and σ_b's, with the sign of the terms depending on the number of σ_a's. The expectation value of the operators $\text{Mermin}_{a,b}$ can be measured based on the decomposition [97]

$$\text{Mermin}_{a,b} = \frac{2^{N-1}}{N} \sum_{k=1}^{N} (-1)^k \left[\cos\left(\tfrac{k\pi}{N}\right) \sigma_a + \sin\left(\tfrac{k\pi}{N}\right) \sigma_b \right]^{\otimes N}. \tag{4.3.10}$$

Hence, $\text{Mermin}_{x,z}$ and $\text{Mermin}_{y,z}$ can be measured with six settings. $\text{Mermin}_{0,z}$, on the other hand, needs only the measurement of the $\{\sigma_z, \sigma_z, \sigma_z, \sigma_z, \sigma_z, \sigma_z\}$ setting.

Knowing that $[A]$, $[A+\mathbb{1}]$ and $[A-\mathbb{1}]$ can be measured with a single setting $\{A, A, A, ..., A\}$, we find that 21 measurement settings are needed to measure $|3,6\rangle\langle 3,6| : x, y, z, x \pm y, x \pm z, y \pm z, \sqrt{3}x \pm z, \sqrt{3}z \pm x, \sqrt{3}y \pm z, \sqrt{3}z \pm y$, and $x \pm y \pm z$. Here, x means measuring σ_x on all qubits, $x + y$ means measuring $\sigma_x + \sigma_y$ on all qubits, etc. The settings are also shown in Fig. 4.1(a).[5]

Observation 4.3.2 *The projector to the four-qubit Dicke state can be decomposed into the linear combination of correlation terms as*

$$\begin{aligned} 16|2,4\rangle\langle 2,4| &= \tfrac{2}{3}([x] + [x \pm \mathbb{1}] + [y] + [y \pm \mathbb{1}]) \\ &+ \tfrac{1}{3}(8[z] - [z \pm \mathbb{1}] - [x \pm z] - [y \pm z]) + \tfrac{1}{6}[x \pm y]. \end{aligned} \tag{4.3.11}$$

The 9 measurement settings are $x, y, z, x \pm y, x \pm z$, and $y \pm z$, shown also in Fig. 4.1(b).

Observation 4.3.1 and Observation 4.3.2 can be verified by simple direct calculation.

4.4 Witnesses with collective operators

Now let us look for criteria for four-qubit system based on collective measurements. Collective measurements are generally much simpler to carry out than fidelity measurements. Remarkably, we can detect genuine multipartite entanglement with these criteria. We will now describe results presented in Ref. [42].

In order to proceed, we will need the followings.

Observation 4.4.1 *For a two-qubit quantum state*

$$\langle M_1\rangle^2 + \langle M_2\rangle^2 + \langle M_3\rangle^2 \leq \frac{16}{3} \tag{4.4.12}$$

holds, where the M_k operators are defined as

$$\begin{aligned} M_1 &:= \sigma_x^{(1)}\sigma_x^{(2)} + \sigma_y^{(1)}\sigma_y^{(2)}, \\ M_2 &:= \sigma_x^{(1)} + \sigma_x^{(2)}, \\ M_3 &:= \sigma_y^{(1)} + \sigma_y^{(2)}. \end{aligned} \tag{4.4.13}$$

[5]Note that Ref. [45] presents another decomposition that needs also 21 settings.

Proof. The proof is rather technical. Let us consider the vector

$$v := (\langle M_1\rangle, \langle M_2\rangle, \langle M_3\rangle). \tag{4.4.14}$$

We want to find an upper bound on $|v|$. We can easily write

$$|v|^2 = \langle M_1\rangle^2 + \langle M_2\rangle^2 + \langle M_3\rangle^2. \tag{4.4.15}$$

We have to look for the maximum of this expression for quantum states. The problem is that it is nonlinear in operator expectation values. Because of that we will employ the following equality

$$|v| \;=\; \max_{|n|=1} vn, \tag{4.4.16}$$

where n is a real unit vector. The meaning of Eq. (4.4.16) is clear: The length of a vector equals to the maximum of its scalar product with a unit vector. Now the right hand side of Eq. (4.4.16) can be rewritten as

$$|v| = \max_{|n|=1} \langle n_1 M_1 + n_2 M_2 + n_3 M_3\rangle. \tag{4.4.17}$$

The advantage of this expression is that it is linear in operator expectation values. The disadvantage is that we have to maximize over n. Now we will find an upper bound on the right hand side of Eq. (4.4.17). We will use the fact that for an operator A the expectation value is bounded as $\langle A\rangle \leq \Lambda_{\max}(A)$. Here $\Lambda_{\max}(A)$ denotes the largest eigenvalue of operator A. Thus

$$|v| \leq \max_{|n|=1} \Lambda_{\max}(n_1 M_1 + n_2 M_2 + n_3 M_3). \tag{4.4.18}$$

The eigenvalues of $(n_1 M_1 + n_2 M_2 + n_3 M_3)$ can easily be obtained analytically as the function of n_k. They are

$$\begin{aligned} \lambda_1 &= 0, \\ \lambda_2 &= -2n_1, \\ \lambda_{3/4} &= n_1 \pm \sqrt{n_1^2 + 4n_2^2 + 4n_3^2}. \end{aligned} \tag{4.4.19}$$

Assuming $|n| = 1$, the eigenvalues given in Eq. (4.4.19) are bounded from above by $\sqrt{16/3}$. Hence, based on Eq. (4.4.18) we obtain $|v|^2 \leq 16/3$ and Eq. (4.4.12) follows. ■

Observation 4.4.2 *For a four-qubit biseparable state*

$$\left\langle J_x^2 \right\rangle + \left\langle J_y^2 \right\rangle \leq \frac{7}{2} + \sqrt{3} \approx 5.23 \tag{4.4.20}$$

holds. For the left-hand side of Eq. (4.4.20) the maximum is 6 *and it is obtained uniquely for the* $|2,4\rangle$ *state.*

Proof. First we present the proof for biseparable pure states with a (12|34) bipartition. For these $\langle J_x^2 \rangle + \left\langle J_y^2 \right\rangle = 2 + v_1 v_2/2$, where

$$\begin{aligned} v_1 &:= (x_1x_2 + y_1y_2,\ x_1 + x_2,\ y_1 + y_2,\ 1), \\ v_2 &:= (1,\ x_3 + x_4, y_3 + y_4,\ x_3x_4 + y_3y_4). \end{aligned} \tag{4.4.21}$$

Here we used the notation $x_1x_2 = \langle \sigma_x^{(1)} \sigma_x^{(2)} \rangle$. Now, note that the elements of v_1 are just the functions of the state of the first two qubits. Three of the elements are the same as the elements v is defined in Eq. (4.4.14), while the fourth element is 1. Hence,

$$|v_1|^2 = |v|^2 + 1 \tag{4.4.22}$$

follows. Then, using Observation 4.4.1, one obtains

$$|v_1|^2 \leq 19/3. \tag{4.4.23}$$

Note also that the elements of v_2 are only the functions of the state of the third and fourth qubit. An argument similar to the previous one leads to

$$|v_2|^2 \leq 19/3. \tag{4.4.24}$$

Hence a bound can be obtained using the Cauchy-Schwarz inequality as

$$\left\langle J_x^2 \right\rangle + \left\langle J_y^2 \right\rangle \leq 2 + |v_1||v_2|/2 \leq 31/6 \approx 5.17. \tag{4.4.25}$$

Note that the upper bound we have just obtained for $\langle J_x^2 \rangle + \left\langle J_y^2 \right\rangle$ is smaller than the bound in Eq. (4.4.20) thus biseparable pure states with a (12|34) bipartition fulfill Eq. (4.4.20).

Now let us take biseparable states with a bipartition (1|234). We will follow similar steps as in the proof of Observation 4.4.1. Let us define the matrices

$$\begin{aligned} Q_a &:= \sigma_a^{(2)} + \sigma_a^{(3)} + \sigma_a^{(4)}; \quad a = x, y, \\ R &:= \sum_{l=x,y} \sigma_l^{(2)}\sigma_l^{(3)} + \sigma_l^{(2)}\sigma_l^{(4)} + \sigma_l^{(3)}\sigma_l^{(4)}. \end{aligned} \tag{4.4.26}$$

Using these matrices we can write

$$\begin{aligned}\left\langle J_x^2\right\rangle + \left\langle J_y^2\right\rangle &= 2 + \frac{1}{2}(x_1\langle Q_x\rangle + y_1\langle Q_y\rangle + \langle R\rangle) \\ &\leq 2 + \frac{1}{2}\max_{x_1^2+y_1^2\leq 1}\Lambda_{\max}(x_1Q_x + y_1Q_y + R).\end{aligned} \tag{4.4.27}$$

Now for finding an upper bound we need the eigenvalues of $(x_1Q_x + y_1Q_y + R)$. These are

$$\begin{aligned}\lambda_{1,2} &= -2 + X, \\ \lambda_{3,4} &= -2 - X, \\ \lambda_{5,6} &= 2 + X \pm 2\sqrt{1 + X + X^2}, \\ \lambda_{7,8} &= 2 - X \pm 2\sqrt{1 - X + X^2},\end{aligned} \tag{4.4.28}$$

where $X = \sqrt{x_1^2 + y_1^2}$. Assuming $|X| \leq 1$, the upper bound of the eigenvalues in Eq. (4.4.28) is $3 + 2\sqrt{3}$. Thus based on Eq. (4.4.27) we obtain Eq. (4.4.20) for biseparable states with a $(1|234)$ bipartition.

Since the measured operators are symmetric under the permutation of qubits, this also proves that Eq. (4.4.20) holds for any biseparable pure state. Due to the convexity of biseparable states, it also holds for mixed biseparable states. ■

4.5 Related experimental and theoretical works

In an experiment aiming at creating a four-qubit Dicke state described in Ref. [43], Observations 4.2.1, and 4.3.2 have been used. In an experiment aiming at creating a six-qubit Dicke state described in Ref. [44], Observations 4.2.1, 4.3.1, and 4.4.2 have been used. In another experiment aiming at creating a six-qubit Dicke state described in Ref. [45], Observation 4.4.2 has been applied, while a decomposition slightly different from the one given in Observation 4.3.1 has been used. References [47, 72] describe entanglement conditions that detect entanglement close to Dicke states, see also Sec. 7.3. References [31, 110] present criteria for multipartite entanglement for states close to Dicke states, which work even for larger systems of spin-1/2 particles. There have been criteria even for ensembles of particles with a higher spin [111].

Chapter 5

Entanglement and permutational symmetry

In this Chapter, the relation between entanglement and permutational symmetry is discussed. We will present symmetric states that are not detected by the criterion based on the positivity of the partial transpose based on Ref. [70].

5.1 Background

5.1.1 Criterion based on the positivity of the partial transpose (PPT)

Definition 5.1.1 *For a density matrix of a bipartite system*

$$\varrho = \sum_{klmn} c_{klmn} |k\rangle\langle l| \otimes |m\rangle\langle n| \tag{5.1.1}$$

the partial transposition according to the first subsystem is defined as

$$\varrho^{T1} = \sum_{klmn} c_{klmn} |l\rangle\langle k| \otimes |m\rangle\langle n|. \tag{5.1.2}$$

The entanglement condition based on the positivity of partial transpose (PPT condition) claims that for every separable state

$$\varrho^{T1} \geq 0. \tag{5.1.3}$$

If a state violates Eq. (5.1.3) *then it is entangled. It is usual to call quantum states satisfying Eq.* (5.1.3) *PPT, while states not satisfying Eq.* (5.1.3) *non-PPT.*

It has been shown that PPT entangled states do not exist in 2×2 and 2×3 systems. For such systems all entangled states violate Eq. (5.1.3). However, for larger systems, there are entangled quantum states that have a positive partial transpose [112, 113]. Such states are called bound entangled states, since their entanglement cannot be distilled with local operations and classical communication.

In a multipartite system, we can talk about partial transposition with respect to a bipartition of the parties. For example, the (1|23) bipartition denotes a bipartition in which particle 1 is in one group, particles 2 and 3 are in the other group. The most interesting bound entangled states have positive semidefinite partial transpose with respect to all bipartitions, while they are not separable. There are also other bound entangled states that have a positive semidefinite partial transpose with respect to some bipartitions, while have a non-positive semidefinite partial transpose with respect to some other bipartitions [114]. Note that separable states given in Eq. (2.1.2) all have a positive semidefinite partial transpose with respect to all bipartitions.

5.1.2 Computable cross norm/realignment criterion (CCNR)

Definition 5.1.2 *Let us consider the matrix Schmidt decomposition of a density matrix*

$$\varrho = \sum_k \lambda_k A_k \otimes B_k, \tag{5.1.4}$$

where $\lambda_k > 0$, *and* A_k *and* B_k *are Hermitian matrices. Here we assume that* $\mathrm{Tr}(A_k A_l) = \delta_{kl}$ *and* $\mathrm{Tr}(B_k B_l) = \delta_{kl}$, *where* δ_{kl} *is the well known Kronecker delta. According to the computable cross norm/realignment criterion (CCNR), for every separable state*

$$\sum_k \lambda_k \leq 1 \tag{5.1.5}$$

holds. If a state violates Eq. (5.1.5) *then it is entangled [115, 116].*

5.2 Entanglement conditions for symmetric states

Before presenting our entanglement conditions, we start with some important definitions. For two d-dimensional quantum systems, there are two types of permutational symmetry.

(i) We call a state *permutationally invariant* if ϱ is invariant under exchanging the particles. This can be formalized by using the flip operator

$$F = \sum_{ij} |ij\rangle\langle ji| \tag{5.2.6}$$

as

$$F\varrho F = \varrho. \tag{5.2.7}$$

(The flip operator is also called swap operator in the literature.) The reduced state of two randomly chosen particles of a larger ensemble has this symmetry. The flip operartor can also be expressed as

$$F = \sum_k M_k \otimes M_k, \tag{5.2.8}$$

where M_k is a full basis of Hermitian matrices such that $\mathrm{Tr}(M_k M_l) = \delta_{kl}$.

(ii) We call a state *symmetric* (or having a bosonic symmetry) if it acts on the symmetric subspace only. This space is spanned by the basis vectors $|\phi^+_{kl}\rangle := (|k\rangle|l\rangle + |l\rangle|k\rangle)/\sqrt{2}$ for $k \neq l$ and $|\psi_k\rangle := |k\rangle|k\rangle$. This is the state space of two d-state bosons.

The projector P_s onto this space can be written as

$$P_s = \frac{1}{2}(\mathbb{1} + F). \tag{5.2.9}$$

This implies that for symmetric states by definition

$$P_s\varrho P_s = P_s\varrho = \varrho P_s = \varrho \tag{5.2.10}$$

and $\varrho F = F\varrho = \varrho$. Based on these, for symmetric states, we have

$$\langle P_s\rangle = 1, \tag{5.2.11a}$$
$$\langle F\rangle = 1. \tag{5.2.11b}$$

Clearly, a symmetric state is also permutationally invariant.

Next, we write down the Schmidt decomposition of a permutationally invariant state of a $d \times d$ system. For that, let us consider a full basis of Hermitian matrices for d state system denoted by M_k which fulfill

$$\mathrm{Tr}(M_k M_l) = \delta_{kl}. \tag{5.2.12}$$

We define the correlation matrix of the bipartite system as

$$\eta_{kl} = \langle M_k \otimes M_l \rangle, \tag{5.2.13}$$

where the quantum state can be written with the correlation matrix as

$$\varrho = \sum_{kl} \eta_{kl} M_k \otimes M_l. \tag{5.2.14}$$

Since our state is symmetric, η is a symmetric matrix with real elements. It can be diagonalized with an orthogonal transformation O as

$$D = O^T \eta O, \tag{5.2.15}$$

where D denotes a diagonal matrix. Let us use the $\Lambda_k = D_{kk}$ notation.The same orthogonal matrix can be used to transform the operators into a new basis as

$$M'_k = \sum_l O_{kl} M_l. \tag{5.2.16}$$

With these, one can write the quantum state as

$$\varrho = \sum_k \Lambda_k M'_k \otimes M'_k. \tag{5.2.17}$$

Equation (5.2.17) is not yet a Schmidt decomposition since Λ_k can also be negative. A Schmidt decomposition of the form Eq. (5.1.4) can be obtained as

$$\begin{aligned} \lambda_k &= |\Lambda_k|, \\ A_k &= \mathrm{sign}(\Lambda_k) M'_k, \\ B_k &= M'_k, \end{aligned} \tag{5.2.18}$$

where $\mathrm{sign}(x)$ is the usual sign function.

Based on these, we can now formulate the following theorem.

Observation 5.2.1 *A bipartite quantum state in the symmetric subspace has a positive partial transpose if and only if for every Hermitian operator A the relation $\langle A \otimes A \rangle \geq 0$ holds.*

Proof. First we have to recognize that for a symmetric state, the PPT and the CCNR criteria are equivalent to each other. For that, let us write down the CCNR criterion as

[117]

$$||(\varrho F)^{\mathrm{T}_1}|| \leq 1, \tag{5.2.19}$$

where $||X|| = \mathrm{Tr}(\sqrt{XX^\dagger})$. Then, for symmetric states $\varrho F = \varrho$. Hence, the statement follows.

Due to Eqs. (5.2.8), (5.2.11b), and (5.2.17), for symmetric states for the sum of the coefficients

$$\sum_k \Lambda_k = 1 \tag{5.2.20}$$

holds. If the CCNR condition given in Eq. (5.1.5) is fulfilled then all $\Lambda_k > 0$, and hence

$$\langle A \otimes A \rangle = \sum_k \Lambda_k \mathrm{Tr}(AA_k)^2 \geq 0 \tag{5.2.21}$$

holds for all A operators. On the other hand, if the CCNR condition is violated then there is a k for which we have $\Lambda_k < 0$. Then, taking $A = A_k$ we obtain

$$\langle A \otimes A \rangle = \sum_k \Lambda_k \mathrm{Tr}(AA_k)^2 = \Lambda_k < 0. \tag{5.2.22}$$

■

Observation 5.2.1 shows that if we find an operator A such that $\langle A \otimes A \rangle < 0$, then the state violates the PPT criterion (5.1.3) and hence it is entangled. Hence, entanglement of symmetric states can be detected with a single correlation measurement.

Next, we show a simple method to generate symmetric entangled states that do not violate the PPT criterion, that is, they are bound entangled states. Here, multiparticle symmetric states mean states in the bosonic subspace.

Observation 5.2.2 *A multiqubit symmetric state is either separable with respect to all bipartitions, or entangled with respect to all bipartitions [70]. This fact has been used in the proofs of [118].*

We now use Observation 5.2.2 to generate bound entangled states. Let us consider a symmetric $2(d-1)$-qubit quantum state, where d is some positive integer. If it is non-PPT with respect to some bipartition, then it is entangled with respect that bipartition. Due to Observation 5.2.2, it is even entangled with respect to all other bipartitions. Let us now consider a state that is PPT with respect to the $(d-1):(d-1)$ bipartition[6], while it is non-PPT with respect to some other bipartition. Then, the state must be entangled

[6]That is, there are $(d-1)$ qubits in one of the subsystems and $(d-1)$ qubits are in the other subsystem.

even with respect to the $(d-1):(d-1)$ bipartition. Hence, we have a bound entangled state of a bipartite system, where both systems have $(d-1)$ qubits.

We have now to remember, that we do not have a general $2(d-1)$-qubit quantum state, but a symmetric one. For such states, even all the different reduced states live in the symmetric subspace. Hence, the two parties of $(d-1)$ qubits mentioned can be mapped to two d-dimensional systems, because we have in general that a symmetric state of an N-qubit system can be mapped to an $(N+1)$-dimensional state.

Observation 5.2.3 *An efficient numerical method obtaining a symmetric PPT entangled state of a $d\times d$ system is as follows. We obtain a random symmetric $2(d-1)$-qubit quantum state such that it is PPT with respect to the $(d-1)$ qubits vs. $(d-1)$ qubits bipartition, while it is not PPT with respect to some other bipartition. Such a state can straightforwardly be mapped to a $d\times d$ symmetric PPT entangled state.*

In more details, one should not try to obtain directly the random state with the properties described in Observation 5.2.3. One should just generate a random symmetric state ϱ_0 as an initial guess. We can require that ϱ_0 is PPT with respect to the $(d-1):(d-1)$ bipartition. If it is non-PPT with respect to one of the bipartitions, we found the state we were looking for. If this is not the case then we generate another random symmetric state σ and use it to step a little starting from ϱ_0 using

$$\varrho' = (1-p)\varrho_0 + p\sigma \tag{5.2.23}$$

with some small p, like $p=0.05$ or $p=0.1$. We accept ϱ' as a new guess if it is still PPT with respect to the $(d-1):(d-1)$ bipartition, and decreases the minimal eigenvalues of all partial tranposes

$$\min_b \lambda_{\min}(\varrho^{Tb}), \tag{5.2.24}$$

where $\lambda_{\min}(A)$ is the minimal eigenvalue of A. When we reach a state for which Eq. (5.2.24) is negative, we arrived at our goal. Note that we have to take care of the fact that symmetric states, and their partial transpose are not full rank and they have several zero eigenvalues. Numerical problems can arise since instead of zero we can obtain a negative number close to zero using various routines calculating the eigenvalues.

Let us see a concrete example for $N=4$. We obtained from numerics the following 4-qubit symmetric state [70]

$$\varrho_{\mathrm{BE4}} = \mathrm{diag}(0.22, 0.176, 0.167, 0.254, 0.183) - 0.059R, \tag{5.2.25}$$

where $R := |3\rangle\langle 0| + |0\rangle\langle 3|$. The basis states are $|0\rangle := |0000\rangle$, $|1\rangle := \mathrm{sym}(|1000\rangle)$, $|2\rangle :=$

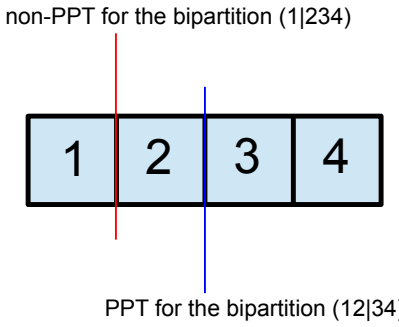

Figure 5.1: Schematic representation of a four-qubit quantum state that is PPT with respect to the (12|34) bipartition, but non-PPT with respect to the (1|234) bipartition.

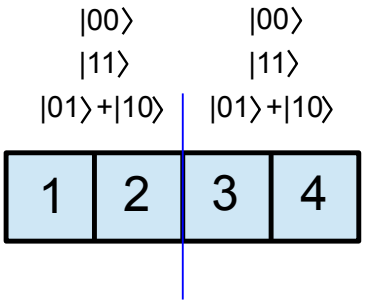

Figure 5.2: Symmetric four-qubit states can be mapped to 3×3 systems, since the state of qubits 1 and 2 can be given in a three-dimensional space. Moreover, similarly the state of qubits 3 and 4 can be given in a three-dimensional space.

$\mathrm{sym}(|1100\rangle), ...$, where $\mathrm{sym}(A)$ denotes an equal superposition of all permutations of A, with an appropriate normalization. The state ϱ_{BE4} is PPT with respect to the 2 qubits vs. 2 qubits bipartition, while it is non-PPT for the 1 qubit vs. 3 qubits bipartition, see Fig. 5.1. Based on Observation 5.2.2, it is bound entangled for the 2 qubits vs. 2 qubits bipartition. The basis states of a symmetric two-qubit system are $|00\rangle, |11\rangle$, and $(|01\rangle + |10\rangle)/\sqrt{2}$, see Fig. 5.2. Hence, we can transform Eq. (5.2.25) into a 3×3 PPT entangled state.

5.3 Related theoretical works

Later, bound entanglement in symmetric systems has been examined, for example, in Refs. [119, 120].

Chapter 6

Permutationally invariant tomography

In this chapter, we discuss an efficient tomographic method for permutationally invariant systems described in Ref. [71]. Its advantage is that the number of measurements needed scales quadratically with the number of qubits. This makes it possible to carry out tomography of large systems.

6.1 Background

6.1.1 Full state tomography

Full state tomography [121] is a procedure that is used to obtain the density matrix of a quantum state, i.e., all the information one can know about a quantum state. The number of degrees of freedom (i.e., the number of independent real parameters) can easily be counted as follows. An N-qubit density matrix can be written as

$$\varrho = \sum_{k_1,k_2,\ldots,k_N} c_{k_1,k_2,\ldots,k_N} \sigma_{k_1} \sigma_{k_2} \ldots \sigma_{k_N}, \tag{6.1.1}$$

where $k_i = 0, 1, 2, 3$. We use the usual notation where σ_0 is the identity, while σ_1,σ_2, and σ_3 are the Pauli spin matrices. In Eq. (6.1.1), ϱ is written as a linear combination of operators that are pairwise orthogonal. The coefficients $c_{k_1,k_2,\ldots,k_N}$ are real numbers defined as expectation values

$$c_{k_1,k_2,\ldots,k_N} = \frac{1}{2^N} \langle \sigma_{k_1} \sigma_{k_2} \ldots \sigma_{k_N} \rangle. \tag{6.1.2}$$

There are 4^N such coefficients. The density matrix has a unit trace, which fixes one of the coefficients as

$$c_{0,0,\ldots,0} = \frac{1}{2^N}. \tag{6.1.3}$$

Hence, we see that a quantum state of N qubits has

$$\mathrm{DOF}_N^{(\mathrm{FST})} = 4^N - 1 \tag{6.1.4}$$

real degrees of freedom, where "FST" refers to full state tomography.

Note that Eq. (6.1.4) agrees with the well-known result that the number of independent generators for the SU(d) group is $d^2 - 1$, where the H_k generators are pairwise orthogonal traceless Hermitian matrices. This also means that the number of linearly independent $d \times d$ traceless Hermitian matrices is $d^2 - 1$. With $d = 2^N$ we obtain Eq. (6.1.4). We presented a different derivation, since it can immediately be used to count real degrees of freedom in other related problems.

Following one of the most usual methods called "overcomplete tomography", we measure a Pauli spin matrix at each qubit and then calculate averages of the correlation terms to obtain the $c_{k_1,k_2,\ldots,k_N}$ coefficients in Eq. (6.1.1) [122]. For instance, for two qubits, we need the following 15 correlations

$$\begin{array}{lll}
\langle \mathbb{1}^{(1)} X^{(2)} \rangle, & \langle \mathbb{1}^{(1)} Y^{(2)} \rangle, & \langle \mathbb{1}^{(1)} Z^{(2)} \rangle, \\
\langle X^{(1)} \mathbb{1}^{(2)} \rangle, & \langle Y^{(1)} \mathbb{1}^{(2)} \rangle, & \langle Z^{(1)} \mathbb{1}^{(2)} \rangle, \\
\langle X^{(1)} X^{(2)} \rangle, & \langle X^{(1)} Y^{(2)} \rangle, & \langle X^{(1)} Z^{(2)} \rangle, \\
\langle Y^{(1)} X^{(2)} \rangle, & \langle Y^{(1)} Y^{(2)} \rangle, & \langle Y^{(1)} Z^{(2)} \rangle, \\
\langle Z^{(1)} X^{(2)} \rangle, & \langle Z^{(1)} Y^{(2)} \rangle, & \langle Z^{(1)} Z^{(2)} \rangle,
\end{array} \tag{6.1.5}$$

where for better readability we use the notation X, Y and Z for the Pauli spin matrices.

Next, we need to think how many local measurement settings (see Sec. 3.1.4) are needed. At every site we measure X, Y or Z. Hence, for N qubits we need

$$\mathcal{D}_N^{(\mathrm{FST})} = 3^N \tag{6.1.6}$$

local measurement settings. For full state tomography for two qubits the following 9 settings are needed

$$\begin{array}{lll}
\{X^{(1)}, X^{(2)}\}, & \{X^{(1)}, Y^{(2)}\}, & \{X^{(1)}, Z^{(2)}\}, \\
\{Y^{(1)}, X^{(2)}\}, & \{Y^{(1)}, Y^{(2)}\}, & \{Y^{(1)}, Z^{(2)}\}, \\
\{Z^{(1)}, X^{(2)}\}, & \{Z^{(1)}, Y^{(2)}\}, & \{Z^{(1)}, Z^{(2)}\},
\end{array} \tag{6.1.7}$$

Here $\{X^{(1)}, X^{(2)}\}$ means that we measure $X^{(1)}$ on the first qubit and $X^{(2)}$ on the second one. (For the definition of the measurement settings, see Sec. 3.1.4.) The number of settings is smaller than the number of correlation terms since several correlation terms can be measured with the same setting. For example, the correlations $\langle \mathbb{1}^{(1)} X^{(2)} \rangle$, $\langle X^{(1)} \mathbb{1}^{(2)} \rangle$ and $\langle X^{(1)} X^{(2)} \rangle$ can all be measured by the setting $\{X^{(1)}, X^{(2)}\}$.

We can see that the number of settings increases exponentially with the number of qubits, which makes full tomography impossible apart from small systems. Indeed, so far the largest full tomography has been carried out for an 8 qubit state in trapped ions [20]. For photonic experiments, the largest full tomography was for 6 qubits [123].

6.1.2 Efficient tomographic schemes

In the previous section we discussed that full state tomography is impossible for large systems, since the number of local measurement settings increases exponentially with the number of qubits. A possible solution to this problem is to consider methods that assume that the quantum state is of a certain form. Very briefly we discuss two such methods available in the literature.

The first approach assumes that the state is a matrix product state (MPS) with a certain bond dimension [124]. For such an ansatz state, the number of free parameters scales polynomially with the system size. A tomographic protocol, called Matrix Product State Tomography, has been worked out assuming that the state is of this form [125]. It works best for ground states of spin chains.

The second approach assumes that the quantum state is of low rank. Then, we do not have to measure all the (6.1.2) coefficients, only a randomly chosen set. This method is called Compressed Sensing [126]. The number of measurements scale still exponentially with the number of qubits, but exponentially better than for full tomography.

6.2 Permutationally invariant tomography

In this section, we will present our method, which works best for permutationally invariant states. Instead of the density matrix of the N-qubit system, it determines the permutationally invariant density matrix

$$\varrho_{\mathrm{PI}} = \frac{1}{N!} \sum_k \Pi_k \varrho \Pi_k^\dagger, \tag{6.2.8}$$

where the summation is over all the permutations Π_k.

Observation 6.2.1 *The number of degrees of freedom for an N-qubit permutationally invariant density matrix of the type* (6.2.8) *is*

$$\mathrm{DOF}_N^{(\mathrm{PI})} = \binom{N+3}{N} - 1, \tag{6.2.9}$$

where "PI" refers to permutationally invariant tomography.

Proof. We can use a technique similar to the one applied in Sec. 6.1.1 to count the number of real degrees of freedom for full tomography. We will have fewer degrees of freedom, since several of the $c_{k_1,k_2,...,k_N}$ coefficients must be equal to each other due to permutational invariance. In particular,

$$c_{k_1,k_2,...,k_N} = c_{k_{i_1},k_{i_2},...,k_{i_N}} \tag{6.2.10}$$

is always true, if $i_1, i_2, ..., i_N$ are some permutations of $1, 2, .., N$. We should now remember that $k_i \in \{0, 1, 2, 3\}$. We have to count how many different ways N numbers can be chosen from $0, 1, 2$, and 3 such that the order does not matter, which is just the well known "stars and bars problem" in combinatorics. We exclude the choice $k_1, k_2, ..., k_N = 0$ since $c_{0,0,...,0}$ is fixed [see Eq. (6.1.3).] Hence, the number of different coefficients is obtained as Eq. (6.2.9). ■

From Observation 6.2.1 we can see that the number of real degrees of freedom depends polynomially on the number of qubits.

Let us now relate the coefficients $c_{k_1,k_2,...,k_N}$ to operator expectation values. Knowing all these coefficients is the same as knowing all the expectation values

$$\langle (X^{\otimes k} \otimes Y^{\otimes l} \otimes Z^{\otimes m} \otimes \mathbb{1}^{\otimes n}) \rangle_{\varrho_{\mathrm{PI}}}. \tag{6.2.11}$$

Let us now relate the coefficients to the density matrix ϱ rather than to ϱ_{PI}. Simple arguments show that knowing all the coefficients $c_{k_1,k_2,...,k_N}$ is the same as knowing all the expectation values

$$\langle (X^{\otimes k} \otimes Y^{\otimes l} \otimes Z^{\otimes m} \otimes \mathbb{1}^{\otimes n})_{\mathrm{PI}} \rangle_{\varrho}, \tag{6.2.12}$$

where we defined the permutationally invariant part of an operartor as

$$X_{\mathrm{PI}} = \frac{1}{N!} \sum_k \Pi_k X \Pi_k^\dagger. \tag{6.2.13}$$

Based on these, now we will calculate the number of measurements needed to obtain ϱ_{PI}.

Observation 6.2.2 *The number of local measurement settings necessary to measure an N-qubit permutationally invariant density matrix of the type* (6.2.8) *is*

$$\mathcal{D}_N^{(\mathrm{PI})} = \binom{N+2}{N}. \tag{6.2.14}$$

Proof. First, one has to recognize that for permutationally invariant tomography, we need to measure settings of the type

$$\{A, A, ..., A\}, \tag{6.2.15}$$

that is, we need to measure the same operator A on all qubits [71]. (For the definition of the measurement settings, see Sec. 3.1.4.) If we measure such a setting, we will know all the expectation values

$$\langle (A^{\otimes(N-n)} \otimes \mathbb{1}^{\otimes n})_{\mathrm{PI}} \rangle \tag{6.2.16}$$

for $n = 0, 1, ..., N-1$.

Let us consider expectation values of the type (6.2.16) for a given n. If we know all such expectation values then we know all correlations of the type (6.2.12) for $k+l+m+n = N$. For a given n, the number of such correlations is $\mathcal{D}_{(N-n)}^{(\mathrm{PI})}$, where $\mathcal{D}_{(N)}^{(\mathrm{PI})}$ is defined in Eq. (6.2.14).

Let us now bound from below the number of measurement settings necessary for permutationally invariant tomography. Any measurement setting of the type (6.2.15) gives at most one expectation value for every such space characterized by a given n. Hence the number of settings cannot be smaller than the largest dimension, which is $\mathcal{D}_N^{(\mathrm{PI})}$. Let us now see, whether $\mathcal{D}_N^{(\mathrm{PI})}$ settings are sufficient. We can see that a generic choice of $\mathcal{D}_N^{(\mathrm{PI})}$ settings is sufficient to recover the correlations in each of these spaces, and hence completely characterizes ϱ_{PI}. ■

Permutationally invariant tomography has been used to study a six-qubit quantum state experimentally. The results can be seen in Fig. 6.1. In Fig. 6.1(a), we can see the results of full tomography vs. the results of permutationally invariant tomography. As Fig. 6.1(b) shows, the A_j operators chosen are distributed in a way that the uncertainties of the reconstruction are small. One can see that the vectors corresponding to A_j seem to be equally distributed on the sphere. In Fig. 6.1(c) and (d), similar results are shown for the case when the A_j operators are chosen randomly. Due to that the uncertainties of the results of the permutationally invariant tomography are much larger. In Fig. 6.2, the density matrices obtained from full tomography and permutationally invariant tomography are shown.

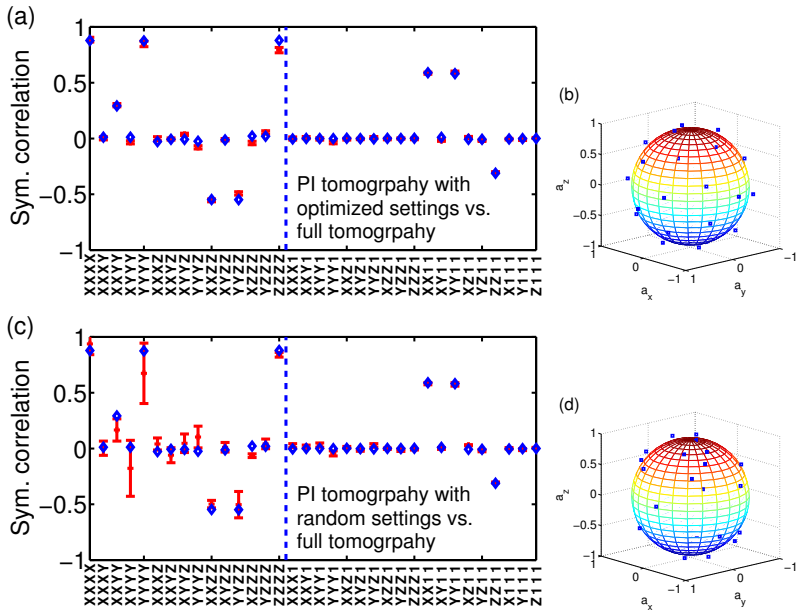

Figure 6.1: (a) Comparison of the 34 symmetrized correlations coming from (crosses with error bars) 15 permutationally invariant measurement settings with optimized A_j matrices for $N = 4$ qubits and (diamonds) from full tomography requiring 81 local settings. The average uncertainty of all symmetrized correlations obtained from full tomography is ± 0.022, and is not shown in the figure. The labels refer to symmetrized correlations of the form given in Eq. (6.2.12). The results corresponding to the 15 full four-qubit correlations are left from the vertical dashed line. (b) Measurement directions. A point at (a_x, a_y, a_z) corresponds to measuring operator $a_x X + a_y Y + a_z Z$. (c) Results for randomly chosen A_j matrices and (d) corresponding measurement directions. Figure taken from Ref. [71].

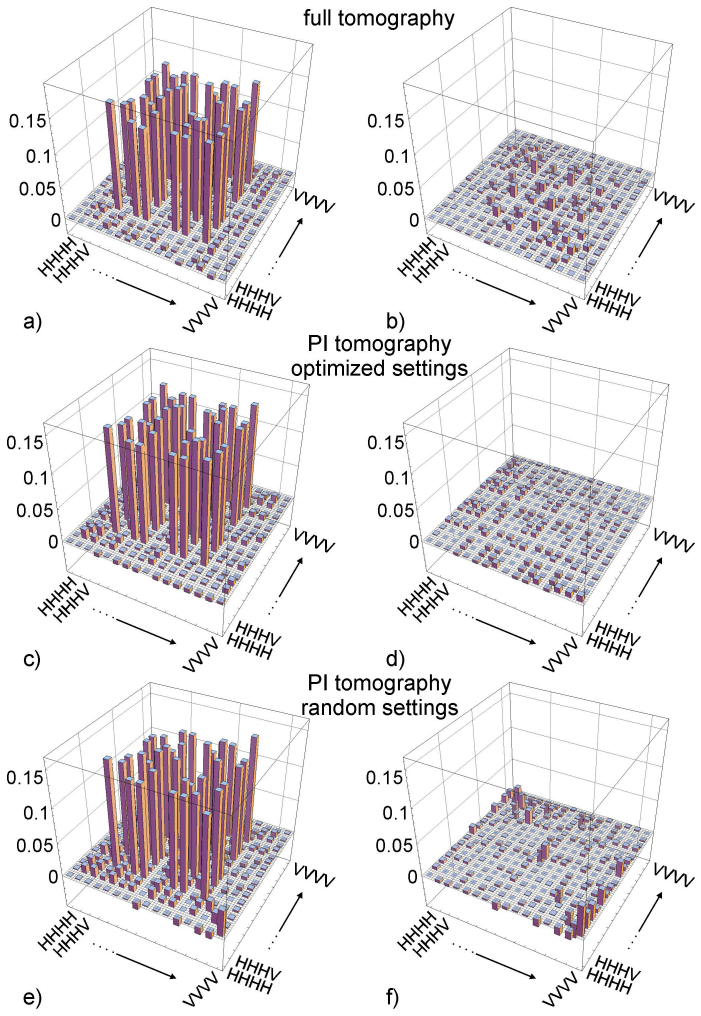

Figure 6.2: (a) The real and (b) imaginary parts of the density matrix coming from full tomography. (c), (d) The same for permutationally invariant tomography with optimized and (e), (f) random measurement directions, respectively. Figure taken from Ref. [71]. The experiment has been carried out and the figure has been drawn by W. Wieczorek, R. Krischek, C. Schwemmer, and H. Weinfurter.

6.3 Connected results

It has been worked out how to store the permutationally invariant state efficiently on a digital computer [127]. Hence, not only the number of measurements needed scales polinomially with the number of qubits, but even the amount of data stored scales that way. It is even shown that fitting the density matrix obtained experimentally to a positive semidefinite density matrix, which is an important task for experimental quantum tomography, can be done efficiently with semidefinite programming. Permutationally invariant tomography has been carried out for a six-qubit photonic quantum state, and compared to compressed sensing and also to full tomography [123]. Permutationally invariant tomography has been combined with the compressed sensing method. Hence, a density matrix can be obtained even before the settings necessary for permutationally invariant tomography are measured [123].

Chapter 7

Optimal spin-squeezing inequalities

In this Chapter, entanglement detection with collective observables are discussed. A generalized spin sqeeezing entanglement condition is presented that detects entanglement close to singlet states, described in Ref. [69]. Later, a complete set of entanglement criteria based on collective observables is presented based on Refs. [47, 72].

7.1 Background

7.1.1 Spin squeezing

Spin squeezing has originally been defined as a notion for spin systems that is analogous to squeezing for bosonic modes. One of the most popular definitions is based on the Heisenberg uncertainty relation [128]

$$(\Delta J_x)^2(\Delta J_y)^2 \geq \frac{1}{4}|\langle J_z\rangle|^2. \tag{7.1.1}$$

A quantum state is spin squeezed if

$$(\Delta J_x)^2 < \frac{1}{2}|\langle J_z\rangle| \tag{7.1.2}$$

holds, where the right-hand side of Eq. (7.1.2) is the square root of the right-hand side of Eq. (7.1.1) and is called the standard quantum limit. It is an important part of the definition that z points into the direction of the mean spin.

Based on Eq. (7.1.2) we see that spin-squeezed states typically have a large spin along the z direction, and have a small spin uncertainty in an orthogonal direction, as shown in Fig. 7.1. We note that there is also a well known, but slightly different definition [6].

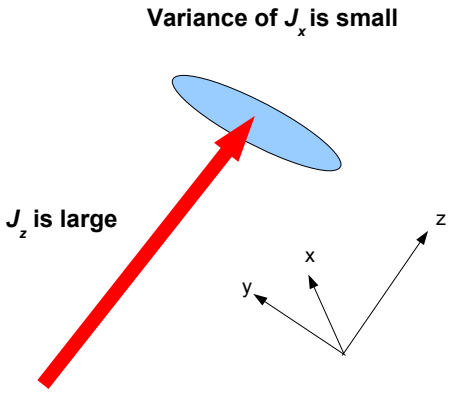

Figure 7.1: A typical spin-squeezed state. The arrow is the collective spin. At the end of the arrow, there is an uncertainty ellipse.

7.1.2 The relation of spin squeezing to entanglement

There is a criterion that can detect the entanglement of spin squeezed states with collective measurements. For N spin-1/2 particles, let us define a spin-squeezing parameter as

$$\xi_{\rm s}^2 = N\frac{(\Delta J_x)^2}{\langle J_y\rangle^2+\langle J_z\rangle^2}. \tag{7.1.3}$$

It has been shown that

$$\xi_{\rm s} < 1 \tag{7.1.4}$$

implies entanglement [7].

It is possible to generalize this approach to an ensemble of spins with $j > 1/2$. One can determine the minimal $(\Delta J_x)^2$ achievable for separable states for a given $\langle J_z\rangle$. If a quantum state reaches a value smaller than this bound, then it is entangled [23]. For $j = 1/2$, this approach detects the same entangled state as the entanglement condition based given in Eq. (7.1.4).

7.2 Entanglement conditions with three variances

A method will now be presented that detects entangled states in optical lattices of two-state atoms even if there are several atoms per lattice site. This is a very useful property of our entanglement detection scheme, since in practice, it is difficult to prepare a lattice with a unit occupancy [129]. Our method needs the measurement of collective observables, which makes it applicable to large ensembles. Our results are described in in Ref. [69].

Observation 7.2.1 *For separable states*

$$(\Delta J_x)^2 + (\Delta J_y)^2 + (\Delta J_z)^2 \geq \frac{\langle N \rangle}{2} \tag{7.2.5}$$

holds, where N is the total particle number and J_l are the collective angular momentum coordinates. They are the sum of the corresponding single site Schwinger type angular momentum operators. For a lattice site, omitting the index (k), these are defined as

$$j_x = \frac{1}{2}(a^\dagger b + a b^\dagger), \tag{7.2.6a}$$

$$j_y = \frac{i}{2}(b^\dagger a - a b^\dagger), \tag{7.2.6b}$$

$$j_z = \frac{1}{2}(a^\dagger a - b^\dagger b), \tag{7.2.6c}$$

where a and b are the bosonic destruction operators corresponding to the two internal states of the atoms. The particle number at a site is $a^\dagger a + b^\dagger b$.

Proof. If the system is in a pure state and a lattice site is not entangled with the other sites, then its state has the form

$$|\Psi\rangle = \sum_m c_m |j_m, z_m\rangle. \tag{7.2.7}$$

A separable state is just the convex combination of products of such single site states. Here $|j, z\rangle$ is an eigenstate of $j_x^2 + j_y^2 + j_z^2$ with eigenvalue $j(j+1)$, and of j_z with eigenvalue z. For example, $|\uparrow\rangle = |1/2, 1/2\rangle$ and $|\downarrow\rangle = |1/2, -1/2\rangle$ denote a single atom at the lattice site in states a and b, respectively, while $|\emptyset\rangle = |0, 0\rangle$ denotes an empty lattice site.

This representation does not take into account entanglement between particles within the lattice site, as expected, and models a lattice site as a particle with a large spin. The spin squeezing criterion [130], however, detects both entanglement between particles on the same site and entanglement between particles on different sites.

As we will show, criterion (7.2.5) is able to distinguish entanglement due to particle number variance (e.g., $|\uparrow\rangle|\emptyset\rangle + |\emptyset\rangle|\uparrow\rangle$) from entanglement in the internal states (e.g., $|\uparrow\rangle|\downarrow\rangle - |\downarrow\rangle|\uparrow\rangle$). Our aim is to detect the second kind of entanglement. In the first case we have a superposition of states with different on-site particle numbers. The Schwinger operators commute with the N_k particle number operators, thus by measuring them one cannot distinguish between a superposition and a mixture of such states [131]. Consequently an entanglement condition in terms of such observables will not take into account entanglement due to particle number variance.

The proof of criterion (7.2.5) is based on the relations

$$\left\langle (j_x^{(k)})^2 + (j_y^{(k)})^2 + (j_z^{(k)})^2 \right\rangle = \left\langle \frac{N_k}{2}\left(1 + \frac{N_k}{2}\right)\right\rangle, \tag{7.2.8a}$$

$$\left\langle j_x^{(k)}\right\rangle^2 + \left\langle j_x^{(k)}\right\rangle^2 + \left\langle j_x^{(k)}\right\rangle^2 \leq \frac{\langle N_k\rangle^2}{4}. \tag{7.2.8b}$$

Here Eq. (7.2.8a) expresses the fact, that a two-mode bosonic system has maximal angular momentum [132]. Subtracting Eq. (7.2.8b) from Eq. (7.2.8a) one obtains the uncertainty relation for spin (k)

$$(\Delta j_x^{(k)})^2 + (\Delta j_y^{(k)})^2 + (\Delta j_z^{(k)})^2 \geq \frac{(\Delta N_k)^2}{4} + \frac{\langle N_k\rangle}{2}. \tag{7.2.9}$$

For separable states

$$\begin{aligned}(\Delta J_x)^2 + (\Delta J_y)^2 + (\Delta J_z)^2 &\geq \sum_l p_l \left\{(\Delta J_x)_l^2 + (\Delta J_y)_l^2 + (\Delta J_z)_l^2\right\} \\ &= \sum_l p_l \sum_k \left\{(\Delta j_x^{(k)})_l^2 + (\Delta j_y^{(k)})_l^2 + (\Delta j_z^{(k)})_l^2\right\}\end{aligned} \tag{7.2.10}$$

holds, which together with Eq. (7.2.9) proves criterion (7.2.5). Thus the uncertainty relations (7.2.9) for the individual lattice sites gave a lower bound for the uncertainties of the corresponding collective quantities for separable states in Eq. (7.2.5)[131]. This lower bound is the highest possible, since *any pure product state* with unit lattice site-occupancy saturates the inequality. [For atoms on the lattice a particle number conserving superselection rule applies, thus $(\Delta N_k)^2 = 0$ for all pure product states.] ■

Inequality (7.2.5) is maximally violated for angular momentum eigenstates with total angular momentum $J = 0$ (many-body spin singlet). The spin squeezing criterion [130] does not detect these states as entangled, since they have $\left\langle J_{x/y/z}\right\rangle = 0$.

7.3 Complete set of inequalities for qubits

As the number of particles is increasing rapidly in recent experiments, it is important to consider entanglement detection in systems in which the particles cannot be individually addressed. Such systems are, for example, clouds of millions of atoms. We determined the full set of entanglement conditions, the Optimal Spin Squeezing Inequalities, that detect entanglement in a system of spin-1/2 particles using first and second order moments of collective quantities. These results are quite general. In any experiment with many two-

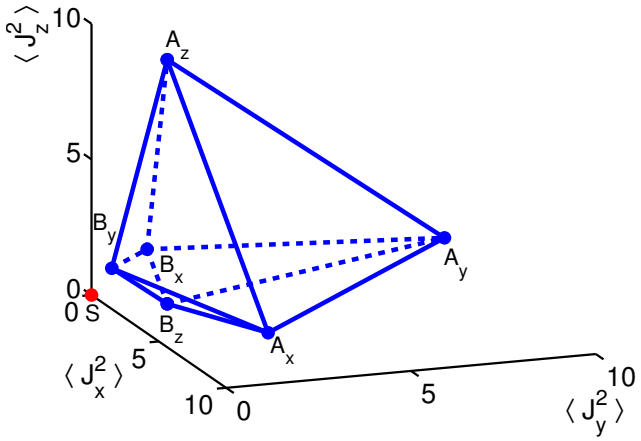

Figure 7.2: The polytope of separable states corresponding to Eqs. (7.3.13) for $N = 6$ and $\vec{J} = 0$. S corresponds to a many body singlet state. Figure from Ref. [47].

state particles our conditions can be used for entanglement detection and, as we proved it, no further conditions can be found. Thus, again, it is expected that our results will be used to verify the success of several many-particle experiments. Our entanglement criteria are described in Refs. [47, 72].

Let us assume that for a physical system the values of the first moments

$$\vec{J} := (\langle J_x \rangle, \langle J_y \rangle, \langle J_z \rangle) \tag{7.3.11}$$

and the second moments

$$\vec{K} := (\langle J_x^2 \rangle, \langle J_y^2 \rangle, \langle J_z^2 \rangle) \tag{7.3.12}$$

are known. Next, we will define a set of entanglement conditions that that detect entanglement with these quantites.

Observation 7.3.1 *Violation of any of the following inequalities implies entanglement:*

$$\langle J_x^2 \rangle + \langle J_y^2 \rangle + \langle J_z^2 \rangle \leq N(N+2)/4, \tag{7.3.13a}$$

$$(\Delta J_x)^2 + (\Delta J_y)^2 + (\Delta J_z)^2 \geq N/2, \tag{7.3.13b}$$

$$\langle J_i^2 \rangle + \langle J_j^2 \rangle - N/2 \leq (N-1)(\Delta J_k)^2, \tag{7.3.13c}$$

$$(N-1)\left[(\Delta J_i)^2 + (\Delta J_j)^2\right] \geq \langle J_k^2 \rangle + N(N-2)/4, \tag{7.3.13d}$$

where i, j, k take all the possible permutations of x, y, z.

Proof. The variance, defined as

$$(\Delta A)^2 := \langle A^2 \rangle - \langle A \rangle^2, \tag{7.3.14}$$

is concave in the state, that is, if we mix two states as

$$\varrho = p\varrho_1 + (1-p)\varrho_2, \tag{7.3.15}$$

then for the variance of the mixture

$$(\Delta A)^2_\varrho \geq p(\Delta A)^2_{\varrho_1} + (1-p)(\Delta A)^2_{\varrho_2} \tag{7.3.16}$$

holds. Thus, it suffices to prove that the inequalities of Observation 7.3.1 are satisfied by pure product states. Based on the theory of angular momentum, inequality Eq. (7.3.13a) is valid for all quantum states and the equality holds for states of the symmetric subspace. However, for separable states it can be proved easily without this knowledge using that for such states Eq. (2.2.11) holds [67]. For Eq. (7.3.13b), one first needs that for product states

$$(\Delta J_k)^2 = \tfrac{N}{4} - \tfrac{1}{4}\sum_i \langle \sigma_k^{(i)} \rangle^2 \tag{7.3.17}$$

holds. Then, for a product state, one has

$$(\Delta J_x)^2 + (\Delta J_y)^2 + (\Delta J_z)^2 = \tfrac{3N}{4} - \tfrac{1}{4}\sum_k x_k^2 + y_k^2 + z_k^2. \tag{7.3.18}$$

Here $x_i := \langle \sigma_x^{(i)} \rangle$, $y_i := \langle \sigma_y^{(i)} \rangle$, and $z_i := \langle \sigma_z^{(i)} \rangle$. Knowing that $x_i^2 + y_i^2 + z_i^2 \leq 1$, the right hand side of Eq. (7.3.18) is bounded from below by $\frac{N}{2}$.

Concerning Eq. (7.3.13c), we have to show that

$$\mathfrak{Y} := (N-1)(\Delta J_x)^2 + \tfrac{N}{2} - \langle J_y^2 \rangle - \langle J_z^2 \rangle \geq 0. \tag{7.3.19}$$

This can be written as

$$\begin{aligned} \mathfrak{Y} &= (N-1)[\tfrac{N}{4} - \tfrac{1}{4}\sum_i x_i^2] - \tfrac{1}{4}\sum_{i\neq j}(y_i y_j + z_i z_j) \\ &= (N-1)[\tfrac{N}{4} - \tfrac{1}{4}\sum_i x_i^2] - \tfrac{1}{4}[(\sum_i y_i)^2 + (\sum_i z_i)^2] + \tfrac{1}{4}\sum_i (y_i^2 + z_i^2). \end{aligned} \tag{7.3.20}$$

Using the inequality

$$\left(\sum_i s_i\right)^2 \leq N \sum_i s_i^2, \tag{7.3.21}$$

and the normalization of the Bloch vector, it follows that

$$\mathfrak{Y} \geq \tfrac{N-1}{4}\sum_i (1 - x_i^2 - y_i^2 - z_i^2) \geq 0. \tag{7.3.22}$$

Equation (7.3.13d) can be proved in a similar way. We have to show that

$$\mathfrak{Z} := (N-1)\left[(\Delta J_k)^2 + (\Delta J_l)^2\right] - \langle J_m^2\rangle - \tfrac{N(N-2)}{4} \geq 0. \tag{7.3.23}$$

This can be proved by rewriting $\mathfrak{Z}$ with the individual spin coordinates and using Eq. (7.3.21):

$$\begin{aligned} \mathfrak{Z} &= (N-1)[\tfrac{N}{4} - \tfrac{1}{4}\sum_i x_i^2 + y_i^2] - \tfrac{1}{4}\sum_{i\neq j} z_i z_j \\ &\geq \tfrac{N-1}{4}\sum_i (1 - x_i^2 - y_i^2 - z_i^2) \geq 0. \end{aligned} \tag{7.3.24}$$

■

For any value of $\vec{J}$ these eight inequalities define a polytope in the three-dimensional $(\langle J_x^2\rangle, \langle J_y^2\rangle, \langle J_z^2\rangle)$-space. Observation 7.3.1 shows that separable states lie inside this polytope. For the case $\vec{J} = 0$ and $N = 6$ the polytope is depicted in Fig. 7.2. Such a polytope is completely characterized by its extreme points. Direct calculation shows that they are

$$A_x := \left[\frac{N^2}{4} - \kappa(\langle J_y\rangle^2 + \langle J_z\rangle^2), \frac{N}{4} + \kappa\langle J_y\rangle^2, \frac{N}{4} + \kappa\langle J_z\rangle^2\right], \tag{7.3.25a}$$

$$B_x := \left[\langle J_x\rangle^2 + \frac{\langle J_y\rangle^2 + \langle J_z\rangle^2}{N}, \frac{N}{4} + \kappa\langle J_y\rangle^2, \frac{N}{4} + \kappa\langle J_z\rangle^2\right], \tag{7.3.25b}$$

where $\kappa := (N-1)/N$. The points $A_{y/z}$ and $B_{y/z}$ can be obtained in an analogous way.

One might ask whether there are separable states corresponding to all points inside the polytope. This would imply that the criteria of Observation 7.3.1 are complete, that is, if the inequalities are satisfied, then the first and second moments of J_k do not suffice to prove entanglement. In other words, it is not possible to find criteria detecting more entangled states based on these moments. Due to the convexity of the set of separable states, it is enough to investigate the extreme points.

Observation 7.3.2 *For any value of $\vec{J}$ there are separable states corresponding to A_k. For certain values of $\vec{J}$ and N there are separable states corresponding to points B_k. However, there are always separable states corresponding to points B_k' such that their distance from B_k is smaller than $1/4$. In the limit $N \to \infty$ for a fixed normalized angular momentum $\vec{j} := \vec{J}/(N/2)$ the difference between the volume of polytope of Eqs. (7.3.13) and the volume of set of points corresponding to separable states decreases with N at least as $\Delta V/V \propto N^{-2}$, hence in the macroscopic limit the characterization is complete.*

Proof. A separable state corresponding to A_x is

$$\rho_{A_x} := p(|\psi_+\rangle\langle\psi_+|)^{\otimes N} + (1-p)(|\psi_-\rangle\langle\psi_-|)^{\otimes N}. \tag{7.3.26}$$

Here $|\psi_{+/-}\rangle$ are the single qubit states with Bloch vector coordinates

$$(\langle\sigma_x\rangle, \langle\sigma_y\rangle, \langle\sigma_z\rangle) = \left(\pm c_x, \frac{\langle J_y\rangle}{J}, \frac{\langle J_z\rangle}{J}\right), \tag{7.3.27}$$

where $J := N/2$ and

$$c_x := \sqrt{1 - \frac{\langle J_y\rangle^2 + \langle J_z\rangle^2}{J^2}}. \tag{7.3.28}$$

The mixing ratio is defined as $p := [1 + \langle J_x\rangle/(Jc_x)]/2$. If $M := Np$ is an integer, we can also define the state corresponding to the point B_x as

$$|\phi_{B_x}\rangle := |\psi_+\rangle^{\otimes M} \otimes |\psi_-\rangle^{\otimes(N-M)}. \tag{7.3.29}$$

If M is not an integer, we can approximate B_x by taking $m := M - \varepsilon$ as the largest integer smaller than M, defining

$$\rho' := (1-\varepsilon)(|\psi_+\rangle\langle\psi_+|)^{\otimes m} \otimes (|\psi_-\rangle\langle\psi_-|)^{\otimes(N-m)} + \varepsilon(|\psi_+\rangle\langle\psi_+|)^{\otimes(m+1)} \otimes (|\psi_-\rangle\langle\psi_-|)^{\otimes(N-m-1)}. \tag{7.3.30}$$

This state has the same coordinates as B_x, except for the value of $\langle J_x^2\rangle$, where the difference is $c_x^2(\varepsilon - \varepsilon^2) \leq 1/4$. The dependence of $\Delta V/V$ on N can be studied by considering the polytopes in the $(\langle J_x^2\rangle, \langle J_y^2\rangle, \langle J_z^2\rangle)$-space corresponding to $\langle J_k\rangle = j_k \times N/2$, where j_k are the normalized angular momentum cordinates. As N increases, the distance of the points A_k to B_k scales as N^2, hence the volume of the polytope increases as N^6. The difference between the polytope and the points corresponding to separable states scales like the surface of the polytope, hence as N^4. ■

7.4 Experimental applications of our results and further work

In Ref. [11], Observation 7.2.1 has been used to detect singlet states in atomic ensembles experimentally (see Ref. [133] for a theoretical description of the method). In Ref. [31], conditions similar to Eq. (7.3.13c) have been developed to detect multipartite entanglement in Dicke states of spin-1/2 particles and have been used in a cold gas experiment. In Ref. [111], general conditions appear for detecting multipartite entanglement in Dicke states of ensembles of spin-j particles. In Refs. [134, 135], the inequalities (7.3.13) have been generalised to ensembles of spin-j particles.

Chapter 8

Entanglement and quantum metrology

In this Chapter the relation of multipartite entanglement and quantum metrology is discussed. Based on that the method given in Ref. [56], we show that full multipartite entanglement is needed to reach the maximum sensitivity.[7]

8.1 Background

8.1.1 Cramér-Rao bound

In metrology, as can be seen in Fig. 8.1, one of the basic tasks is phase estimation connected to the unitary dynamics of a linear interferometer

$$\varrho_{\text{output}} = e^{-i\theta J_{\vec{n}}} \varrho e^{+i\theta J_{\vec{n}}}, \tag{8.1.1}$$

where ϱ is the input state of the interferometer, while ϱ_{output} is the output state, and $J_{\vec{n}}$ is a component of the collective angular momentum in the direction $\vec{n}$.

The important question is, how well we can estimate the small angle θ by measuring ϱ_{output}. For such an interferometer the phase estimation sensitivity, assuming *any* type of measurement, is bounded by the Quantum Cramér-Rao inequality as [137, 138]

$$\Delta\theta \geq \frac{1}{\sqrt{F_Q[\varrho, J_{\vec{n}}]}}, \tag{8.1.2}$$

where F_Q is the quantum Fisher information.

[7] In Ref. [136], an independent work about a similar topic has been published. The two articles appeared next to each other in Phys. Rev. A.

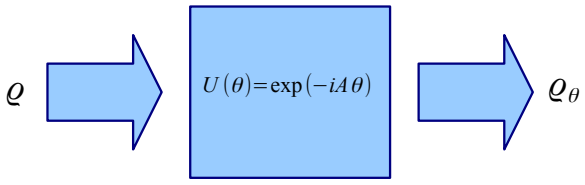

Figure 8.1: A basic problem of linear interferometry. The parameter θ must be estimated by measuring ϱ_θ.

8.1.2 Quantum Fisher information

The quantum Fisher information is defined as [137–140]

$$F_Q[\varrho, A] = 2\sum_{i,j} \frac{(\lambda_i - \lambda_j)^2}{\lambda_i + \lambda_j} |A_{ij}|^2. \tag{8.1.3}$$

Here λ_i are the eigenvalues of the density matrix and A_{ij} are the matrix elements of the operator A in the eigenbasis of the density matrix.

We summarize now some important properties of the quantum Fisher information.

1. For pure states $F_Q[|\Psi\rangle, A] = 4(\Delta A)^2_\Psi$ holds.
2. It is convex in the state. Hence, for mixed states $F_Q[\varrho, A] \leq 4(\Delta A)^2_\varrho$.

8.2 Entanglement and the quantum Fisher information

The relationship between phase estimation sensitivity and entanglement in linear interferometers has already been examined [55], and an entanglement condition has been formulated with the sensitivity of the phase estimation, that is, with the quantum Fisher information. It has been found that for separable states of N-qubit states of the form Eq. (2.1.2) we obtain [55]

$$F_Q[\varrho, J_l] \leq N, \tag{8.2.4}$$

where J_l is an angular momentum component. All states violating Eq. (8.2.4) are entangled. Based on Eq. (8.2.4) we see that entanglement is needed for having a precision better than what can be reached by separable states. It has also been shown that not all entangled states are useful for phase estimation, at least in a linear interferometer [141].

It is instructive to find an upper bound on the left-hand side of Eq. (8.2.4) for general

states. For pure states, we have

$$F_Q[\varrho, J_l] = 4(\Delta J_l)^2 \leq N^2, \tag{8.2.5}$$

which is a valid bound even for mixed states. By comparing Eq. (8.2.4) and Eq. (8.2.5), one can see the large difference between the precision achievable by separable states and by entangled states.

After defining the basic notions, we will find the bounds for the metrological sensitivity of quantum states with various levels of multipartite entanglement.

Observation 8.2.1 *For N-qubit k-producible states, the quantum Fisher information is bounded from above by [56, 136]*

$$F_Q[\varrho, J_l] \leq sk^2 + (N - sk)^2, \tag{8.2.6}$$

where

$$s = \lfloor \tfrac{N}{k} \rfloor, \tag{8.2.7}$$

and $\lfloor \frac{N}{k} \rfloor$ denotes the integer part of $\frac{N}{k}$.

Proof. Let us consider pure k-producible states of the form (2.1.6) where $|\psi_m\rangle$ are multiparticle states with $k_m \leq k$ particles. Clearly, $\sum_m k_m = N$. For such states

$$(\Delta J_l)^2 = \sum_m (\Delta J_l)^2_{\psi_m} \leq \sum_m \frac{k_m^2}{4}. \tag{8.2.8}$$

Let us now maximize the right-hand side of Eq. (8.2.8) for the case when k is a divisor of N. It is maximized by a state of the type

$$|\Psi\rangle^{\otimes s}, \tag{8.2.9}$$

where $|\Psi\rangle$ is a state of k qubits and $s = N/k$. For this state, $k_m = k$ for $m = 1, 2, .., s$. If k is not a divisor of N then a state maximizing Eq. (8.3.17) is of the type

$$|\Psi\rangle^{\otimes s} \otimes |\Phi\rangle, \tag{8.2.10}$$

where $|\Psi\rangle$ is a state of k qubits and $|\Phi\rangle$ is a state of $(N - sk)$ qubits. For this state, k_m equals k for $m = 1, 2, .., s$ while $k_{s+1} = N - sk$. Based on these, we arrive at Eq. (8.2.6). ■

It is instructive to write Eq. (8.2.6) for the case N divisible by k as

$$F_Q[\varrho, J_{\vec{n}}] \leq Nk. \tag{8.2.11}$$

Equation (8.2.11) is saturated by a tensor product of k-qubit GHZ-states $|\mathrm{GHZ}_k\rangle^{\otimes(N/k)}$. Based on Eq. (8.2.11) we can see that the bounds reached by k-producible states are distributed linearly, i.e., $(2k)$-poducible states can reach a twice as large value for $F_Q[\varrho, J_l]$ as k-producible states can.

Note the criterion (8.2.11) for k-producible states for $k = 1$ is just the same as the criterion for separable states given in Eq. (8.2.4). Moreover, the criterion (8.2.11) for $k = N - 1$ is fulfilled by all biseparable states. Hence, states that violate Eq. (8.2.11) for $k = N - 1$ are genuine multipartite entangled. Thus, genuine multipartite entanglement is needed to reach the maximum sensitivity in metrology.

Note also that if N is not divisible by k then Eq. (8.2.11) is still a valid bound, which can be seen as follows. We need to prove that

$$sk^2 + (N - sk)^2 \leq Nk. \tag{8.2.12}$$

By substracting sk^2 from both sides of Eq. (8.2.12), we arrive at

$$(N - sk)^2 \leq k(N - sk). \tag{8.2.13}$$

Equation (8.2.13) is evidently true, knowing that $N - sk < k$.

8.3 Condition with three quantum Fisher information terms

Next we show that it is possible to obtain relations similar to Eq. (8.2.4), but for the sum of several quantum information terms. In order to construct such a relation, let us consider the average quantum Fisher information defined as

$$\mathrm{avg}_{\vec{n}} F_Q[\varrho, J_{\vec{n}}] = \int_{|\vec{n}|=1} F_Q[\varrho, J_{\vec{n}}] d\vec{n}. \tag{8.3.14}$$

Equation (8.3.14) is relevant for the following metrological task. It gives an upper bound on the average $(\Delta\theta)^{-2}$ for a quantum state ϱ, if the direction of the magnetic field is chosen randomly based on a uniform distribution. Simple calculations show that the integral (8.3.14) equals the average of the quantum Fisher information corresponding to

the three angular momentum components

$$\mathrm{avg}_{\vec{n}} F_Q[\varrho, J_{\vec{n}}] = \tfrac{1}{3}(F_Q[\varrho, J_x] + F_Q[\varrho, J_y] + F_Q[\varrho, J_z]). \tag{8.3.15}$$

Next, we present an entanglement condition with the average quantum Fisher information.

Observation 8.3.1 *For N-qubit k-producible states, for $k \geq 2$, the sum of the three Fisher information terms is bounded from above by [56, 136]*

$$\mathrm{avg}_{\vec{n}} F_Q[\varrho, J_{\vec{n}}] \leq \begin{cases} \frac{1}{3}sk(k+2) + \frac{1}{3}(N-sk)(N-sk+2) & \text{if } N - sk \neq 1, \\ \frac{1}{3}sk(k+2) + \frac{2}{3} & \text{if } N - sk = 1, \end{cases} \tag{8.3.16}$$

where s is again the integer part of $\frac{N}{k}$. Any state that violates this bound is not k-producible and contains $(k+1)$-particle entanglement. These inequalities have been used to detect experimentally useful multipartite entanglement in Ref. [9].

Proof. Let us again consider pure k-producible states of the form (2.1.6) where $|\psi_m\rangle$ are multiparticle states with $k_m \leq k$ particles. Clearly, $\sum_m k_m = N$. For such states

$$(\Delta J_x)^2 + (\Delta J_y)^2 + (\Delta J_z)^2 \;\; = \;\; \sum_m (\Delta J_x)^2_{\psi_m} + (\Delta J_y)^2_{\psi_m} + (\Delta J_z)^2_{\psi_m}. \tag{8.3.17}$$

We will now bound the righ-hand side of Eq. (8.3.17). We know that

$$\langle J_x^2 + J_y^2 + J_z^2 \rangle_{\psi_m} \leq \frac{k_m}{2}\left(1 + \frac{k_m}{2}\right), \tag{8.3.18}$$

where the bound is tight. Equation (8.3.18) can be used to bound the sum of the three variances as follows

$$(\Delta J_x)^2_{\psi_m} + (\Delta J_y)^2_{\psi_m} + (\Delta J_z)^2_{\psi_m} = \langle J_x^2 + J_y^2 + J_z^2 \rangle_{\psi_m} - (\langle J_x \rangle^2_{\psi_m} + \langle J_y \rangle^2_{\psi_m} + \langle J_z \rangle^2_{\psi_m}). \tag{8.3.19}$$

Now we will consider two cases depending on k_m.

(i) For $k_m = 1$, for pure states $(\langle J_x \rangle^2_{\psi_m} + \langle J_y \rangle^2_{\psi_m} + \langle J_z \rangle^2_{\psi_m}) = 1/4$.

(ii) For $k_m > 1$, there are pure states that maximize $\langle J_x^2 + J_y^2 + J_z^2 \rangle_{\psi_m}$, while

$$(\langle J_x \rangle^2_{\psi_m} + \langle J_y \rangle^2_{\psi_m} + \langle J_z \rangle^2_{\psi_m}) = 0. \tag{8.3.20}$$

Hence, the sum of variances are bounded from above as

$$(\Delta J_x)^2_{\psi_m} + (\Delta J_y)^2_{\psi_m} + (\Delta J_z)^2_{\psi_m} \leq \begin{cases} \frac{k_m}{2}\left(1+\frac{k_m}{2}\right) & k_m > 1, \\ \frac{1}{2} & k_m = 1. \end{cases} \tag{8.3.21}$$

Let us now maximize Eq. (8.3.17) for the case when k is a divisor of N. Then we need to calculate the maximum for states of the type (8.2.9), similarly to the proof of Observation 8.2.1. If k is not a divisor of N then we have to consider states of the type (8.2.10). Based on these, we arrive at Eq. (8.3.16). ■

Note that the two cases in Eq. (8.3.16) and the two cases in Eq. (8.3.21) are strongly connected to each other. If we consider states with $N - sk = 1$, corresponding to the bottom line in Eq. (8.3.16), then the the state $|\Phi\rangle$ in the expression Eq. (8.2.10) is a single qubit state, hence for its uncertainties the bottom line must be used in Eq. (8.3.21).

Let us see some special cases of Observation 8.3.1. The bound for the average of the three variances for all quantum states, including entangled states, can be obtained from Observation 8.3.1 with the substitution $k = N$ as

$$\mathrm{avg}_{\vec{n}} F_Q[\varrho, J_{\vec{n}}] \leq \tfrac{1}{3}N(N+2). \tag{8.3.22}$$

Finally, we obtain the bound for separable states, which are just 1-producible states. Note that the bound in Observation 8.3.1 was valid only for k-producible states with $k \geq 2$.

Observation 8.3.2 *For separable states*

$$\mathrm{avg}_{\vec{n}} F_Q[\varrho, J_{\vec{n}}] \leq \tfrac{2}{3}N. \tag{8.3.23}$$

holds.

Proof. Let us again consider pure k-producible states of the form (2.1.6), where $|\psi_m\rangle$ are multiparticle states with $k = 1$ particles. For such states we have that the collective variances can be given as a sum of individual single-qubit variances as in Eq. (8.3.17). Moreover, for the single-qubit state ψ_m the relation $(\Delta J_x)^2_{\psi_m} + (\Delta J_y)^2_{\psi_m} + (\Delta J_z)^2_{\psi_m} \leq 1/4$ holds, see also Eq. (8.3.21). From these, an upper bound can be obtained for the sum of the three variances for pure product states. Then, a bound for the sum of the three quantum Fisher information terms can be obtained using that the quantum Fisher information is convex. ■

Comparing Eq. (8.2.4) with Eq. (8.3.23) shows that the bound for separable states for the average quantum Fisher information is lower than the bound for quantum Fisher

information for a single metrological task for a given direction.

8.4 Connected experimental and theoretical work

The quantum Fisher information is estimated based on collective measurements, and used to detect multipartite entanglement in a cold gas experiment creating Dicke states in Ref. [142]. In Ref. [143], a method is presented to estimate the quantum Fisher information based on some von Neumann measurements. The method can be applied in general, and can be used in a wide range of experiments with cold gases, cold trapped ions or photons. After estimating the quantum Fisher information, we can also detect multipartite entanglement based on the ideas of this chapter.

Chapter 9

Bell inequalities for graph states

In this Chapter, Bell inequalities detecting the non-locality of graph states are presented based on Ref. [66].

9.1 Background

9.1.1 Bell inequalities

In this section, we very briefly introduce Bell inequalities [58]. These inequalities are constraining the correlations in a bipartite system that we can obtain in an experiment. They are based on the assumption that in quantum mechanics, as in the case in classical physics, the measurement results "exist" locally at the parties, and the measurement is merely reading them out.

Of course, quantum mechanics does not fulfill the requirements mentioned above, hence some quantum states have correlations that violate Bell inequalities. Interestingly, all states that violate a Bell inequality are entangled, however, not all entangled states violate a Bell inequality [35]. [8]

In order to see how Bell inequalities work, let us consider a paradigmatic example, the Clauser-Horne-Shimony-Holt (CHSH) Bell inequality [62]

$$X_1X_2 - X_1Y_2 + Y_1X_2 + Y_1Y_2 \leq 2. \tag{9.1.1}$$

Here, on the first party we measure either X_1 or Y_1, while on the second party we measure either X_2 or Y_2. All these observables can have a measurement result $+1$ or -1. The setup

[8] In

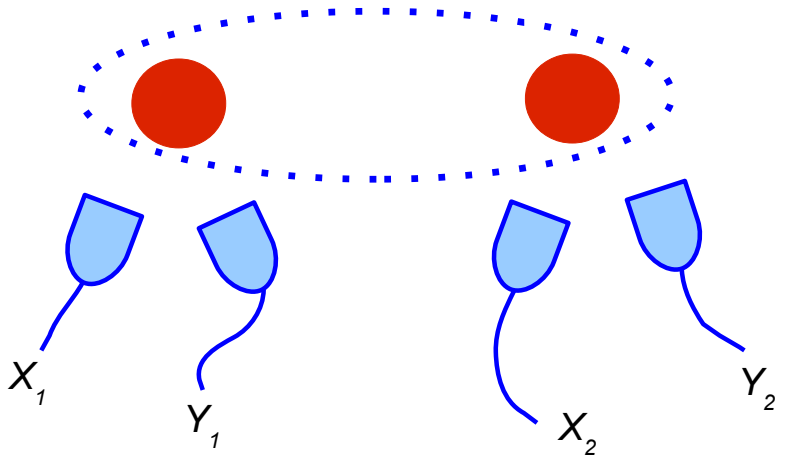

Figure 9.1: Measurements for a Bell inequality for a bipartite system. In both parties, we measure either X_k or Y_k. Both of these have possible outcomes $+1$ and -1.

is shown in Fig. 9.1.

Next, let us consider how we obtained the bound for Eq. (9.1.1). Simply, we have to substitute all the 16 possibilities for the four measurement outcomes, i.e., $(-1,-1,-1,-1)$, $(-1,-1,-1,+1)$, $(-1,-1,+1,-1)$, $(-1,-1,+1,+1)$, ..., $(+1,+1,+1,+1)$. We can observe that the largest value we can obtain for the left-hand side of Eq. (9.1.1) is 2. Note that for obtaining the bound, we did not need any physical model, did not need to know the quantities measured, and, in particular, we did not need the knowledge of quantum mechanics.

Finally, let us show a quantum state that can violate the Bell inequality Eq. (9.1.1). When we evaluate a Bell inequality on a quantum state, we have to define what quantum operators have to be measured. We will consider the case when X_k and Y_k correspond to measuring Pauli spin matrices $X^{(k)}$ and $Y^{(k)}$, respectively. For the quantum state

$$|\Psi\rangle = \frac{1-i}{2}|01\rangle + \frac{1}{\sqrt{2}}|10\rangle, \tag{9.1.2}$$

we get $2\sqrt{2}$. This is also the maximum that can be obtained for any quantum state and is called Tsirelson's bound [144].

Let us fix the notation for formulating Bell inequalities. A Bell operator is typically presented as the sum of many-body correlation terms. Now we will consider Bell operators $\mathcal{B}$ which are the sums of some of the stabilizing operators of graph states

$$\mathcal{B} = \sum_{m \in J} S_m, \tag{9.1.3}$$

where set J tells us which stabilizing operators we use for $\mathcal{B}$. (Stabilizing operators are discussed in Sec. 3.1.1.) Since all S_m are the products of Pauli spin matrices $X^{(k)}$, $Y^{(k)}$ and $Z^{(k)}$, we naturally assume that for our Bell inequalities for each qubit these spin coordinates are measured.

The maximum of the mean value $\langle\mathcal{B}\rangle$ for quantum states can immediately be obtained: For the graph state $|G_n\rangle$ all stabilizing operators have an expectation value $+1$ thus $\langle\mathcal{B}\rangle$ is an integer and it equals the number of stabilizing operators used for constructing $\mathcal{B}$ as given in Eq. (9.1.3). Clearly, there is no quantum state for which $\langle\mathcal{B}\rangle$ could be larger.

Now we will determine the maximum of $\langle\mathcal{B}\rangle$ for LHV models. It can be obtained in the following way. We take the definition Eq. (9.1.3). We then replace the Pauli spin matrices with real (classical) variables X_k, Y_k and Z_k. Let us denote the expression obtained this way by $\mathcal{E}(\mathcal{B})$:

$$\mathcal{E}(\mathcal{B}) := [\mathcal{B}]\big|_{X^{(k)}\to X_k, Y^{(k)}\to Y_k, Z^{(k)}\to Z_k}. \tag{9.1.4}$$

It is known that when maximizing $\mathcal{E}(\mathcal{B})$ for LHV models it is enough to consider deterministic LHV models which assign a definite $+1$ or -1 to the variables X_k, Y_k and Z_k. The value of our Bell operators for a given deterministic local model $\mathcal{L}$, i.e., an assignment of $+1$ or -1 to the classical variables will be denoted by $\mathcal{E}_{\mathcal{L}}(\mathcal{B})$. Thus we can obtain the maximum of the absolute value of $\langle\mathcal{B}\rangle$ for LHV models as

$$\mathcal{C}(\mathcal{B}) := \max_{\mathcal{L}} |\mathcal{E}_{\mathcal{L}}(\mathcal{B})|. \tag{9.1.5}$$

Based on Eq. (9.1.5), for LHV models we have

$$\langle\mathcal{B}\rangle \leq \mathcal{C}(\mathcal{B}). \tag{9.1.6}$$

If the maximum for quantum states is larger than the classical maximum, i.e., $\max_\Psi |\langle\mathcal{B}\rangle_\Psi| > \mathcal{C}(\mathcal{B})$ then Eq. (9.1.6) is a Bell inequality, and some quantum states violate it. The usefulness of a Bell inequality in experiments can be characterized by the visibility defined as a ratio of the quantum and the classical maxima as

$$\mathcal{V}(\mathcal{B}) := \frac{\max_\Psi |\langle\mathcal{B}\rangle_\Psi|}{\max_{\mathcal{L}} |\mathcal{E}_{\mathcal{L}}(\mathcal{B})|}. \tag{9.1.7}$$

The quantity $\mathcal{V}(\mathcal{B})$ is also called the maximal violation of local realism allowed by the Bell operator $\mathcal{B}$. The larger $\mathcal{V}(\mathcal{B})$, the better our Bell inequality.

The visibility is clearly a quantity similar to the robustness of entanglement witnesses discussed in Sec. 2.1.5. Let us consider a pure state $|\Psi\rangle$ mixed with white noise of the

form (2.1.7). We can assume that

$$\langle \mathcal{B} \rangle_{\varrho_{\rm cm}} = 0, \tag{9.1.8}$$

which is typically the case. Here, $\varrho_{\rm cm}$ is the compeletely mixed state defined in Eq. (2.1.8). Then, the noisy quantum state violates a Bell inequality given by Eq. (9.1.6) if the noise fraction $p_{\rm noise}$ is smaller than

$$p_{\rm noise\ limit} = 1 - \frac{\mathcal{C}(\mathcal{B})}{\langle \mathcal{B} \rangle_\Psi}. \tag{9.1.9}$$

Based on Eq. (9.1.7), if the state $|\Psi\rangle$ maximizes $\langle \mathcal{B} \rangle_\Psi$ then the noise limit is

$$p_{\rm max.\ noise\ limit} = 1 - [\mathcal{V}(\mathcal{B})]^{-1}. \tag{9.1.10}$$

If any pure state is mixed with more noise than $p_{\rm max.\ noise\ limit}$ then it cannot be detected by the Bell inequality (9.1.6).

9.1.2 Local hidden variable (LHV) models

As we discussed before, local hidden variable models assume that the a quantity existed before its measurement and when we measure it, we just read it out, without disturbing it. There are several possible formulations. A simple one is the following. In a bipartite system the correlations between $A^{(1)}$ and $B^{(2)}$ can be described by a hidden variable model, if there are p_k, a_k, and b_k such that

$$\left\langle A^{(1)} B^{(2)} \right\rangle = \sum_k p_k a_k b_k, \tag{9.1.11}$$

where $p_k > 0$ are probabilities. The formula can be interpreted as an expectation value of a random process that gives with p_k probability a measurement result a_k for $A^{(1)}$ and b_k for $B^{(2)}$. Clearly, a_k and b_k must be then valid measurement results, that is, they have to be in the range of allowed outcomes for $A^{(1)}$ and $B^{(2)}$.

If we measure only a single operator on the first party, and a single operator on the second, there is always a hidden variable model that describes their correlations. However, if we measure at least two operators per party, this is already not the case. Hence, we could find the state (9.1.2) that violates the CHSH inequality.

Let us consider $N^{(1)}$ operators on party 1 denoted by $\{A_m^{(1)}\}_{m=1}^{N^{(1)}}$, and $N(2)$ operators on party 2 denoted by $\{B_n^{(2)}\}_{n=1}^{N^{(2)}}$. Then, for states that do not violate any Bell inequality with these measurements, there must exist a hidden variable model for all possible measurements assuming that we measure one of the $A_m^{(1)}$ on party 1 and $B_n^{(2)}$ on party 2. That

is, we need $p_k, a_k^{(m)}$, and $b_k^{(n)}$ such that

$$\left\langle A_m^{(1)} B_n^{(2)} \right\rangle = \sum_k p_k a_k^{(m)} b_k^{(n)} \tag{9.1.12}$$

for all $1 \leq m \leq N^{(1)}$ and $1 \leq n \leq N^{(2)}$.

It can happen that there is an LHV model for a quantum state for a set of operators, however, there is not an LHV model for another set of operators. Then, such a state could violate a Bell inequality with these second set of operators. There are even quantum states, for which there is an LHV model for all possible operators that can be measured on party A and party B, respectively. Such quantum states do not violate any Bell inequality.

9.1.3 Multipartite Bell inequalities

So far we presented Bell inequalities for bipartite systems. In this section, we will present a Bell inequality, called Mermin's inequality, which works for multipartite systems [63]. Let us denote the number of parties by N. Then, let us consider the operator

$$\begin{aligned}
\mathcal{B}_N^{(\text{Mermin})} &:= X^{(1)}X^{(2)}X^{(3)}X^{(4)}X^{(5)}X^{(6)}X^{(7)}\cdots X^{(N)} \\
&- (Y^{(1)}Y^{(2)}X^{(3)}X^{(4)}X^{(5)}X^{(6)}X^{(7)}\cdots X^{(N)} + \text{perm.}) \\
&+ (Y^{(1)}Y^{(2)}Y^{(3)}Y^{(4)}X^{(5)}X^{(6)}X^{(7)}\cdots X^{(N)} + \text{perm.}) \\
&- (Y^{(1)}Y^{(2)}Y^{(3)}Y^{(4)}Y^{(5)}Y^{(6)}X^{(7)}\cdots X^{(N)} + \text{perm.}) \\
&+ \ ...,
\end{aligned} \tag{9.1.13}$$

where "perm" denotes all permutations. [In Eq. (4.3.9), we have already defined the Mermin operator. With that notation, $\mathcal{B}_N^{(\text{Mermin})} = \text{Memin}_{xy}$.]

Note that the first term in Eq. (9.1.13), has only X's, no $Y's$. Then, the second term has 2 Y's, the third term has 4 Y's, and so on. The signs of the terms are alternating. It has been shown that for states with a multipartite LHV model we have the Bell inequality

$$|\langle \mathcal{B}_N^{(\text{Mermin})} \rangle| \leq L_{\text{Mermin}}(N) \tag{9.1.14}$$

with the upper bound given as

$$L_{\text{Mermin}}(m) := \begin{cases} 2^{\frac{m-1}{2}} & \text{for odd } m, \\ 2^{\frac{m}{2}} & \text{for even } m, \end{cases} \tag{9.1.15}$$

The state $|\text{GHZ}\rangle$ maximally violates the Mermin inequality given in Eq. (9.1.14) with $\langle \mathcal{B}_N^{(\text{Mermin})} \rangle = 2^{N-1}$. [Note again that the variables X_k and Y_k in the Bell inequality are

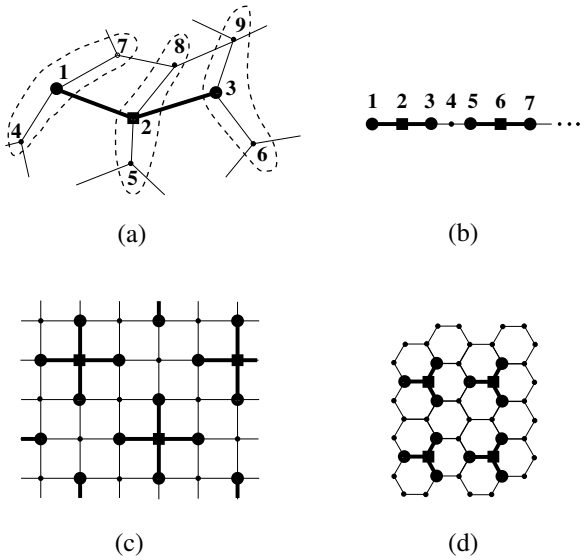

Figure 9.2: Bell inequalities for graph states. (a) The graphical representation of a Bell inequality involving the generators of vertices 1, 2 and 3. The corresponding three-vertex subgraph is shown in bold. The dashed lines indicate the three qubit-groups involved in this inequality. For the interpretation of symbols at the vertices see text. (b) Graphical representation for Bell inequalities for linear cluster states, (c) a two-dimensional lattice and (d) a hexagonal lattice. Figure is taken from Ref. [66].

identified with the Pauli spin matrices $X^{(k)}$ and $Y^{(k)}$.]

For clarity, we write out explicitly the Mermin's inequality for $N = 3$ parties

$$\langle X^{(1)}X^{(2)}X^{(3)}\rangle - \langle Y^{(1)}X^{(2)}X^{(3)}\rangle - \langle X^{(1)}Y^{(2)}X^{(3)}\rangle - \langle X^{(1)}X^{(2)}Y^{(3)}\rangle \geq 2 \qquad (9.1.16)$$

and $N = 4$ parties

$$\begin{aligned}&\langle X^{(1)}X^{(2)}X^{(3)}X^{(4)}\rangle - \langle Y^{(1)}Y^{(2)}X^{(3)}X^{(4)}\rangle - \langle Y^{(1)}X^{(2)}Y^{(3)}X^{(4)}\rangle - \langle Y^{(1)}X^{(2)}X^{(3)}Y^{(4)}\rangle \\ &-\langle X^{(1)}Y^{(2)}Y^{(3)}X^{(4)}\rangle - \langle X^{(1)}Y^{(2)}X^{(3)}Y^{(4)}\rangle - \langle X^{(1)}X^{(2)}Y^{(3)}Y^{(4)}\rangle + \langle Y^{(1)}Y^{(2)}Y^{(3)}Y^{(4)}\rangle \\ &\geq 4. \qquad (9.1.17)\end{aligned}$$

These Bell inequalities can simply be verified by substituting all possible combination of $+1$ and -1 for $X^{(k)}$ and $Y^{(k)}$.

9.2 Two-setting Bell inequalities

Now we present an approach providing a Bell inequality for any graph state, discussed in Sec. 3.1.2. Our method assigns a Bell inequality to each vertex in the graph. The

inequality is constructed such that it is maximally violated by the $|G\rangle$ state, having stabilizing operators $S_k^{(\mathrm{G}_N)}$.

Before starting the proof of a main result, let us recall an important fact which simplifies the calculation of the maximum mean value for local realistic models:

Observation 9.2.1 *Let $\mathcal{B}$ be a Bell operator consisting of a subset of the stabilizer for some graph state. Then, when computing the classical maximum $\mathcal{C}(\mathcal{B})$ one can restrict the attention to LHV models which assign $+1$ to all Z_k.*

Proof. From the construction of graph states and the multiplication rules for Pauli matrices it is easy to see that for an element S of the stabilizer the following fact holds: we have $Y^{(i)}$ or $Z^{(i)}$ at the qubit i in S iff the number of $Y^{(k)}$ and $X^{(k)}$ in the neighborhood $\mathcal{N}(i)$ in S is odd. Thus, if a LHV model assigns -1 to $Z^{(i)}$, we can, by changing the signs for $Z^{(i)}$ at the qubit i and for all $X^{(k)}$ and all $Y^{(k)}$ with $k \in \mathcal{N}(i)$, obtain a LHV model with the same mean value of $\mathcal{B}$ and the desired property. ■

Now we are in the position to present the main result of this section.

Observation 9.2.2 *Let i be a vertex and let*

$$I \subseteq \mathcal{N}(i) \tag{9.2.18}$$

be a subset of its neighborhood, such that none of the vertices in I are connected by an edge. Then the following operator

$$\mathcal{B}(i, I) := S_i^{(\mathrm{G}_N)} \prod_{j \in I} (1 + S_j^{(\mathrm{G}_N)}), \tag{9.2.19}$$

defines a Bell inequality $|\langle \mathcal{B}(i, I) \rangle| \leq L_{\mathrm{Mermin}}(|I|+1)$ with $L_{\mathrm{Mermin}}(m)$ given in Eq. (9.1.15), and $|G\rangle$ maximally violates it with $\langle \mathcal{B}(i, I) \rangle = 2^{|I|}$. The notation $\mathcal{B}(i, I)$ indicates that the Bell operator for our inequality is constructed with the generators corresponding to vertex i and to some of its neighbors given by set I. Note that $S_i^{(\mathrm{G}_N)}$ contains not only operators of site (i), but also of other sites. However, stabilizing operator corresponding to different sites commute with each other.

Proof. Consider a Bell inequality with the Bell operator Eq. (9.2.19) with vertex 2 and its two neighbors, vertices 1 and 3. The example is depicted in Fig. 9.2(a). The three-vertex subgraph with bold edges now represents the Bell inequality $\mathcal{B}(2, \{1, 3\})$. In this case, $i = 2$, which is indicated by a square at vertex 2. On the other hand, $I = \{1, 3\}$, which is indicated by circles at vertices 1 and 3.

Now constructing the Bell operator $\mathcal{B}$ involves $S_2^{(\mathrm{G}_N)}$ and $(1 + S_{1/3}^{(\mathrm{G}_N)})$, defined as

$$\begin{aligned} S_1^{(\mathrm{G}_N)} &= X^{(1)}Z^{(4)}Z^{(7)}Z^{(2)}, \\ S_2^{(\mathrm{G}_N)} &= X^{(2)}Z^{(1)}Z^{(3)}Z^{(5)}Z^{(8)}, \\ S_3^{(\mathrm{G}_N)} &= X^{(3)}Z^{(6)}Z^{(9)}Z^{(2)}. \end{aligned} \tag{9.2.20}$$

Then by expanding the brackets in Eq. (9.2.19), one obtains

$$\begin{aligned} \mathcal{B}(2,\{1,3\}) = {} & Z^{(1)}(Z^{(5)}Z^{(8)}X^{(2)})Z^{(3)} \\ & +(Z^{(4)}Z^{(7)}Y^{(1)})(Z^{(5)}Z^{(8)}Y^{(2)})Z^{(3)} \\ & +Z^{(1)}(Z^{(5)}Z^{(8)}Y^{(2)})(Z^{(6)}Z^{(9)}Y^{(3)}) \\ & -(Z^{(4)}Z^{(7)}Y^{(1)})(Z^{(5)}Z^{(8)}X^{(2)})(Z^{(6)}Z^{(9)}Y^{(3)}). \end{aligned} \tag{9.2.21}$$

Equation (9.2.21) corresponds to measuring two multi-spin observables at each of the three parties, where a party is formed out of several qubits. In fact, in Eq. (9.2.21) one can recognize the three-body Mermin inequality with multi-qubit observables. These observables are indicated by bracketing. The corresponding three qubit groups are indicated by dashed lines in Fig. 9.2(a).

Let us now turn to the general case of an inequality involving a vertex and its $N_{\mathrm{neigh}} \geq 2$ neighbors given in $\{I_k\}_{k=1}^{\mathrm{N_{neigh}}}$. Then, similarly to the previous tripartite example, this inequality is effectively a $(|I|+1)$-body Mermin's inequality. In order to see that, let us define the reduced neighborhood of vertex k as

$$\tilde{\mathcal{N}}(k) := \mathcal{N}(k) \backslash (I \cup \{i\}). \tag{9.2.22}$$

Then we define the following $2(N_{\mathrm{neigh}}+1)$ multi-qubit observables

$$\begin{aligned} A^{(1)} &:= Y^{(i)} \prod_{k \in \tilde{\mathcal{N}}(i)} Z^{(k)}, & B^{(1)} &:= X^{(i)} \prod_{k \in \tilde{\mathcal{N}}(i)} Z^{(k)}, \\ A^{(j+1)} &:= Z^{(I_j)}, & B^{(j+1)} &:= Y^{(I_j)} \Bigg(\prod_{k \in \tilde{\mathcal{N}}(I_j)} Z^{(k)} \Bigg), \end{aligned} \tag{9.2.23}$$

for $j = 1, 2, ..., N_{\mathrm{neigh}}$ and I_j denotes the j-th element of I. Then we can write down our Bell operator given in Eq. (9.2.19) as the Bell operator of a Mermin inequality with $A^{(i)}$

and $B^{(i)}$

$$\begin{aligned}\mathcal{B}(i,I) &= \sum_{\pi} B^{(1)}A^{(2)}A^{(3)}A^{(4)}A^{(5)}\cdots \\ &- \sum_{\pi} B^{(1)}B^{(2)}B^{(3)}A^{(4)}A^{(5)}\cdots \\ &+ \sum_{\pi} B^{(1)}B^{(2)}B^{(3)}B^{(4)}B^{(5)}\cdots, \end{aligned} \tag{9.2.24}$$

where $\sum_{\pi}$ represents the sum of all possible permutations of the qubits that give distinct terms. Hence the bound for local realism for Eq. (9.2.19) is the same as for the $(|I|+1)$-partite Mermin inequality [63]. To be more specific, if one takes the Bell operator presented in Ref. [63] and replaces $A^{(k)}$ and $B^{(k)}$ by $X^{(k)}$ and $Y^{(k)}$, respectively, then the Bell operator Eq. (9.2.24) is obtained. For $|\mathrm{G}_N\rangle$ all the terms in the Mermin inequality using the variables defined in Eq. (9.2.23) have an expectation value $+1$ thus $\langle\mathcal{B}(i,I)\rangle = 2^{|I|}$. ■

There is also an alternative way to understand why the extra $Z^{(k)}$ terms in the Bell operator do not influence the maximum for LHV models. That is, the maximum is the same as for the $(|I|+1)$-qubit Mermin inequality. For that we have to use Observation 9.2.1 described for computing the maximum for LHV models for an expression constructed as a sum of stabilizer elements of a graph state. Observation 9.2.1 says that the Z_k terms can simply be set to $+1$ and for computing the maximum it is enough to vary the X_k and Y_k terms. Thus from the point of view of the maximum, the extra Z_k terms can be neglected and would not change the maximum for LHV models even if it were not possible to reduce our inequality to a $(|I|+1)$-body Mermin inequality using the definitions Eq. (9.2.23).

Furthermore, it is worth noting that the above presented inequalities can be viewed as conditional Mermin inequalities for qubits $\{i\}\cup I$ after $Z^{(j)}$ measurements on the neighboring qubits are performed[9]. Indeed, after measuring $Z^{(j)}$ on these qubits, a state locally equivalent to a GHZ state is obtained. Knowing the outcomes of the $Z^{(j)}$ measurements, one can determine which state it is exactly and can write down a Mermin-type inequality with two single-qubit measurements per site which is maximally violated by this state. Indeed, this Mermin-type inequality can be obtained from the Bell inequality presented in Observation 9.2.2, after substituting in it the ±1 measurement results for these $Z^{(j)}$ measurements. Our scheme shows some relation to the Bell inequalities presented in Ref. [145]. These were essentially two-qubit Bell inequalities conditioned on measurement results on the remaining qubits.

[9] J. I. Cirac, private communication

9.3 Composite Bell inequalities

Observation 9.2.2 can also be used to obtain families of Bell inequalities with a degree of violation increasing exponentially with the number of qubits. In order to do this, let us start from two Bell inequalities of the form

$$|\mathcal{E}_1| \leq \mathcal{C}_1, \qquad |\mathcal{E}_2| \leq \mathcal{C}_2, \tag{9.3.25}$$

where $\mathcal{E}_{1/2}$ denote two expressions with classical variables X_k's, Y_k's and Z_k's. Then it follows immediately that

$$|\mathcal{E}_1\mathcal{E}_2| \leq \mathcal{C}_1\mathcal{C}_2. \tag{9.3.26}$$

Concerning Bell inequalities, one has to be careful at this point: Eq. (9.3.26) is not necessarily a Bell inequality. It may happen that $\mathcal{E}_1\mathcal{E}_2$ have correlation terms which contain two or more variables of the same qubit, e.,g., $(X_1Z_2)(Z_1X_2) = X_1Z_1X_2Z_2$. Such a correlation term cannot appear in a Bell inequality. Because of that we need the following theorem.

Observation 9.3.1 *Let us consider two Bell inequalities of the form Eq.* (9.3.25)*. If for each qubit k at most only one of the inequalities contain variables corresponding to the qubit, then Eq.* (9.3.26) *describes a composite Bell inequality. If both of the inequalities contain variables corresponding to qubit k, then Eq.* (9.3.26) *still describes a Bell inequality if the inequalities contain the same variable for qubit k.*

Proof. If the conditions mentioned above are satisfied then none of the correlation terms of the Bell inequality Eq. (9.3.26) contain more than two variables for a qubit. They may contain quadratic terms such as X_k^2, however, these can be replaced by 1. ■

Based on these ideas, composite Bell inequalities can be created from several inequalities. Let us see a concrete example. For an N-qubit cluster state we have the stabilizing operators $g_i^{(\mathrm{C}_N)} := Z^{(i-1)}X^{(i)}Z^{(i+1)}$ where $i \in \{1, 2, .., n\}$ and for the boundaries $Z^{(0)} = Z^{(n+1)} = \mathbb{1}$. Then we can define the following Bell inequality for vertex i

$$\begin{aligned}\mathcal{B}_i^{(\mathrm{C}_N)} &:= g_i^{(\mathrm{C}_N)}(1 + g_{i+1}^{(\mathrm{C}_N)})(1 + g_{i-1}^{(\mathrm{C}_N)}) \\ &= Z^{(i-1)}X^{(i)}Z^{(i+1)} \qquad + Z^{(i-2)}Y^{(i-1)}Y^{(i)}Z^{(i+1)} \\ &+ Z^{(i-1)}Y^{(i)}Y^{(i+1)}Z^{(i+2)} - Z^{(i-2)}Y^{(i-1)}X^{(i)}Y^{(i+1)}Z^{(i+2)}.\end{aligned} \tag{9.3.27}$$

The maximal violation of the Bell inequality is

$$\mathcal{V}(\mathcal{B}_i^{(\mathrm{C}_N)}) = 2. \tag{9.3.28}$$

Now we can combine these Bell inequalities, for different i as illustrated in Fig. 9.2(b). Here $\mathcal{B}_2^{(\mathrm{C}_N)}$ and $\mathcal{B}_6^{(\mathrm{C}_N)}$ are represented by two bold subgraphs. If N is divisible by four then we obtain a composite inequality characterized by the Bell operator

$$\mathcal{B}^{(\mathrm{C}_N)} := \prod_{i=1}^{N/4} \mathcal{B}_{4i-2}^{(\mathrm{C}_N)}, \tag{9.3.29}$$

and the maximal violation of the Bell inequality is

$$\mathcal{V}(\mathcal{B}^{(\mathrm{C}_N)}) = 2^{N/4}. \tag{9.3.30}$$

Thus, the violation increases exponentially with N.

Figs. 9.2(c-d) show the graphical representation of other composite Bell inequalities, where a similar argument can be applied to show that the violation increases exponentially with the number of qubits.

9.4 Comparison with existing Bell inequalities

The systematic study of Bell inequalities for graph states was initiated in an important paper by Scarani, Acín, Schenck, and Aspelmeyer [64]. In this paper, a Bell inequality for a four-qubit cluster state was presented which has already been used for detecting the violation of local realism experimentally [146]. The inequality of Ref. [64] is also a Mermin's inequality with composite observables

$$X_1X_3Z_4 + Z_1Y_2Y_3Z_4 + X_1Y_3Y_4 - Z_1Y_2X_3Y_4 \leq 2. \tag{9.4.31}$$

It is instructive to write down its Bell operator with the stabilizing operator of a cluster state

$$\mathcal{B}^{(\mathrm{C}_4)} = S_3^{(\mathrm{C}_4)}(S_1^{(\mathrm{C}_4)} + S_2^{(\mathrm{C}_4)})(\mathbb{1} + S_4^{(\mathrm{C}_4)}). \tag{9.4.32}$$

This is different from our ansatz in Eq. (9.2.19). The inequality obtained from our ansatz Eq. (9.2.19) for $i = 3$ is

$$Z_2X_3Z_4 + Z_1Y_2Y_3Z_4 + Z_2Y_3Y_4 - Z_1Y_2X_3Y_4 \leq 2. \tag{9.4.33}$$

The following two four-qubit Bell inequalities are also built with stabilizing terms and

have a factor of two violation of local realism:

$$X_1X_3Z_4 - Y_1X_2Y_3Z_4 + X_1Y_3Y_4 + Y_1X_2X_3Y_4 \leq 2,$$
$$Z_2X_3Z_4 - Y_1X_2Y_3Z_4 + Z_2Y_3Y_4 + Y_1X_2X_3Y_4 \leq 2. \quad (9.4.34)$$

Further four inequalities can be obtained by exchanging qubits 1 and 4, and qubits 2 and 3, in the previous four Bell inequalities. These eight inequalities are all maximally violated by the four-qubit cluster state $|\mathrm{C}_4\rangle$, however, not only by the cluster state. The maximum of the Bell operator for these inequalities is doubly degenerate. Thus, as discussed in Ref. [64] for the case of Eq. (9.4.31), they are maximally violated also by some mixed states.

9.5 Connected experimental and theoretical work

Bell inequalities for graph states based on the decomposition of the projector have been presented in Ref. [65]. Bell inequalities for graph states have been tested in trapped ions in Ref. [147]. Bell inequalities were also tested for four-photon six-qubit graph states in Ref. [148]. Bell inequalities are presented for hypergraph states in Ref. [149].

Acknowledgments

Concerning many of the works in this thesis, I would like to thank Otfried Gühne for the long-term, very fruitful collaboration. We were collaborating on several projects of the Thesis, in particular, on the works on witnesses for GHZ states and cluster states, on the relations of symmetry and entanglement, on the optimal spin squeezing inequalities, and on Bell inequalities for graph states. I thank J. Ignacio Cirac for important inputs for the paper about entanglement detection with energy measurement, and also for the project about detecting entanglement in optical lattices of cold atoms. I thank Hans J. Briegel for collaborating on the project on spin squeezing inequalities, and on Bell inequalities. I thank Christian Knapp for collaborating on the project on spin squeezing inequalities. I would like to thank the group of Harald Weinfurter including Witlef Wieczorek, Roland Krischek, Nikolai Kiesel and Patrick Michelberger, for collaboration on the entanglement conditions on Dicke states. I would like to thank the group of Harald Weinfurter including Witlef Wieczorek, Roland Krischek, and Christian Schwemmer, for collaborating on the work on permutationally invariant tomography. I would also like to thank David Gross for the theoretical collaboration in that project. In the Thesis, I also referred to the experimental papers of the group of Harald Weinfurter, in several of which I had the opportunity to collaborate. Many entanglement witnesses were constructed to detect entanglement in these experiments. I would like to thank Harald Weinfurter and his research group for the long term, very fruitful collaboration. I thank István Rácz for important advice and discussions about the thesis. I thank Iagoba Apellaniz for a critical reading of the Thesis. I thank Szilárd Szalay and Tamás Vértesi for a very careful reading of the manuscript, and also for many suggestions how to improve it. I thank János Asbóth and Gergely Szirmai for helpful comments.

I am thankful to all members of the Department of Quantum Optics and Quantum Information of the Wigner Research Centre for Physics in Budapest and the Department of Theoretical Physics at the University of the Basque Country, or their helpfulness and the friendly atmosphere, which was essential in preparing the thesis. I thank Ikerbasque, the Basque Foundation for Science for their continuing strong support. The preparation of this work has been supported also by the OTKA grants No. K124351 and KH129601. We

thank also the EU (QuantERA CEBBEC, ERC Starting Grant 258647/GEDENTQOPT, CHIST-ERA QUASAR, COST Action CA15220). We thank also the Spanish Ministry of Economy, Industry and Competitiveness and the European Regional Development Fund FEDER through Grant No. FIS2015-67161-P (MINECO/FEDER, EU), the Basque Government (Project No. IT986-16).

Bibliography

[1] R. Horodecki, P. Horodecki, M. Horodecki, and K. Horodecki, Rev. Mod. Phys. **81**, 865 (2009).

[2] O. Gühne and G. Tóth, Phys. Rep. **474**, 1 (2009).

[3] L. K. Grover, eprint arXiv:quant-ph/9605043 (1996).

[4] P. W. Shor, SIAM Review **41**, 303 (1999).

[5] C. H. Bennett, G. Brassard, C. Crépeau, R. Jozsa, A. Peres, and W. K. Wootters, Phys. Rev. Lett. **70**, 1895 (1993).

[6] D. J. Wineland, J. J. Bollinger, W. M. Itano, and D. J. Heinzen, Phys. Rev. A **50**, 67 (1994).

[7] A. Sørensen, L.-M. Duan, J. Cirac, and P. Zoller, Nature (London) **409**, 63 (2001).

[8] M. Bourennane, M. Eibl, C. Kurtsiefer, S. Gaertner, H. Weinfurter, O. Gühne, P. Hyllus, D. Bruß, M. Lewenstein, and A. Sanpera, Phys. Rev. Lett. **92**, 087902 (2004).

[9] R. Krischek, C. Schwemmer, W. Wieczorek, H. Weinfurter, P. Hyllus, L. Pezzé, and A. Smerzi, Phys. Rev. Lett. **107**, 080504 (2011).

[10] B. Julsgaard, A. Kozhekin, and E. S. Polzik, Nature (London) **413**, 400 (2001).

[11] N. Behbood, F. Martin Ciurana, G. Colangelo, M. Napolitano, G. Tóth, R. J. Sewell, and M. W. Mitchell, Phys. Rev. Lett. **113**, 093601 (2014).

[12] W. Muessel, H. Strobel, D. Linnemann, D. B. Hume, and M. K. Oberthaler, Phys. Rev. Lett. **113**, 103004 (2014).

[13] L. Diósi, Phys. Rev. A **40**, 1165 (1989).

[14] D. M. Greenberger, M. A. Horne, A. Shimony, and A. Zeilinger, Am. J. Phys. **58**, 1131 (1990).

[15] J. K. Stockton, J. M. Geremia, A. C. Doherty, and H. Mabuchi, Phys. Rev. A **67**, 022112 (2003).

[16] R. H. Dicke, Phys. Rev. **93**, 99 (1954).

[17] R. Raussendorf and H. J. Briegel, Phys. Rev. Lett. **86**, 5188 (2001).

[18] W.-B. Gao, C.-Y. Lu, X.-C. Yao, P. Xu, O. Gühne, A. Goebel, Y.-A. Chen, C.-Z. Peng, Z.-B. Chen, and J.-W. Pan, Nat. Phys. **6**, 331 (2010).

[19] A. Chiuri, C. Greganti, M. Paternostro, G. Vallone, and P. Mataloni, Phys. Rev. Lett. **109**, 173604 (2012).

[20] H. Häffner, W. Hänsel, C. Roos, J. Benhelm, M. Chwalla, T. Körber, U. Rapol, M. Riebe, P. Schmidt, C. Becher, et al., Nature (London) **438**, 643 (2005).

[21] T. Monz, P. Schindler, J. T. Barreiro, M. Chwalla, D. Nigg, W. A. Coish, M. Harlander, W. Hänsel, M. Hennrich, and R. Blatt, Phys. Rev. Lett. **106**, 130506 (2011).

[22] K. Hammerer, A. S. Sørensen, and E. S. Polzik, Rev. Mod. Phys. **82**, 1041 (2010).

[23] A. S. Sørensen and K. Mølmer, Phys. Rev. Lett. **86**, 4431 (2001).

[24] A. Furusawa, J. L. Sørensen, S. L. Braunstein, C. A. Fuchs, H. J. Kimble, and E. S. Polzik, Science **282**, 706 (1998).

[25] B. Julsgaard, J. Sherson, J. I. Cirac, J. Fiurasek, and E. S. Polzik, Nature (London) **432**, 482 (2004).

[26] O. Hosten, N. J. Engelsen, R. Krishnakumar, and M. A. Kasevich, Nature (London) **529**, 505 (2016).

[27] J. Esteve, C. Gross, A. Weller, S. Giovanazzi, and M. Oberthaler, Nature (London) **455**, 1216 (2008).

[28] C. Gross, T. Zibold, E. Nicklas, J. Esteve, and M. K. Oberthaler, Nature (London) **464**, 1165 (2010).

[29] M. F. Riedel, P. Böhi, Y. Li, T. W. Hänsch, A. Sinatra, and P. Treutlein, Nature (London) **464**, 1170 (2010).

[30] B. Lücke, M. Scherer, J. Kruse, L. Pezzé, F. Deuretzbacher, P. Hyllus, J. Peise, W. Ertmer, J. Arlt, L. Santos, et al., Science **334**, 773 (2011).

[31] B. Lücke, J. Peise, G. Vitagliano, J. Arlt, L. Santos, G. Tóth, and C. Klempt, Phys. Rev. Lett. **112**, 155304 (2014).

[32] O. Mandel, M. Greiner, A. Widera, T. Rom, T. W. Hansch, and I. Bloch, Nature (London) **425**, 937 (2003).

[33] D. Jaksch, H.-J. Briegel, J. I. Cirac, C. W. Gardiner, and P. Zoller, Phys. Rev. Lett. **82**, 1975 (1999).

[34] W. S. Bakr, J. I. Gillen, A. Peng, S. Fölling, and M. Greiner, Nature (London) **462**, 74 (2009).

[35] R. F. Werner, Phys. Rev. A **40**, 4277 (1989).

[36] S. Gharibian, Quantum Inf. Comp. **10**, 343 (2010).

[37] A. Acín, D. Bruß, M. Lewenstein, and A. Sanpera, Phys. Rev. Lett. **87**, 040401 (2001).

[38] C. Sackett, D. Kielpinski, B. King, C. Langer, V. Meyer, C. Myatt, M. Rowe, Q. Turchette, W. Itano, D. Wineland, et al., Nature (London) **404**, 256 (2000).

[39] G. Tóth and O. Gühne, Phys. Rev. Lett. **94**, 060501 (2005).

[40] N. Kiesel, C. Schmid, U. Weber, G. Tóth, O. Gühne, R. Ursin, and H. Weinfurter, Phys. Rev. Lett. **95**, 210502 (2005).

[41] G. Tóth and O. Gühne, Phys. Rev. A **72**, 022340 (2005).

[42] G. Tóth, J. Opt. Soc. Am. B **24**, 275 (2007).

[43] N. Kiesel, C. Schmid, G. Tóth, E. Solano, and H. Weinfurter, Phys. Rev. Lett. **98**, 063604 (2007).

[44] W. Wieczorek, R. Krischek, N. Kiesel, P. Michelberger, G. Tóth, and H. Weinfurter, Phys. Rev. Lett. **103**, 020504 (2009).

[45] R. Prevedel, G. Cronenberg, M. S. Tame, M. Paternostro, P. Walther, M. S. Kim, and A. Zeilinger, Phys. Rev. Lett. **103**, 020503 (2009).

[46] G. Tóth, W. Wieczorek, R. Krischek, N. Kiesel, P. Michelberger, and H. Weinfurter, New J. Phys. **11**, 083002 (2009).

[47] G. Tóth, C. Knapp, O. Gühne, and H. J. Briegel, Phys. Rev. Lett. **99**, 250405 (2007).

[48] V. Giovannetti, S. Lloyd, and L. Maccone, Science **306**, 1330 (2004).

[49] M. G. A. Paris, Int. J. Quant. Inf. **07**, 125 (2009).

[50] R. Demkowicz-Dobrzanski, M. Jarzyna, and J. Kolodynski, Prog. Optics **60**, 345 (2015), `arXiv:1405.7703`.

[51] L. Pezze and A. Smerzi, in *Atom Interferometry (Proc. Int. School of Physics 'Enrico Fermi', Course 188, Varenna)*, edited by G. Tino and M. Kasevich (IOS Press, Amsterdam, 2014), pp. 691–741, `arXiv:1411.5164`.

[52] G. Tóth and I. Apellaniz, J. Phys. A: Math. Theor. **47**, 424006 (2014).

[53] L. Pezzè, A. Smerzi, M. K. Oberthaler, R. Schmied, and P. Treutlein, arxiv:1609.01609 (2016).

[54] D. Petz, *Quantum information theory and quantum statistics* (Springer, Berlin, Heilderberg, 2008).

[55] L. Pezzé and A. Smerzi, Phys. Rev. Lett. **102**, 100401 (2009).

[56] G. Tóth, Phys. Rev. A **85**, 022322 (2012).

[57] A. Einstein, B. Podolsky, and N. Rosen, Phys. Rev. **47**, 777 (1935).

[58] J. S. Bell, *Speakable and unspeakable in quantum mechanics: Collected papers on quantum philosophy* (Cambridge university press, 2004).

[59] N. Brunner, D. Cavalcanti, S. Pironio, V. Scarani, and S. Wehner, Rev. Mod. Phys. **86**, 419 (2014).

[60] A. Peres, Found. Phys. **29**, 589 (1999).

[61] T. Vértesi and N. Brunner, Nat. Commun. **5**, 5297 (2014).

[62] J. F. Clauser, M. A. Horne, A. Shimony, and R. A. Holt, Phys. Rev. Lett. **23**, 880 (1969).

[63] N. D. Mermin, Phys. Rev. Lett. **65**, 1838 (1990).

[64] V. Scarani, A. Acín, E. Schenck, and M. Aspelmeyer, Phys. Rev. A **71**, 042325 (2005).

[65] O. Gühne, G. Tóth, P. Hyllus, and H. J. Briegel, Phys. Rev. Lett. **95**, 120405 (2005).

[66] G. Tóth, O. Gühne, and H. J. Briegel, Phys. Rev. A **73**, 022303 (2006).

[67] G. Tóth, Phys. Rev. A **71**, 010301(R) (2005).

[68] G. Tóth and O. Gühne, Appl. Phys. B **82**, 237 (2006).

[69] G. Tóth, Phys. Rev. A **69**, 052327 (2004).

[70] G. Tóth and O. Gühne, Phys. Rev. Lett. **102**, 170503 (2009).

[71] G. Tóth, W. Wieczorek, D. Gross, R. Krischek, C. Schwemmer, and H. Weinfurter, Phys. Rev. Lett. **105**, 250403 (2010).

[72] G. Tóth, C. Knapp, O. Gühne, and H. J. Briegel, Phys. Rev. A **79**, 042334 (2009).

[73] J. K. Asbóth, J. Calsamiglia, and H. Ritsch, Phys. Rev. Lett. **94**, 173602 (2005).

[74] D. Bouwmeester, J.-W. Pan, M. Daniell, H. Weinfurter, and A. Zeilinger, Phys. Rev. Lett. **82**, 1345 (1999).

[75] J.-W. Pan, D. Bouwmeester, M. Daniell, H. Weinfurter, and A. Zeilinger, Nature (London) **403**, 515 (2000).

[76] Z. Zhao, T. Yang, Y.-A. Chen, A.-N. Zhang, M. Żukowski, and J.-W. Pan, Phys. Rev. Lett. **91**, 180401 (2003).

[77] C.-Y. Lu, X.-Q. Zhou, O. Gühne, W.-B. Gao, J. Zhang, Z.-S. Yuan, A. Goebel, T. Yang, and J.-W. Pan, Nat. Phys. **3**, 91 (2007).

[78] O. Gühne, G. Tóth, and H. J. Briegel, New J. Phys. **7**, 229 (2005).

[79] O. Gühne and G. Tóth, Phys. Rev. A **73**, 052319 (2006).

[80] S. Szalay, Phys. Rev. A **92**, 042329 (2015).

[81] S. Szalay and Z. Kökényesi, Phys. Rev. A **86**, 032341 (2012).

[82] M. Lewenstein, B. Kraus, P. Horodecki, and J. I. Cirac, Phys. Rev. A **63**, 044304 (2001).

[83] B. M. Terhal, Theoretical Computer Science **287**, 313 (2002).

[84] J. Eisert, P. Hyllus, O. Gühne, and M. Curty, Phys. Rev. A **70**, 062317 (2004).

[85] A. C. Doherty, P. A. Parrilo, and F. M. Spedalieri, Phys. Rev. A **71**, 032333 (2005).

[86] X. Wang, Phys. Rev. A **66**, 044305 (2002).

[87] X. Wang and P. Zanardi, Phys. Lett. A **301**, 1 (2002).

[88] P. Pfeuty, Ann. Phys. **57**, 79 (1970).

[89] C. Brukner and V. Vedral, eprint arXiv:quant-ph/0406040 (2004).

[90] M. R. Dowling, A. C. Doherty, and S. D. Bartlett, Phys. Rev. A **70**, 062113 (2004).

[91] L.-A. Wu, S. Bandyopadhyay, M. S. Sarandy, and D. A. Lidar, Phys. Rev. A **72**, 032309 (2005).

[92] D. Gottesman, Phys. Rev. A **54**, 1862 (1996).

[93] M. Hein, J. Eisert, and H. J. Briegel, Phys. Rev. A **69**, 062311 (2004).

[94] O. Gühne, P. Hyllus, D. Bruß, A. Ekert, M. Lewenstein, C. Macchiavello, and A. Sanpera, Phys. Rev. A **66**, 062305 (2002).

[95] O. Gühne and P. Hyllus, International Journal of Theoretical Physics **42**, 1001 (2003), ISSN 1572-9575.

[96] O. Gühne, P. Hyllus, D. Bruss, A. Ekert, M. Lewenstein, C. Macchiavello, and A. Sanpera, J. Mod. Opt. **50**, 1079 (2003).

[97] O. Gühne, C.-Y. Lu, W.-B. Gao, and J.-W. Pan, Phys. Rev. A **76**, 030305 (2007).

[98] M. Eibl, N. Kiesel, M. Bourennane, C. Kurtsiefer, and H. Weinfurter, Phys. Rev. Lett. **92**, 077901 (2004).

[99] H. J. Briegel and R. Raussendorf, Phys. Rev. Lett. **86**, 910 (2001).

[100] M. A. Nielsen, Phys. Rev. Lett. **83**, 436 (1999).

[101] G. Vallone, E. Pomarico, P. Mataloni, F. De Martini, and V. Berardi, Phys. Rev. Lett. **98**, 180502 (2007).

[102] K. Chen, C.-M. Li, Q. Zhang, Y.-A. Chen, A. Goebel, S. Chen, A. Mair, and J.-W. Pan, Phys. Rev. Lett. **99**, 120503 (2007).

[103] Y. Tokunaga, S. Kuwashiro, T. Yamamoto, M. Koashi, and N. Imoto, Phys. Rev. Lett. **100**, 210501 (2008).

[104] S. M. Lee, H. S. Park, J. Cho, Y. Kang, J. Y. Lee, H. Kim, D.-H. Lee, and S.-K. Choi, Opt. Express **20**, 6915 (2012).

[105] W.-B. Gao, P. Xu, X.-C. Yao, O. Gühne, A. Cabello, C.-Y. Lu, C.-Z. Peng, Z.-B. Chen, and J.-W. Pan, Phys. Rev. Lett. **104**, 020501 (2010).

[106] C. Reimer, S. Sciara, P. Roztocki, M. Islam, L. Romero Cortés, Y. Zhang, B. Fischer, S. Loranger, R. Kashyap, A. Cino, et al., Nat. Phys. **15**, 148 (2019).

[107] S. Sciara, C. Reimer, M. Kues, P. Roztocki, A. Cino, D. J. Moss, L. Caspani, W. J. Munro, and R. Morandotti, Phys. Rev. Lett. **122**, 120501 (2019).

[108] P. Erker, M. Krenn, and M. Huber, Quantum **1**, 22 (2017).

[109] P. Erker, Ph.D. thesis, Universitat Autònoma de Barcelona and Università della Svizzera Italiana (2019).

[110] L.-M. Duan, Phys. Rev. Lett. **107**, 180502 (2011).

[111] G. Vitagliano, I. Apellaniz, M. Kleinmann, B. Lücke, C. Klempt, and G. Tóth, New J. Phys. **19**, 013027 (2017).

[112] M. Horodecki, P. Horodecki, and R. Horodecki, Phys. Rev. Lett. **80**, 5239 (1998).

[113] A. Peres, Phys. Rev. Lett. **77**, 1413 (1996).

[114] A. Ferraro, D. Cavalcanti, A. García-Saez, and A. Acín, Phys. Rev. Lett. **100**, 080502 (2008).

[115] K. Chen and L.-A. Wu, Quant. Inf. Comp. **3**, 193 (2003).

[116] O. Rudolph, Quant. Inf. Proc. **4**, 219 (2005).

[117] M. Wolf, Ph.D. thesis, Technical University of Braunschweig (2003).

[118] K. Eckert, J. Schliemann, D. Bruss, and M. Lewenstein, Ann. Phys. **299**, 88 (2002).

[119] J. Tura, R. Augusiak, P. Hyllus, M. Kuś, J. Samsonowicz, and M. Lewenstein, Phys. Rev. A **85**, 060302 (2012).

[120] R. Augusiak, J. Tura, J. Samsonowicz, and M. Lewenstein, Phys. Rev. A **86**, 042316 (2012).

[121] R. Schmied, J. Mod. Opt. **63**, 1744 (2016).

[122] N. Kiesel, Ph.D. thesis, Ludwig-Maximilians-Universität, München (2007).

[123] C. Schwemmer, G. Tóth, A. Niggebaum, T. Moroder, D. Gross, O. Gühne, and H. Weinfurter, Phys. Rev. Lett. **113**, 040503 (2014).

[124] F. Verstraete, V. Murg, and J. Cirac, Adv. Phys. **57**, 143 (2008).

[125] M. Cramer, M. B. Plenio, S. T. Flammia, R. Somma, D. Gross, S. D. Bartlett, O. Landon-Cardinal, D. Poulin, and Y.-K. Liu, Nat. Comm. **1**, 149 (2010).

[126] D. Gross, Y.-K. Liu, S. T. Flammia, S. Becker, and J. Eisert, Phys. Rev. Lett. **105**, 150401 (2010).

[127] T. Moroder, P. Hyllus, G. Tóth, C. Schwemmer, A. Niggebaum, S. Gaile, O. Gühne, and H. Weinfurter, New J. Phys. **14**, 105001 (2012).

[128] M. Kitagawa and M. Ueda, Phys. Rev. A **47**, 5138 (1993).

[129] J. J. García-Ripoll and J. I. Cirac, Phys. Rev. Lett. **90**, 127902 (2003).

[130] A. Sørensen and K. Mølmer, Phys. Rev. Lett. **83**, 2274 (1999).

[131] H. F. Hofmann and S. Takeuchi, Phys. Rev. A **68**, 032103 (2003).

[132] T.-L. Ho and L. Yin, Phys. Rev. Lett. **84**, 2302 (2000).

[133] G. Tóth and M. W. Mitchell, New J. Phys. **12**, 053007 (2010).

[134] G. Vitagliano, P. Hyllus, I. L. Egusquiza, and G. Tóth, Phys. Rev. Lett. **107**, 240502 (2011).

[135] G. Vitagliano, I. Apellaniz, I. L. Egusquiza, and G. Tóth, Phys. Rev. A **89**, 032307 (2014).

[136] P. Hyllus, W. Laskowski, R. Krischek, C. Schwemmer, W. Wieczorek, H. Weinfurter, L. Pezzé, and A. Smerzi, Phys. Rev. A **85**, 022321 (2012).

[137] C. Helstrom, *Quantum Detection and Estimation Theory* (Academic Press, New York, 1976).

[138] A. Holevo, *Probabilistic and Statistical Aspects of Quantum Theory* (North-Holland, Amsterdam, 1982).

[139] S. L. Braunstein and C. M. Caves, Phys. Rev. Lett. **72**, 3439 (1994).

[140] S. L. Braunstein, C. M. Caves, and G. J. Milburn, Ann. Phys. **247**, 135 (1996).

[141] P. Hyllus, O. Gühne, and A. Smerzi, Phys. Rev. A **82**, 012337 (2010).

[142] I. Apellaniz, B. Lücke, J. Peise, C. Klempt, and G. Tóth, New J. Phys. **17**, 083027 (2015).

[143] I. Apellaniz, M. Kleinmann, O. Gühne, and G. Tóth, Phys. Rev. A **95**, 032330 (2017).

[144] B. S. Cirel'son, Lett. Math. Phys. **4**, 93 (1980).

[145] S. Popescu and D. Rohrlich, Phys. Lett. A **166**, 293 (1992).

[146] P. Walther, M. Aspelmeyer, K. J. Resch, and A. Zeilinger, Phys. Rev. Lett. **95**, 020403 (2005).

[147] B. P. Lanyon, M. Zwerger, P. Jurcevic, C. Hempel, W. Dür, H. J. Briegel, R. Blatt, and C. F. Roos, Phys. Rev. Lett. **112**, 100403 (2014).

[148] W.-B. Gao, X.-C. Yao, P. Xu, H. Lu, O. Gühne, A. Cabello, C.-Y. Lu, T. Yang, Z.-B. Chen, and J.-W. Pan, Phys. Rev. A **82**, 042334 (2010).

[149] M. Gachechiladze, C. Budroni, and O. Gühne, Phys. Rev. Lett. **116**, 070401 (2016).